



KTH Industrial Engineering  
and Management



## MASTER THESIS

# Performance Calculations and Optimization of a Fresnel Direct Steam Generation CSP Plant with Heat Storage

Perrine SCHLAIFER

### Supervisors:

Christophe LEHAUT (CNIM)  
James SPELLING (KTH)  
Marcellin MOUEZA (ECP)

July 2012 - December 2012

Master of Science Thesis EGI-2012-118MSC EKV929



**KTH Industrial Engineering  
and Management**

**Master of Science Thesis EGI-2012-118MSC EKV929**

**Performance Calculations and Optimisation of a Fresnel Direct Steam Generation CSP Plant with Heat Storage**

Perrine SCHLAIFER

Approved	Examiner Björn LAUMERT	Supervisor James SPELLING
	Commissioner	Contact person

## Abstract

This master thesis deals with the performance calculations of a 9MW linear Fresnel CSP plant with direct steam generation built by the Solar Division of the CNIM Company. The aim was to calculate the annual electricity production taking into account the weather conditions as well as some steam storage. At first, a steam accumulator model was developed with Excel, in order to estimate the pressure evolution in the tanks during the charging, storage and discharging processes. The data obtained with this model was then integrated to the thermodynamic cycle model, programmed with Excel, which calculated the electrical power production knowing the thermal power available in the solar field. The electricity production calculations were made every 600 seconds during one year.

To improve the results accuracy, the influence of the plant location slope was estimated, calculating the equivalent azimuth and elevation angles in a new spherical coordinates system. For an average slope of  $4.21^\circ$  at the plant location, the annual thermal energy gain is 14.4% (with a gain up to 60% during winter days) and the annual electricity production is increased by 12.59%. The influence of frost on the mirrors during cold and humid nights was also estimated with a simple model of the energy needed to heat up a constant layer of ice. Depending on the assumptions, the electricity production losses were between 1.27 and 2.84% of annual electricity production. The losses due to plant shutdowns set by the electrical network manager RTE during the snowmelt months were also estimated. The annual electricity production could decrease by 8.02 to 11.57 % because of the load management, depending on the days during which the plant is shutdown.

Finally, an economic optimisation was led with prices estimated by CNIM, which gave an optimal solar field design with 31 lines and 5 steam accumulators. The payback time would then be 9.887 years.

**Keywords:** CSP plant, thermal solar plant, linear Fresnel technology, direct steam generation, steam accumulator, steam turbine.

Ce rapport de stage traite du calcul du productible d'une centrale solaire à technologie de Fresnel et génération directe de vapeur de 9MW. Le stage a été effectué au sein de la division solaire de la compagnie CNIM. L'objectif était de calculer la production annuelle d'électricité d'une centrale, en prenant en compte les conditions climatiques ainsi que du stockage d'énergie.

Dans un premier temps, un accumulateur de vapeur a été modélisé, dans le but d'estimer les variations de pression lors de la charge, du stockage et de la décharge de l'accumulateur. Ces données ont ensuite été intégrées à la modélisation du cycle thermodynamique de la centrale, permettant d'estimer la production électrique, en connaissant la puissance thermique disponible dans le champ solaire.

L'influence de la pente sur le terrain de la centrale a ensuite été estimée, en calculant l'azimut et la hauteur équivalents dans un nouveau repère, après changement de coordonnées sphériques. Pour une pente moyenne de  $4.21^\circ$ , le gain thermique annuel est de 14.4% alors que la production électrique augmente de 12.59%. L'influence du givre sur les miroirs a aussi été estimée, en prenant en compte un modèle simple de l'énergie nécessaire pour faire fondre une couche de glace d'épaisseur constante. Les pertes dues au givre varient entre 1.27 et 2.84% de la production annuelle d'électricité, en fonction de l'épaisseur de givre considérée. Les pertes dues aux heures d'effacement imposées par RTE lors de la fonte des neiges ont aussi été évaluées. La production d'électricité pourrait baisser de 8.02 à 11.57% pour cette raison.

Enfin, une optimisation de la conception du champ solaire a été réalisée, en prenant en compte des données de prix estimées par CNIM. Le champ solaire optimal serait constitué de 31 lignes et aurait 5 accumulateurs de vapeur, ce qui correspondrait à un temps de retour sur investissement de 9.887 ans.

**Mots-clés:** centrale solaire thermique, centrale solaire thermodynamique, technologie de Fresnel, génération directe de vapeur, accumulateur de vapeur, turbine à vapeur.

**Sökord:** solenergi, termisk solkraft, termiskt solkraftverk, ångturbin.

I hereby declare that I did this work independently, using only the listed sources and aids.

La Seyne-sur-Mer, December 2012

## Acknowledgement

I would like to express my gratitude to James SPELLING, my supervisor at KTH, for his support and assistance during the whole project, as well as for having shown interest for the thesis from the beginning.

I would like to thank my supervisor at CNIM Christophe LEHAUT for his patience, his useful critiques and teachings, as well as for the trust he placed in my work.

Special thank should be given to Florent CASSAR for his guidance, and his helpful suggestions throughout the whole time I spent at CNIM.

My grateful thanks are also extended to Roger PUJOL and Anne-Marie FOURNIER for welcoming me in the Solar Division.

I finally wish to thank the whole solar team: Cyril CRUCY, Sylvain DENIAU, Thomas FELEDZIAK, Cindy LIOTARD and Mathieu MARTIN for their welcome and cheerfulness.

## Table of Content

ABSTRACT .....	3
ACKNOWLEDGEMENT .....	5
LIST OF FIGURES .....	8
LIST OF TABLES .....	10
NOMENCLATURE.....	11
ABBREVIATIONS .....	11
INDICES .....	11
SYMBOLS.....	11
I- INTRODUCTION .....	13
II- BACKGROUND.....	15
1- ENERGY FROM THE SUN.....	15
a- Global Solar Resource.....	15
b- Energy balance on a receiver.....	19
c- Optical Losses.....	21
2- CONCENTRATION TECHNOLOGIES.....	23
a- Why concentrate?.....	23
b- Parabolic Trough .....	24
c- Linear Fresnel collector .....	26
d- Solar Tower .....	27
e- Dish Stirling.....	30
3- POWER PRODUCTION.....	31
a- Heat transfer fluids.....	31
b- Rankine cycle.....	32
c- Organic Rankine cycle .....	34
d- Solutions to increase the efficiency of a solar power plant.....	35
4- ENERGY STORAGE IN CSP .....	36
a- Why an energy storage?.....	36
b- Steam accumulator.....	37
c- Molten-salts energy storage .....	38
d- Thermocline storage system .....	39
III- CASE STUDY .....	41
1- PRESENTATION OF CNIM- SOLAR DIVISION.....	41
a- CNIM Solar Division.....	41
b- CNIM technology .....	41
c- The projects.....	43
2- OBJECTIVES .....	43
IV- STEAM ACCUMULATOR MODELING .....	45
1- METHOD .....	45
a- Mass balance.....	45
b- Energy balance.....	46
c- Energy losses.....	47
d- Volume balance.....	48
e- Discretisation .....	48
2- RESULTS .....	49

3- DISCUSSION .....	54
4- CONCLUSION .....	55
<b>V- PERFORMANCES CALCULATIONS .....</b>	<b>56</b>
1- METHOD .....	56
a- Piping and Instrumentation Diagram.....	56
b- Solar field .....	57
c- Expansion tank.....	57
d- Turbine.....	58
e- Air condenser .....	59
f- Condensate tank.....	61
g- Deaerator.....	62
h- Pre-heaters.....	62
i- Drums.....	62
j- Storage (charging / discharging).....	63
k- Pumps.....	64
l- Thermal losses.....	64
m- Pressure losses .....	69
n- Pre-heating.....	69
2- RESULTS .....	70
3- DISCUSSION .....	71
<b>VI- RESULTS IMPROVEMENT.....</b>	<b>72</b>
1- INFLUENCE OF THE LOCATION SLOPE .....	72
Results.....	74
2- MODIFICATION OF TURBINE OPERATION CONDITIONS.....	75
3- INFLUENCE OF THE WEATHER CONDITIONS.....	75
Results.....	77
4- LOAD MANAGEMENT .....	77
Results.....	78
5- RESULTS .....	78
6- DISCUSSION .....	82
<b>VII - ECONOMIC OPTIMISATION .....</b>	<b>86</b>
1- METHOD .....	86
2- RESULTS .....	88
3- DISCUSSION .....	89
<b>CONCLUSION .....</b>	<b>90</b>
<b>REFERENCES .....</b>	<b>91</b>

## List of figures

- Figure II.1 Distance between the Sun and the Earth and relation between their diameters.
- Figure II.2 Extraterrestrial radiation spectrum and 5800K black body spectrum
- Figure II.3 Modification of the incoming solar radiation
- Figure II.4 Solar radiation spectrum at sea level compared to extraterrestrial radiation spectrum.
- Figure II.5 Definition of the zenith angle  $\theta_z$
- Figure II.6 Direct Normal Irradiation (DNI) in the world, in kWh/m<sup>2</sup> per year.
- Figure II.7 Direct Normal Irradiation in Southern Europe and North Africa in kWh/m<sup>2</sup> per year.
- Figure II.8 Consequence of an incoming radiation on a body
- Figure II.9 Definition of the different parameters used in the equations
- Figure II.10 Illustration of the cosine effect
- Figure II.11 Illustration of the shadowing effect (left) and the blocking effect (right)
- Figure II.12 Illustration of the tube-end losses
- Figure II.13 Definition of the geometric concentration ratio
- Figure II.14 Parabolic trough technology principle (left) and SEGS parabolic trough power plant in California (right)
- Figure II.15 Layout of a SEGS plant
- Figure II.16 Layout of an "Andasol" type of plant.
- Figure II.17 Layout of a linear Fresnel collector
- Figure II.18 Kimberlina liner Fresnel power plant (California)
- Figure II.19 Solar tower power plant principle (left) and Abengoa PS10 power plant (Seville, Spain)
- Figure II.20 Heliostats field for medium latitudes (left) and low latitudes (right)
- Figure II.21 THEMIS thermal solar power plant, in Targassonne (France)
- Figure II.22 Dish Stirling system principle
- Figure II.23 Parabolic dish system of Infinia
- Figure II.24 Typical two-phases flow pattern map for horizontal pipes.
- Figure II.25 Simplified layout of a solar power plant with direct steam generation and Rankine cycle
- Figure II.26 T-s diagram of a simplified Rankine cycle.
- Figure II.27 Layout of a typical steam cycle with two pre-heaters and one feed-water tank.
- Figure II.28 Simplified layout of a power plant with water as heat transfer fluid and an organic fluid as working fluid.
- Figure II.29 T-s diagram of an Organic Rankine Cycle
- Figure II.30 Layout of an Integrated Solar Combined Cycle System
- Figure II.31 Advantages of thermal energy storage in solar power plant operation
- Figure II.32 Steam accumulator layout
- Figure II.33 ANDASOL solar power plant's layout
- Figure II.34 GEMASOLAR power plant's layout
- Figure II.35 Thermocline tank layout
- Figure II.36 Operation of a thermocline energy storage system
- Figure III.1 Scheme of a module of CNIM linear Fresnel concentrator viewed from above.
- Figure III.2 Cut of the receiver
- Figure III.3 Linear Fresnel direct steam generation prototype in La Seyne-sur-Mer (France)
- Figure IV.1 Steam accumulator layout
- Figure IV.2 Layout of a tank with a layer of insulator
- Figure IV.3 Evolution of the pressure, the inlet and outlet steam mass-flows during the simulation
- Figure IV.4 Evolution of the pressure with the time during the low-pressure storage process
- Figure IV.5 Evolution of the pressure with the time during the high-pressure storage process

- Figure IV.6 Evolution of the pressure with the mass of steam charged inside the accumulator  
 Figure IV.7 Evolution of the pressure with the mass of steam discharged from the accumulator  
 Figure IV.8 Evolution of the pressure with the sum of mass-flow of steam charged in the accumulator  
 Figure IV.9 Evolution of the pressure with the sum of mass-flow of steam discharged from the accumulator  
 Figure IV.10 Results obtained for the charging process in [Stevanovic et al. 2012]
- Figure V.1 Piping and Instrumentation Diagram of the plant (Llo project)  
 Figure V.2 Calculation of the design ambient temperature  
 Figure V.3 Modelling of a pipe  
 Figure V.4 Representation of a tank  
 Figure V.5 Casing of the receiver tube  
 Figure V.6 Modelling of the receiver tube and casing, and its electrical equivalent  
 Figure V.7 Monthly electrical production with and without storage.
- Figure VI.1 Definition of the angles used in the thermal power calculation program  
 Figure VI.2 Change of spherical coordinates system  
 Figure VI.3 Thermal-power gain with location slope at solar noon  
 Figure VI.4 Monthly electrical energy production with and without storage.  
 Figure VI.5 Utilisation of thermal power on a summer day.  
 Figure VI.6 Electrical power production with and without storage on a summer day  
 Figure VI.7 Utilisation of thermal power on a winter day  
 Figure VI.8 Electrical power production with and without storage on a winter day

## List of tables

Table IV.1	Initial conditions for optimal initial water volume calculation
Table IV.2	Results of simulations for initial water volume calculation
Table V.1	Thermodyn 70 bars and 9 MW turbine data sheet
Table V.2	Estimated partial loads for the turbine
Table V.3	Coefficients for Knudsen & Katz equation
Table V.4	Monthly electrical energy production with and without storage (dimensionless results, compared to $P_{BP}$ )
Table VI.1	Repartition of hours during which the production must be cut-off
Table VI.2	Electricity production losses with the load management
Table VI.3	Dimensionless results of the simulations for different cases.
Table VI.4	Dimensionless monthly electrical energy production with and without storage
Table VI.5	Results summary

# Nomenclature

## Abbreviations

CPC	Compound Parabolic Collector
CSP	Concentrated Solar Power
DNI	Direct Normal Irradiation (kWh/m <sup>2</sup> )
ISCCS	Integrated Solar Combined Cycle System

## Indices

1	Liquid
2	Steam
c	Condensation
e	Evaporation

## Symbols

### Background Part

$A_a$	Aperture area	$\text{m}^2$
$A_r$	Receiver area	$\text{m}^2$
$CR_g$	Geometric concentration ratio	
$h_r$	Radiation heat transfer coefficient	$\text{W}/\text{m}^2 \cdot ^\circ\text{C}$
$h_w$	Convection heat transfer coefficient	$\text{W}/\text{m}^2 \cdot ^\circ\text{C}$
$I(r)$	Intensity received at a distance $r$ from the Sun	$\text{W}/\text{m}^2$
$I_a$	Insolation	$\text{W}/\text{m}^2$
$I_b$	Beam radiation	$\text{W}/\text{m}^2$
$I_c$	Radiation incoming on the surface of the collector	$\text{W}/\text{m}^2$
$I_{d,h}$	Diffuse radiation on a horizontal surface	$\text{W}/\text{m}^2$
$I_{sc}$	Solar constant	$\text{W}/\text{m}^2$
$I_{\text{Sun}}$	Power at the sun surface	$\text{W}$
$I_{t,h}$	Global radiation on a horizontal surface	$\text{W}/\text{m}^2$
$L$	Characteristic length of the receiver	$\text{m}$
$Q_{\text{losses}}$	Power lost because of convection or radiation	$\text{W}$
$Q_{\text{sun}}$	Power received from the Sun through the collector	$\text{W}$
$Q_{\text{useful}}$	Useful power in the receiver	$\text{W}$
$r$	Distance from the sun	$\text{m}$
$R$	Receiver-intercept factor	
$S$	Receiver-shading factor	
$T$	Mean radiation temperature	$^\circ\text{C}$
$T_a$	Ambient temperature	$^\circ\text{C}$
$T_r$	Average temperature of the receiver	$^\circ\text{C}$
$U_{\text{cond}}$	Conduction heat transfer coefficient	$\text{W}/\text{m}^2 \cdot ^\circ\text{C}$

$U_1$	Overall heat transfer coefficient	W/m <sup>2</sup> .°C
$V$	Wind speed	m/s
$\alpha$	Absorbance	
$\alpha_r$	Absorbance of the receiver	
$\epsilon$	Emissivity	
$\epsilon_{\cos}$	Cosine effectiveness	
$\theta$	Angle of incidence of the beam radiation	
$\theta_z$	Solar zenith angle	
$\rho$	Reflectance	
$\rho_{CPC}$	Reflectance of the CPC	
$\rho_m$	Mirrors reflectance	
$\sigma$	Stefan's constant	5,67.10 <sup>-8</sup> J/s.m <sup>2</sup> .K <sup>4</sup>
$\tau$	Transmittance	

### Performance calculation and results improvement parts

$C_p$	Air heat capacity	kJ/kg.K
$\epsilon_{LLO}$	Location slope in Llo	°
$h$	Enthalpy	kJ/kg
$H$	Enthalpy	kJ
$h'$	Saturated liquid enthalpy	kJ/kg
$h''$	Saturated steam enthalpy	kJ/kg
$M$	Mass of steam/liquid	kg
$m$	Mass flow of steam/liquid	kg/s
$Nu$	Nusselt number	
$P$	Pressure	bar
$P_{BP}$	Electrical energy production in business plan	GWhe
$Pr$	Prandt number	
$P_{th}$	Thermal power	kWth
$Q$	Heat received by a system	kJ
$Re$	Reynolds number	
$R_{th}$	Thermal resistance	K/W
$T$	Temperature	°C
$t$	Time	s
$U$	Internal energy	kJ
$V$	Volume	m <sup>3</sup>
$W'$	Work applied on a system	kJ
$x$	Steam quality	
$\Delta t$	Time step	s
$\eta_{is}$	Isentropic efficiency	
$\vartheta_m$	Logarithmic mean temperature difference	°C
$\lambda$	Thermal conductivity	W/mK
$\mu$	Dynamic viscosity	N/sm <sup>2</sup>
$\tau$	Condensation/evaporation relaxation time	s

## I- Introduction

Two phenomena nowadays jeopardize people's comfort and way of living: global warming and the fossil fuel resources depletion. Those two events are linked together and trigger, as the main consequence for humans, a need to change their way of consuming, most of all energy, without changing their comfort. More and more countries and organisations turn thus themselves to renewable and greener energies.

Almost all the renewable energies that are known today (except for geothermal energy) come from the Sun. Indeed, when reaching the Earth, the sunrays bring four different forms of energy. Latent energy is used to vaporise the water from the sea, which is then transformed into rain and is used in hydropower. Sensible heat is used to heat up fluids, in thermal solar energy as well as in ocean thermal energy. The uneven heating of the Earth creates winds whose kinetic energy is used to run wind turbines and oscillating water columns using waves energy. Finally, the energy of photons is used in photovoltaic cells, but also by the plants during the photosynthesis, thus creating biomass.

Of all those renewable energies, hydropower is the most advanced one, developed to full power in most of the developed countries, and still developing in developing countries. Wind power and photovoltaic are developing quickly, even though they suffer from their unpredictability and variability, which make them difficult to link to the electrical network. Biomass is used in power plants, in complement or not to fossil fuel, but can also be turned directly into fuel for car engines. Ocean thermal energy and waves energy are still at an early stage in the development process as there is a need to find solutions to withstand complex situations as sea storms and icing.

Among all of these renewable energies, concentrated solar power (CSP) is a fast developing technology with great potential. The amount of solar energy striking the Earth every day (600 TW) is about ten times larger than the daily global electricity consumption (60 TW) [Krothapalli 2011]. A mirror of about 20 square metres in the desert would be enough to provide the need of one person, day and night, with no CO<sub>2</sub> emission [<http://www.desertec.org>]. The potential is thus huge. And the technology to convert the heat into electricity is a proven and well-known one that has been used for years in thermal power plants: Rankine cycles with a steam turbine.

Another great advantage of CSP is the possibility of thermal energy storage that is offered by the technology, with steam accumulators or molten salts tanks for example. The storage of thermal energy is much more efficient and easily implemented than electricity storage in batteries. This storage possibility is thus impossible on the developing technologies that are wind power and photovoltaic.

With energy storage, producing a constant power with a renewable energy becomes possible. Indeed, buffer storage allows smoothing the production, even when clouds pass above the thermal solar plant. Storage allows also producing power even when there is no sun anymore. It would then be possible, with adapted storage technologies, to produce at constant rate, even during the night, to meet the demand. This makes thus concentrated solar power much easier to link to the electrical network, as it does not bring instabilities, contrary to the intermittent and variable technologies that are wind power and photovoltaic.

Four different concentrator technologies are currently developed to convert the radiation into useful energy for a steam turbine. Parabolic trough and linear Fresnel technologies use mirrors approximating a parabolic reflexion onto a tube placed in the focal point of the mirrors. Solar tower power plants use a field of heliostats (or planar mirrors) to concentrate the sunrays onto a receiver atop a tower. Finally, parabolic dish technology is the only modular technology, using a parabolic dish that reflects the light on a receiver placed in the middle of the reflector.

After estimating the amount of energy that can be received on the solar receiver of a CSP plant, all the technologies of collecting and concentrating the energy will be presented, as well as the technologies to convert the energy into electricity and to store thermal energy. Then, the company into which this thesis

is led will be presented, as well as the projects onto which the thesis is based. The steam accumulator model will then be described, as well as the results that were obtained. The method to calculate the annual performances of the solar plant will be also detailed, as well as the calculations made to estimate the influence of the location slope, the frost on the mirrors and the shutdowns due to load management. Finally, a quick economic optimisation will be led to determine the best solar field design.

## II- Background

This section aims at explaining all the processes that take place between the fusion of two atoms of hydrogen inside the core of the Sun and the production of electricity at the output of thermal solar power plants. At first, an estimation of the energy that can be used in a solar plant is given; taking into account the energy that is received from the Sun as well as the optical and thermodynamic losses. Then the different types of solar power plants are described, with all their different components. The third part of this section details the different cycles that can be used to extract the energy from the Sun and convert it into electricity. Finally, the question of energy storage is approached, with a description of several types of thermal energy storage. This whole section is inspired of [Spelling 2011], [Kalogirou 2009], [Soler 2010], and [Krothapalli 2011].

### 1- Energy from the Sun

#### a- Global Solar Resource

When two atoms of hydrogen fuse into one atom of helium in the Sun core, energy is produced, which is then brought to the surface thanks to radiation and convection. This ensures a production rate of  $3.85 \times 10^{26} \text{ W}$  and a temperature of around 6000K at the surface.

This energy is then radiated through space with electro-magnetic waves travelling at the speed of light. The intensity of the solar radiation decreases with the inverse-square law, given by the following formula:

$$I(r) = \frac{I_{\text{Sun}}}{4\pi r^2} \quad (\text{II.1})$$

Where  $I(r)$  is the intensity received at a distance  $r$  from the Sun, in  $\text{W/m}^2$  and  $I_{\text{Sun}}$  is the power at the sun surface in  $\text{W}$ .

The distance between the Sun and the Earth is  $1.5 \times 10^{11}$  metres, as shown on figure II.1.

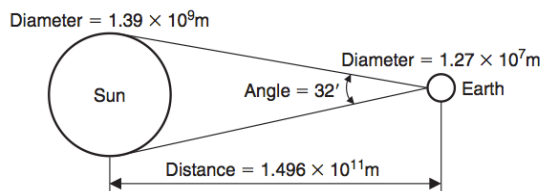
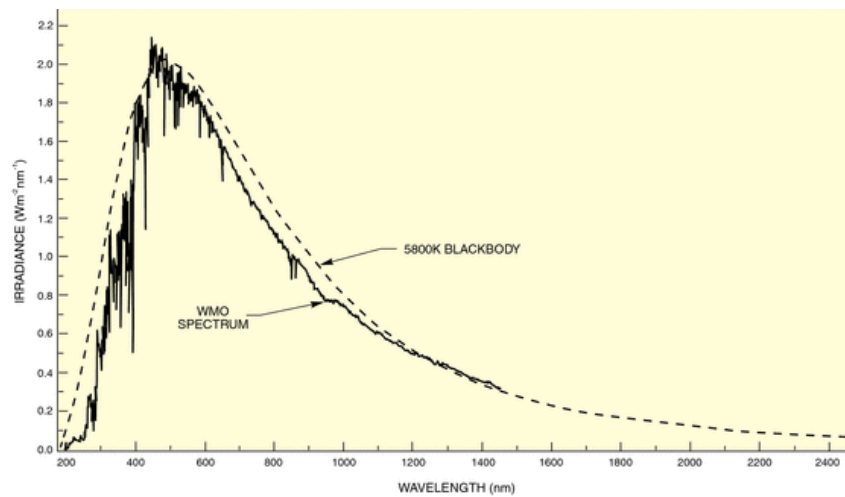


Figure II.1: Distance between the Sun and the Earth and relation between their diameters [Kalogirou 2009]

At this distance, the global radiation received by the Earth from the Sun is equal to the solar constant,  $I_{sc}=1367 \text{ W/m}^2$ . The solar constant is the mean power received from the Sun on a unit area surface perpendicular to the sunrays, outside of the atmosphere. This radiation varies of about 3.4% throughout the year, because of the variation of the distance between the Earth and the Sun.

Outside the atmosphere, the solar radiation can be approximated by the distribution of the radiation of a black body at temperature 5800K, as shown in figure II.2. It gives the irradiance (in  $\text{W/m}^2$ ) as a function of the wavelength.



*Figure II.2: Extraterrestrial radiation spectrum and 5800K black body spectrum  
[<http://www.newport.com/Introduction-to-Solar-Radiation/411919/1033/content.aspx>]*

However, the extraterrestrial radiation is not the radiation that is received at the surface of the Earth. Only 51% of the incident radiation reach the surface and can be absorbed. The rest being reflected by the surface of the Earth, the clouds or the atmosphere toward the outer space, or being scattered by the clouds and the atmosphere. Figure II.3 shows what happens to the incoming solar radiation.

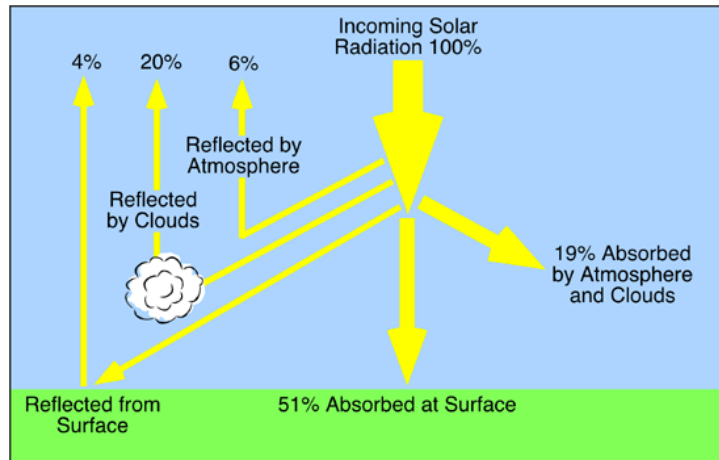


*Figure II.3: Attenuation of the incoming solar radiation [[www.physicalgeography.net](http://www.physicalgeography.net)]*

This attenuation of the incident radiation can be seen on the following figure, which shows the distribution of the solar radiation that reaches the surface of the Earth, compared to the radiation outside the atmosphere.

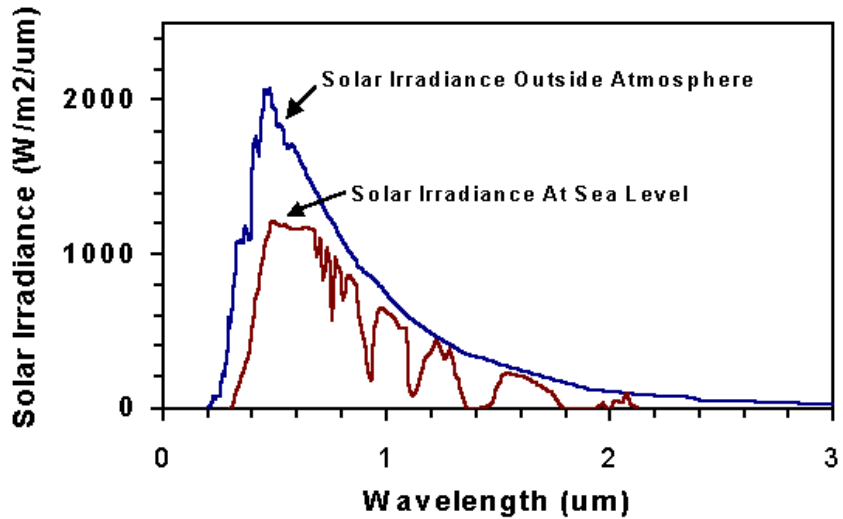


*Figure II.4: Solar radiation spectrum at sea level compared to extraterrestrial radiation spectrum  
[<http://www.crisp.nus.edu.sg/~research/tutorial/optical.htm>]*

Several definitions can then be given.

The **beam radiation** is the radiation that is incident from the direction of the Sun. It means that it has not been scattered. The beam radiation is the one that is useful in concentrated solar power (CSP). Its intensity depends a lot on the orientation of the surface on which it is collected. This is why the collectors in CSP technology have to be orientated during the day, to maximise the beam radiation that is received.

The orientation of the beam radiation can be calculated for every place in the world (every latitude and longitude), every time of the year, thanks to geometrical relations that will not be described further in this thesis. The intensity of the beam radiation can be measured with a normal incidence pyrheliometer.

The **diffuse radiation** is the radiation that is received from the Sun after being scattered by the atmosphere and the clouds. The diffuse radiation can be up to 100% of incoming radiation on cloudy days, and remains higher than 10% even on very bright days. The diffuse radiation can be measured by a shadow-band pyrheliometer that blocks the direct radiation.

The **global radiation** is the sum of the beam and the diffuse radiations. The global radiation can be measured by a pyrheliometer.

Those different radiations are linked together by the following equation:

$$I_{t,h} = I_b \cos \theta_z + I_{d,h} \quad (\text{II.2})$$

Where  $I_{t,h}$  is the global radiation on a horizontal surface,  $I_{d,h}$  is the diffuse radiation on a horizontal surface,  $I_b$  is the beam radiation and  $\theta_z$  is the solar zenith angle represented in figure II.5.

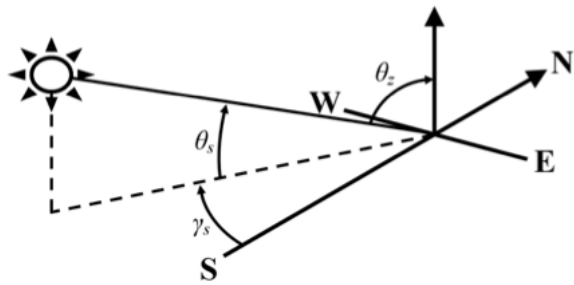


Figure II.5: Definition of the zenith angle  $\theta_z$  [Spelling 2011]

The **irradiance** is given in  $\text{W/m}^2$  and gives the rate at which radiant energy is incident on a unit area surface. It is also the intensity of the solar radiation.

The **irradiation** (given in  $\text{J/m}^2$ ) gives the amount of energy that is received per unit area.

The **insolation** is the solar energy irradiation.

The intensity of solar radiation is not the same everywhere on the planet. It depends on the latitude of the place. The higher the latitude (in northern hemisphere), the lower the intensity of solar radiation. It depends also on the humidity of the place. When a place is humid, solar radiation is more scattered by clouds and thus its intensity is lower. Figure II.6 gives the Direct Normal Irradiation or DNI (in  $\text{kWh/m}^2$  per year) in the world.

One can see that the places in the world that are the most suitable for concentrated solar power are situated in the Middle East, North Africa, South Africa, Australia and the United States.

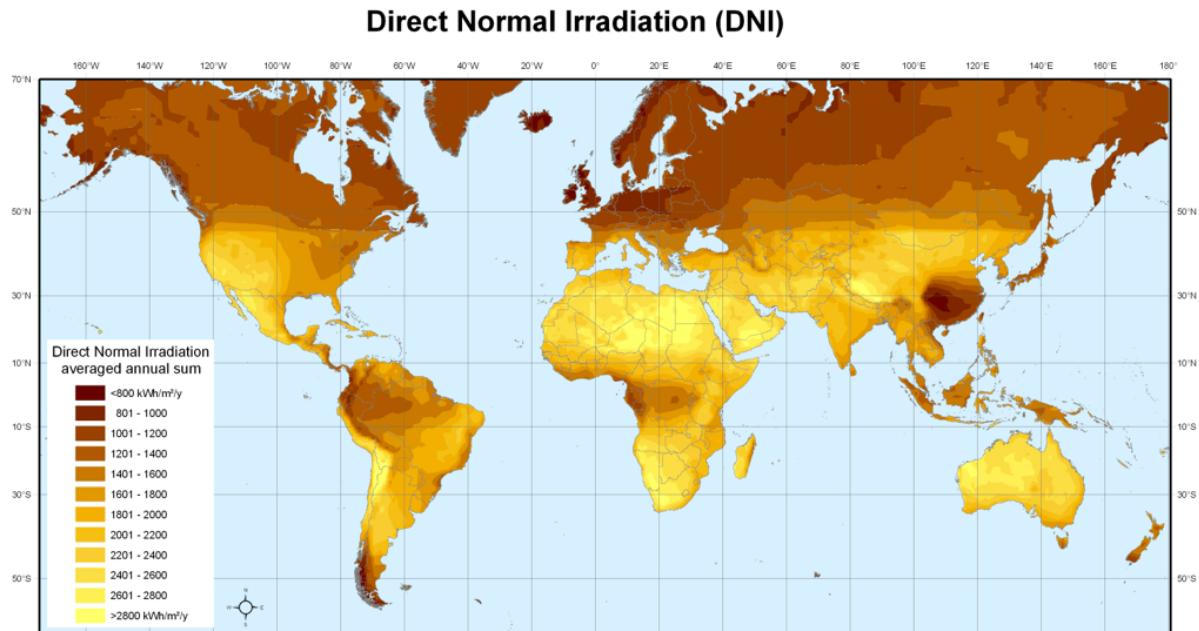


Figure II.6: Direct Normal Irradiation (DNI) in the world, in  $\text{kWh/m}^2$  per year [Trieb 2009]

As the present thesis focuses on projects that are led in Morocco and in France, a more precise map of this area is given in figure II.7, showing that Morocco has a good potential for CSP plants.

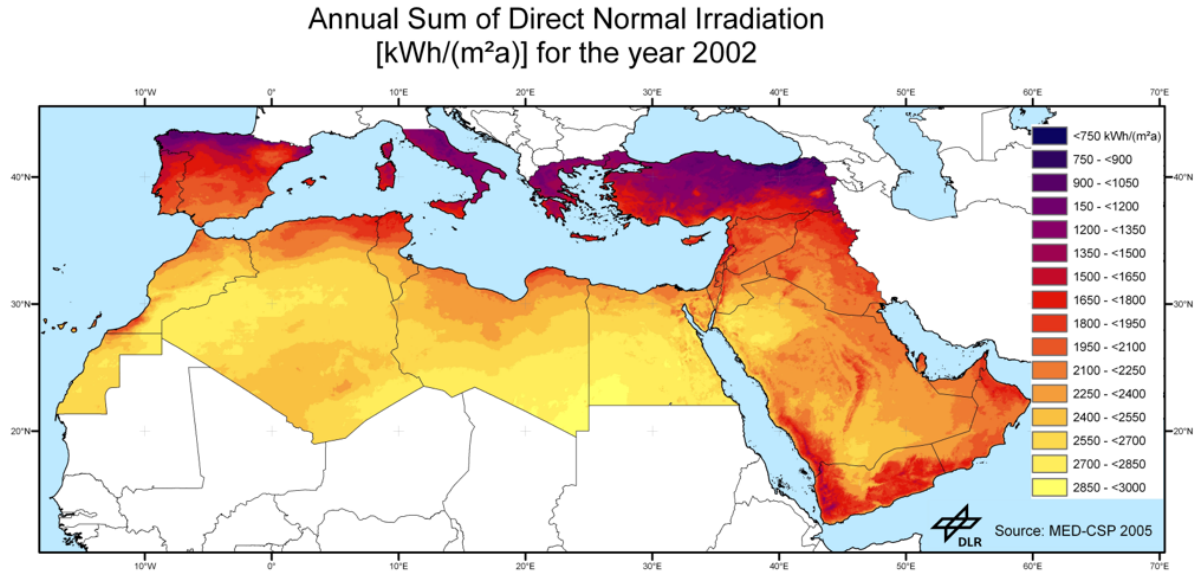


Figure II.7: Direct Normal Irradiation in Southern Europe and North Africa in kWh/m<sup>2</sup> per year [Trieb 2009]

Those maps, but also measures with pyrheliometers or geometrical calculations give the insolation on the locations where CSP plants can be installed. However, this energy from the Sun is not the useful energy for the plant. Some losses have to be taken into account and are described in the two following parts.

### b- Energy balance on a receiver

Knowing the beam radiation at a specific location, one is able to calculate the energy that can be extracted from the sun in a receiver. This useful energy is the difference between the energy received from the collector and the energy lost because of radiation and convection, as given by the following equation:

$$\dot{Q}_{useful} = \dot{Q}_{Sun} - \dot{Q}_{losses} \quad (\text{II.3})$$

Where the first term is the useful power in the receiver, the second term is the power received from the Sun via the collector and the third term represents the losses.

To estimate the amount of energy that is received from the sun on the receiver, some definitions need to be given.

An incoming radiation on a body can be either reflected, absorbed or transmitted by the body, as represented on figure II.8.

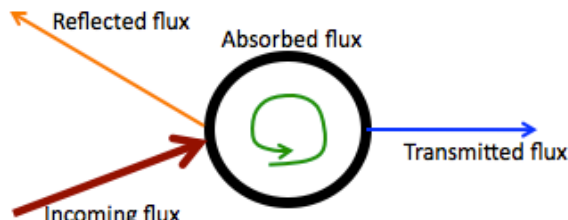


Figure II.8: Consequence of an incoming radiation on a body

Four dimensionless numbers then define a body that receives a radiation: the absorbance, the transmittance, the reflectance and the emissivity.

The **absorbance**, noted  $\alpha$ , is the ratio of the flux that is absorbed by the body and the incoming flux on the body.

The **transmittance**, noted  $\tau$ , is the ratio of the flux that is transmitted by the body to the incoming flux on the body.

The **reflectance**, noted  $\rho$ , is the ratio of the flux that is reflected by the body to the incoming flux on the body.

The **emissivity**, noted  $\epsilon$ , is the ratio of the flux that is emitted by the body by radiation to the flux that would be radiated by the body if it were a black body at the same temperature.

The following equation links the absorbance, the transmittance and the reflectance:

$$\alpha + \rho + \tau = 1$$

Now, the incoming energy on the receiver tube is the energy that is reflected by the mirrors, transmitted by the glass pane covering the receiver, and finally absorbed by the receiver.

The power reflected by the mirrors is  $I_{reflected} = I_{incident} \rho_m A_a = I_a \rho_m A_a$  with  $\rho_m$  being the reflectance of the mirrors,  $A_a$  the aperture area and  $I_a$  the insolation ( $\text{W/m}^2$ ).

The flux transmitted by the glass pane is  $I_{transmitted} = I_{incident} \tau = I_a \rho_m A_a \tau$  with  $\tau$  being the transmittance of the glass pane.

The flux absorbed by the receiver is  $I_{absorbed} = I_{incident} \alpha_r = I_a \rho_m A_a \tau \alpha_r$  with  $\alpha_r$  being the absorbance of the receiver.

Thus, the power received from the sun in the receiver is  $\dot{Q}_{received} = I_a \rho_m A_a \tau \alpha_r$  (in  $\text{W}$ ).

However, one should also take into account the effects linked to the whole solar field, for example, shadowing and blocking effects between the mirrors, but also the fact that the receiver does not intercept the whole reflected beam. Those effects are further described in the next section but can be taken into account with two dimensionless numbers:

The receiver-shading factor  $S$  is the fraction of the collector aperture that is not shadowed and not blocked.

The receiver-intercept factor  $R$  is the fraction of the reflected beam that is intercepted by the receiver.

This gives the following equation in the end:  $\dot{Q}_{useful} = I_a \rho_m A_a \tau \alpha_r R S \quad (\text{II.4})$

As the receiver does not intercept all of the reflected radiation, some power plants manufacturers use a second reflector, called CPC (Compound Parabolic Collector). Its reflectance  $\rho_{CPC}$  could also be taken into account.

All the parameters of the equations are defined in figure II.9.

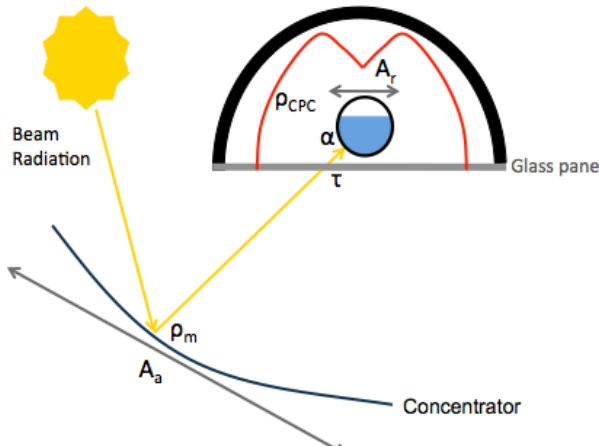


*Figure II.9: Definition of the different parameters used in the equations*

The thermal losses need also to be expressed. They are due to radiation, convection and conduction in and around the receiver. The conduction can usually be neglected in this case. The convection is mainly due to the wind, and this is why the wind speed data is really important for the calculations of the power plant production. At high temperature however, the phenomenon that has the greatest influence is radiation.

$$\dot{Q}_{losses} = A_r U_l (T_r - T_a) \quad (\text{II.5})$$

Where  $A_r$  is the receiver area,  $U_l$  is the overall heat transfer coefficient ( $\text{W}/\text{m}^2 \cdot ^\circ\text{C}$ ),  $T_r$  is the average temperature of the receiver and  $T_a$  is the ambient temperature.

The overall heat transfer coefficient is given by the sum of all the transfer coefficients for radiation  $h_r$ , convection due to the wind  $h_w$  and conduction  $U_{cond}$ .

$$U_l = h_w + h_r + U_{cond} \quad (\text{II.6})$$

The convection heat transfer coefficient can be given by:  $h_w = \frac{8.6V^{0.6}}{L^{0.4}}$ , where  $V$  is the wind speed ( $\text{m}/\text{s}$ ) and  $L$  is the characteristic length of the receiver ( $\text{m}$ ).

And the radiation heat transfer coefficient can be given by a first order approximation of the Stefan's law:  $h_r = 4\sigma\epsilon T^3$  where  $\epsilon$  is the emissivity of the receiver,  $\sigma$  is Stefan's constant equal to  $5,67 \cdot 10^{-8} \text{ J}/\text{s} \cdot \text{m}^2 \cdot \text{K}^4$  and  $T$  is the mean radiation temperature.

At high temperatures, the energy losses can be approximated by Stefan's law, as the convection and the conduction can be neglected, thus giving:  $\dot{Q}_{losses} = A_r \epsilon \sigma T_{surface}^4$ .

$$\text{Finally, the useful energy is given by: } \dot{Q}_{useful} = I_a \rho_m A_a \tau \alpha_r R S - A_r \epsilon \sigma T_{surface}^4 \quad (\text{II.7})$$

### c - Optical Losses

The following section describes some optical losses that one must take into account to estimate the amount of energy that is received by the receiver. Those losses are of different kind. Some are due to the geometry of the field, while others are due to the atmosphere and the environment.

One of the most important losses to be considered is the loss due to the **cosine effect**. It has a great influence, most of all for horizontal reflectors.

It can be explained as follow: the amount of energy that passes through the surface  $A_0$  is the same as the amount of energy that arrives on the surface  $A_c$  of the collector (see figure II.10). It gives:

$$I_b A_0 = I_c A_c = I_c \frac{A_0}{\cos \theta}$$

Where  $I_b$  is the beam radiation,  $I_c$  is the radiation incoming on the surface of the collector  $A_c$  and  $\theta$  is the angle of incidence of the beam radiation.  $A_c$  is defined on figure II.10.

Thus, the insolation on the surface of the collector is  $I_c = I_b \cos \theta$ .

The cosine effectiveness is defined as  $\varepsilon_{\cos} = \frac{I_c}{I_b} = \cos \theta$ . (II.8)

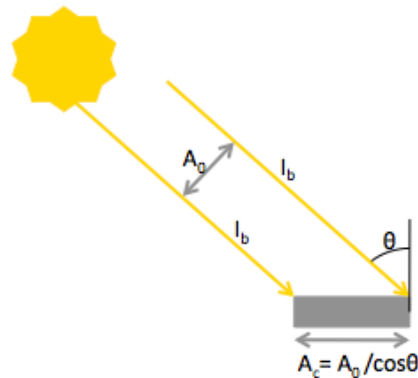


Figure II.10: Illustration of the cosine effect

**Shadowing** can also trigger losses; most of all on solar fields were collectors are placed close to one another (parabolic trough, linear Fresnel and solar tower plants). It is due to the shadow that is created by the collectors all around, thus preventing the direct beam to reach the collector, as illustrated in figure II.11 (left).

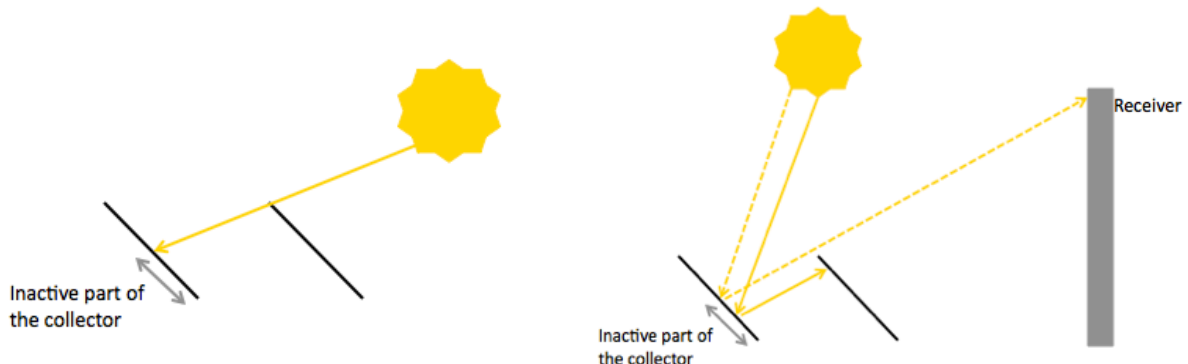


Figure II.11: Illustration of the shadowing effect (left) and the blocking effect (right)

**Blocking** is another cause of optical losses on solar fields, mainly where the collectors are close one another and far from the receiver, that is to say on solar tower power plants.

Blocking is also due to the geometrical design of the solar field and means that the light cannot be reflected to the receiver because other collectors block the rays, as illustrated in figure II.11 (right).

Once the light has been reflected, a part of it can be scattered by the atmosphere or by dust in the air. This is called **atmospheric attenuation** and has an influence on plants where the collectors are placed far from the receiver, most of all in tower power plants.

**Tube-End losses** are the last losses due to the geometry of the solar field. As the mirror field and the receiver tube are not infinite, parts of the tube are sometimes inactive, while a part of the light is reflected outside the tube, as shown on figure II.12.

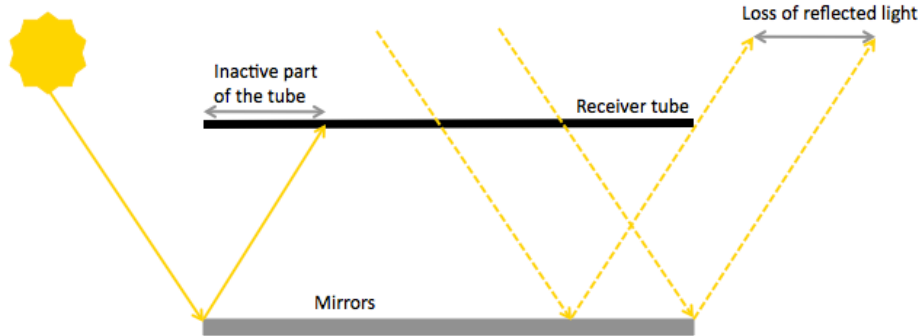


Figure II.12: Illustration of the tube-end losses

Finally, part of the light that is reflected can miss the receiver, as the spot of reflected light is wider than the receiver itself. This is called **spillage** and has an influence in plants where the receiver is far from the collectors, most of all solar tower plants but also linear Fresnel plants. In linear Fresnel plants, those losses can be reduced using a Compound Parabolic Collector that reflects the light missing the receiver, onto the receiver.

All those losses have to be taken into account when calculating the solar energy reaching the receiver. It is most of the time a complex calculation, depending on the geometry of the mirrors field. But it is of the utmost importance to have an accurate prevision of the plant production.

## 2- Concentration technologies

In this section, the different types of concentrated solar power (CSP) plants are described, with their advantages and drawbacks.

### a- Why concentrate?

Some solar energy collectors do not concentrate the energy that is received from the sun. They are called stationary collectors and are mainly used to heat water for domestic purposes.

One can define the geometric concentration ratio as the ratio of the receiver area to the aperture area, as shown in figure II.13.

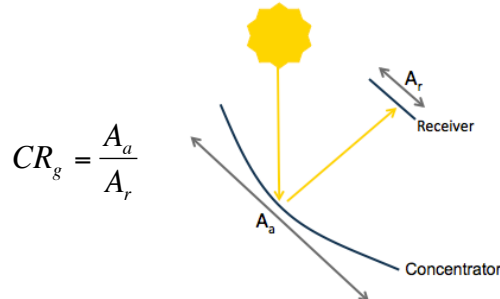


Figure II.13: Definition of the geometric concentration ratio

A non-concentrating collector has a concentration ratio equal to 1. This means that the area of concentration of the radiation is the same as the heat collection area. Most of the non-concentrating collectors are indeed flat, for example, flat plate collectors.

As they do not concentrate the radiation flux from the Sun, those collectors can reach only low temperatures, for example, up to about 120°C. This is perfect for domestic use but not good enough for power production.

Concentrating the radiation flux has thus several advantages. First, when the radiation is concentrated onto a receiver, the heat transfer fluid inside the receiver can reach higher temperatures (up to 2000°C) than with non-concentrating collectors. As a consequence, the thermodynamic efficiency of the cycle is a lot higher.

Then, as the area where the energy is received is smaller than with non-concentrating collectors, the heat losses due to convection, conduction and radiation are lower. The heat losses can be further reduced using vacuum installation inside the casing of the receiver, to decrease convection losses, and selective surface treatment on the receiver tube, to increase the amount of energy that is transmitted to the tube. This cannot be done on non-concentrating collectors as the heat collection area is larger, and thus the investment is not profitable.

Finally, the reflective surfaces (mirrors) are structurally simpler and thus cheaper than flat plate collectors.

However, the concentrating systems use mainly direct radiation and little diffuse radiation. In order to maximize the energy that is received by the collector, the concentrators need to track the sun all day long, the tracking system thus increasing the investment costs. Finally, cleaning is needed in order to maintain the reflectivity of the concentrator surface at its highest point.

Different technologies of solar concentrating collectors exist. All of them have advantages and drawbacks that are studied in this section.

Each collector is made of two distinct parts: a concentrator, which reflects the incident solar radiation onto a receiver, thus increasing the energy received; and a receiver in which flows a fluid that extracts the energy from the radiation.

The technologies of collectors can be divided into different types. Some are line focusing, which means that they focus the radiation on a tube with one-axis sun tracking. Those kinds of collectors are parabolic troughs or linear Fresnel collectors. They can reach medium temperatures, between 120°C and 450°C.

Others are point focusing, which means that they focus the sunrays on a point, with two-axis sun tracking. Those kinds of reflectors are for example solar tower power plants or parabolic dishes concentrators. They can reach high temperatures, up to 2000°C.

Then, some collectors are large scale (from 10MWe to several hundred MWe), while others are modular (<50kWe).

### b- Parabolic Trough

In the parabolic trough technology, the concentrator is a parabolic dish, which reflects the solar radiation onto a tube that is placed along the focal line of the collector, as can be seen on figure II.14. This technology belongs to the linear collectors category. The concentration ratio for parabolic trough collectors is between 30 and 100.

During the day, the parabolic dish turns around a horizontal axis, in order to track the Sun and thus receive the maximum radiation all day long. The reflectors lines can be oriented following a North-South axis, thus tracking the sun from East to West, or an East-West axis.



*Figure II.14: Parabolic trough technology principle (left) and SEGS parabolic trough plant in California (right)*  
[NREL]

The receiver tube is usually made of stainless steel covered with a special coating, with a high absorbance at short wavelengths (visible spectrum) and a low emissivity at long wavelengths (infrared), which means that the radiation received by the tube is mainly absorbed, a small part being re-emitted. A glass envelope with a high transmittance then covers the tube, in order to decrease the convection losses.

One advantage of parabolic trough technology is that the parabolic shape ensures a high optical efficiency. However, this shape is difficult to produce, which increases the production costs. The costs are further increased by the structure to maintain the mirrors. Indeed, as the area of mirror is quite large, it increases the wind loading. The structure needs to be stronger than, for example, with linear Fresnel collectors.

Another advantage of parabolic trough is that it is the most mature technology to reach medium temperatures. Indeed, about 90% of all the thermal solar plants in the world are built with a parabolic trough technology and a Rankine cycle scheme. The first plants were built in the 1980's and the experience that was gained since then has permitted to decrease the solar electricity prices to about 10 US\$/kWh. The experience shows also that it is a robust and reliable technology, thus making it easier to get some funding when needed.

An example of parabolic trough power plant is the group of 9 plants called SEGS, standing for Solar Electric Generation Systems, with a total installed capacity of 350 MW. Those plants were built in Mojave Desert in California in the 1980's and 1990's to meet midday peak electricity demand. The heat transfer fluid is a synthetic oil, which is used in a heat exchanger to heat (and reheat) water into steam, as described in figure II.15. A natural gas system is used as a back up, thus contributing to 25% of the plants output. This permits to reach a temperature of 390°C and pressure of 100 bar at the turbine inlet, while the water entering the solar field has a temperature of about 304°C. However, there is no possible storage in SEGS plants.

Another example of parabolic trough plant is the plant built by the Spanish company Andasol in 2009. It was built in order to meet the day load, as well as the evening peak. In this purpose, a storage technology was designed. In this type of plant, the heat transfer fluid is the same as the storage medium: molten salts of nitrate ( $\text{NaNO}_3$  and  $\text{KNO}_3$ ). The salts are stored in tanks, as explained in section II.4.c, and are then used in a heat exchanger to heat (and reheat) some water into steam to run the turbine. This permits to reach temperatures up to 390°C and pressure up to 100 bar at the turbine inlet. Figure II.16 represents the layout of an "Andasol" type of plant.

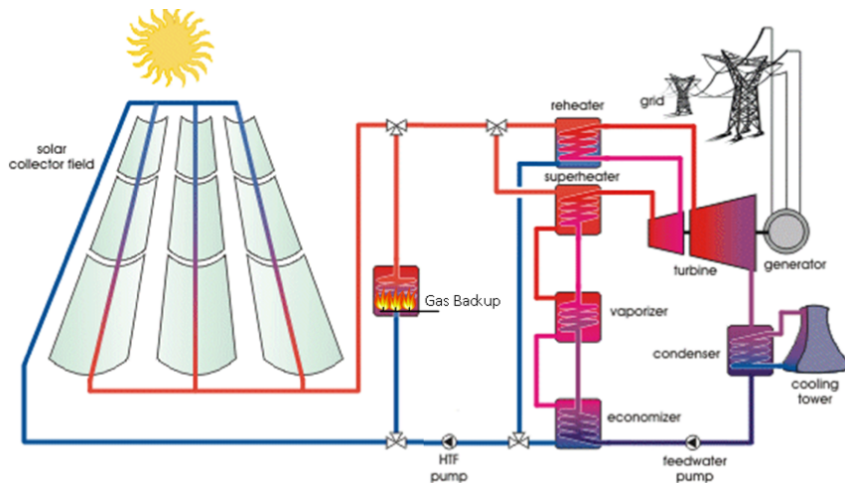


*Figure II.15: Layout of a SEGS plant [Spelling 2011]*

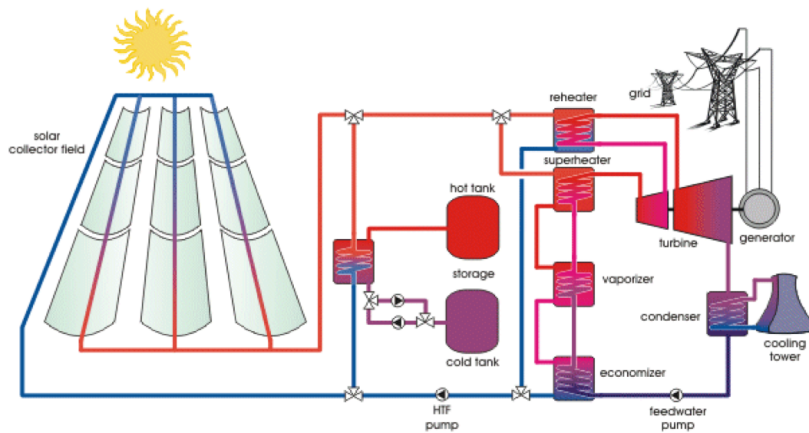


*Figure II.16: Layout of an “Andasol” type of plant [Spelling 2011]*

### c- Linear Fresnel collector

A linear Fresnel collector is made of several planar or slightly bended mirrors that can be orientated independently in order to track the sun and approximate a parabolic concentration on an absorber tube situated above the mirrors, on a tower (about 10 metres high). Figure II.17 represents a linear Fresnel collector.

The mirrors are smaller and simpler than those used in parabolic trough. They can thus be placed closer to the ground. As a consequence, the costs linked to the mirrors and to the structure are reduced compare to the previous technology. However, the mirrors in a Fresnel collector can only approximate a parabolic concentration, and the optical efficiency is thus lower.

As it is a line focusing technology, it needs only a one-axis sun tracking and can only reach medium temperatures (lower than 400°C). The geometric concentration ratio for a linear Fresnel collector is between 25 and 100.

The receiver tubes used in this technology are the same as for the parabolic trough technology.

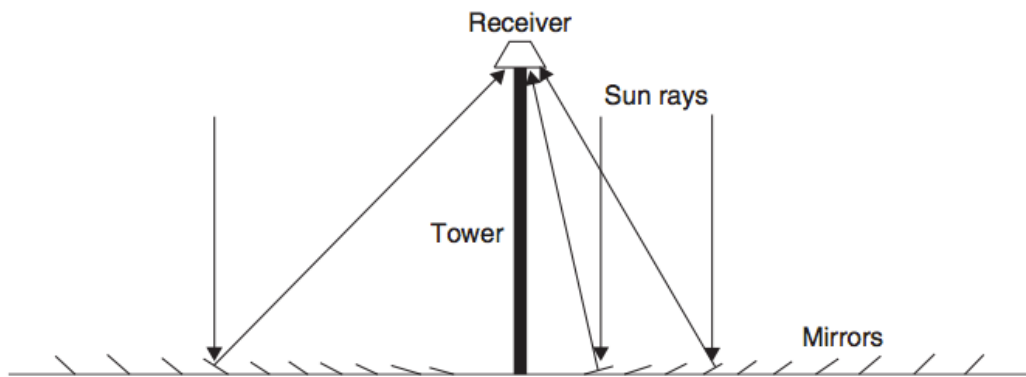


Figure II.17: Layout of a linear Fresnel collector [Kalogirou 2009]

This is not a mature technology, even though the investment costs are lower than for parabolic trough projects and the land requirement is lower than for any other technology.

This technology being the one on which is led this study, it will be further described in part III.1.b.

An example of a Linear Fresnel power plant is Kimberlina plant, built in Bakersfield (California) in 2008 by Ausra (now AREVA Solar). It produces 5MWe during peak hours and uses steam up to 400°C and 106 bars. Figure II.18 shows a line of reflector at Kimberlina power plant.

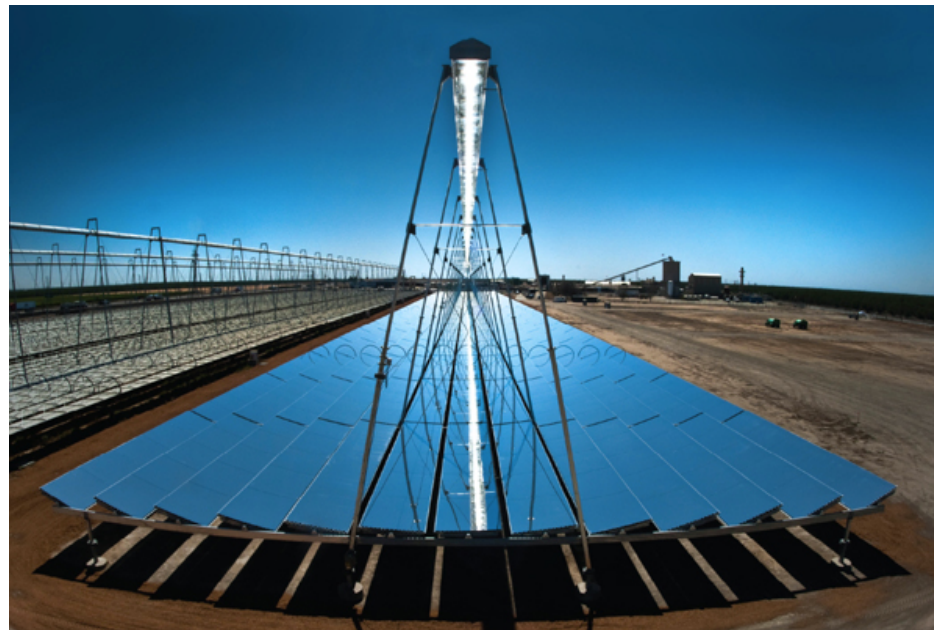


Figure II.18: Kimberlina liner Fresnel power plant (California) [Areva Solar]

#### d- Solar Tower

In the solar tower power plant technology, the solar field is made of several thousands planar mirrors called heliostats, individually tracking the sun with a two-axis system and concentrating the radiations on a receiver mounted atop a high tower (more than 100 metres high), as shown on figure II.19. Heat transfer fluids can be either molten salt or nitrates ( $\text{NaNO}_3$  and  $\text{KNO}_3$ ) or water that is turned into

steam. Other heat transfer fluids, such as air, sodium or helium are also currently tested. Then, power is produced usually with a Rankine cycle. Storage is possible with the molten salts.

The geometric concentration ratio for solar tower power plants is between 500 and 800. The sunlight is concentrated between 300 and 1500 times on the receiver, allowing to reach temperatures between 800 and 2000°C. Solar tower power plants can thus reach higher rated power than the others technologies.

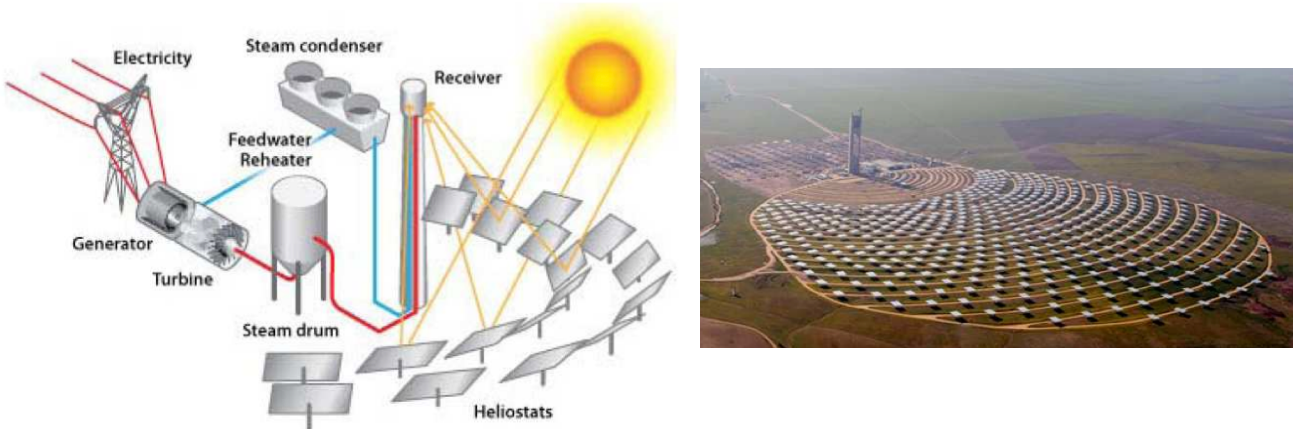


Figure II.19: Solar tower power plant principle (left) and Abengoa PS10 power plant (Seville, Spain) [Soler 2010] [[www.enerzine.com](http://www.enerzine.com)]

The heliostats field can be placed all around the tower, or only on the north side of the tower. The first case is better for low latitudes ( $<35^\circ$ ), while the second case is better for medium latitudes. In any case, the design of the field is different for each plant. Figure II.20 shows two types of heliostats fields that can be encountered.

When increasing the space between heliostats, the losses because of shadowing and blocking decrease, while the atmospheric attenuation increases. The design of a heliostats field must thus be a compromise between all those elements.

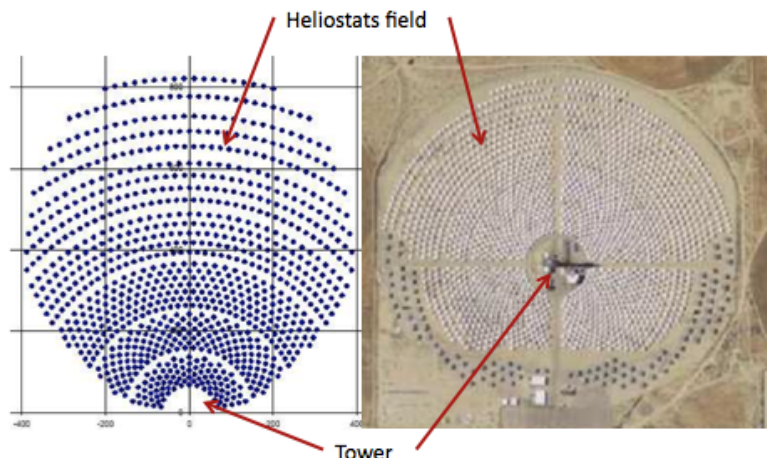


Figure II.20: Heliostats field for medium latitudes (left) and low latitudes (right) [Soler 2011]

Several types of receiver in the tower can be used, depending on the type of heliostats field implemented. The type of receiver that is used has a great influence on the maximal temperature that can be reached, and thus on the energy output and plant efficiency. The receiver material must have the same characteristics as the receiver tube in parabolic trough and linear Fresnel collector technologies, that is to say: high absorbance for the visible spectrum and low emissivity for long wavelengths.

External receivers, being able to receive radiation from all directions are used with heliostats fields all around the tower, while cavity receivers, that can receive radiation only from a specific direction, are

used with heliostats fields situated in the North of the tower. Finally, volumetric receivers can be used to increase the flux density that can be absorbed by the heat transfer fluid, as volumetric material allows heat transfer not only on the surface but also in the volume.

This technology has several advantages. First of all, the high concentration rate on the receiver means high temperature, high efficiency and thus a high power production. Then flat mirrors are simple and cheap to mass-produce and the fact that there is only one receiver allows benefiting from economies of scale. Finally, it is a proven technology that is becoming mature and allows high storage possibilities. Solar thermal power plants could produce electricity at 0.04 US\$ /kWh by 2020. [Kalogirou 2009]

However, the heliostats field and receiver design, as well as the sun tracking implementation are difficult tasks, which are time and money consuming. The structure is also heavier than for other technologies. Finally, the fact that the heat transfer fluid has to go down the tower to run the turbine creates a problem for direct steam generation power plants, as the steam cannot go down easily.

There is no standard design for thermal solar tower power plants, but several different concepts, among which direct steam generation and towers using molten salts as heat transfer fluid. Other concepts, using air as working fluid, for example, are also currently developed, but are only at an early stage nowadays.

One of the first thermal solar power plants to be built was the THEMIS plant, in Targassonne (South of France), in 1983. It was made of 201 heliostats, concentrating the solar radiation onto a 105 meters high tower, where molten salts were heated up to 500°C. The heat was then transferred to water turned into steam in a heat exchanger to run a turbine. It could produce up to 2MWe electricity and used molten salts tanks to store thermal energy. Figure II.21 shows the THEMIS plant when not in operation.



*Figure II.21: THEMIS thermal solar power plant, in Targassonne (France) [Wikipedia]*

An example of a direct steam generation solar tower plant is the PS10 plant in Spain (figure II.19), which was built and started by Abengoa near Seville (Andalucía) in 2007. It is made of more than 600 heliostats and can produce 11 MW. Water/steam is used as heat transfer and working fluid. It is heated up to 265°C and 40 bars and then is used to run the turbine. Steam buffer storage is also used to store thermal energy for one hour worth production.

### e- Dish Stirling

The dish Stirling technology is a point focusing technology as well. However, this is the only technology that is modular, meaning that it can be used either in large power plants, with several dishes, but also as stand alone power systems, in remote areas to produce energy for villages or for water pumping.

The collector is made of a parabolic dish, reflecting the radiation onto a receiver placed in the focal point of the dish. A two-axis sun tracking system ensures an optimal irradiation of the mirrors. The dishes always facing the sun, it is the most efficient technology among all thermal solar collectors. The concentration ratio can reach 2000. The dishes are usually between 5 and 15 meters wide. The parabolic dish can be made of one surface, or of several small facets.

Figure II.22 represents the principle of a dish Stirling system.

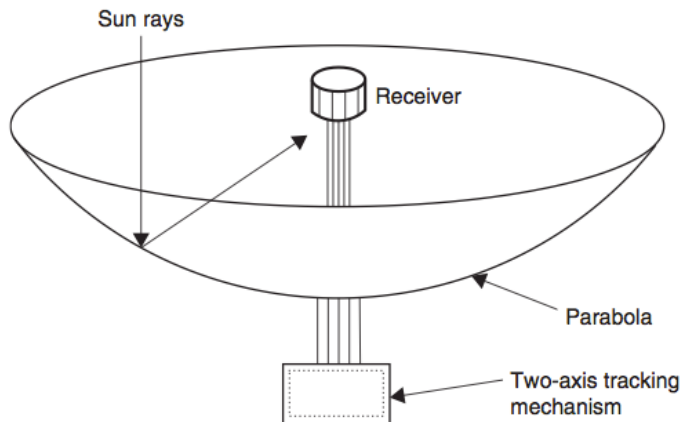


Figure II.22: Dish Stirling system principle [Kalogirou 2009]

The solar radiation heats a fluid that can be either hydrogen or helium up to 1500°C and 150 bars. The heat transfer fluid is then used to run an engine, usually a Stirling engine, and finally a generator converts the mechanical energy into electricity. A dish Stirling system can produce between 5 and 25 kW<sub>e</sub> per dish.

There is no thermal energy storage nor thermal energy transportation possibility. The energy is directly converted into electricity.

The main disadvantages of this technology are that it needs complex reflector geometry, which is thus expensive to manufacture. Then, the need for maintenance is increased, as each dish system has its own engine and generator. Finally, it is not a mature technology, still under development.

One example of parabolic dish Stirling system is the PowerDish of Infinia, shown in figure II.23.



Figure II.23: Parabolic dish system of Infinia [Infinia]

### 3- Power production

Power is produced when extracting the heat from the radiation and transforming it into mechanical energy (with a turbine) and then into electricity with a generator. Several fluids can be used as heat transfer fluid, to extract the heat from the solar radiation, as well as working fluid, to run the turbine. Those are described in the next section.

Then the main thermodynamic cycles used to produce power in solar thermal power plants will be described: the Rankine and organic Rankine cycles. Other cycles can also be used, such as the Stirling cycle or the Brayton cycle. However those two are not described in this thesis.

#### a- Heat transfer fluids

Different fluids can be used as heat transfer fluid, extracting the energy from the solar radiation in the absorber tube to use it to produce power or heat.

Water can be used with **saturated or superheated steam turbines**. The main advantage of steam is that it is cheap. It can also reach quite high temperatures, above 400°C sometimes. However, the fact that a two-phases liquid flows in the absorber tube can create some problems. A lot depend on the type of flow inside the tube. The different patterns for two-phases flows inside a tube are described in figure II.24.

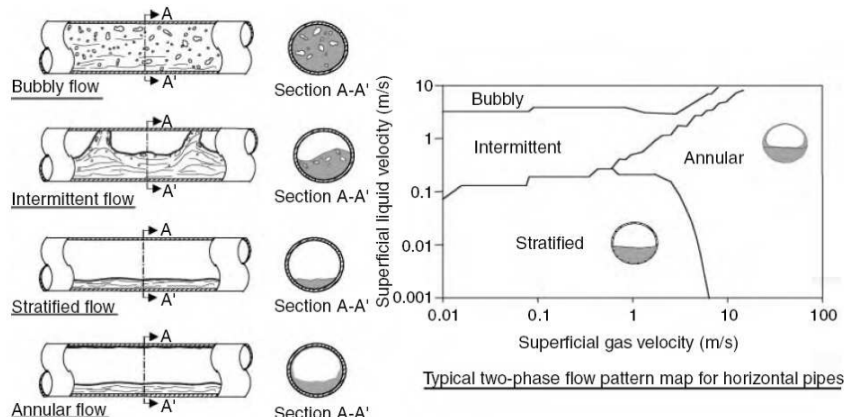


Figure II.24: Typical two-phases flow pattern map for horizontal pipe [Soler 2010]

In order to ensure a proper cooling of the absorber tube, it is important to have liquid water all around the tube (and not, for example, a stratified flow). Indeed, liquid water has a higher specific heat than steam, and thus heat transfer is thus better with water than with steam.

A two-phases flow triggers thus problems to control the solar field and ensure a proper cooling of the tube, otherwise, the stresses on the tube increase. Then, having steam inside the tube increases the possibility of coolant leakages.

This type of heat transfer liquid is used in all kinds of solar power plants, but mainly in linear Fresnel collectors, with direct steam generation (which means that the steam is used both as a heat transfer fluid and a working fluid in the turbine).

**Molten salts of nitrate** (a mix of 60% of NaNO<sub>3</sub> and 40% of KNO<sub>3</sub>) are commonly used in solar tower power plants, as it needs higher operating temperatures. Molten salts are used between 290°C and 550°C, as below 220°C they become solid. Using molten salts adds complexity to the power plant, as it creates a need for molten salts temperature control, to ensure that it does not drop below their solidification point. And as molten salts cannot run a turbine, several loops need to be created in the circuit, with at least one heat exchanger between the molten salts and the working fluid (most of the time water/steam) that runs the turbine.

Another advantage of the molten salts is that it is a good storage medium, with high specific heat and high energy density.

Finally, molten salts are not toxic, nor inflammable, contrary to mineral or synthetic oils.

**Mineral or synthetic oils** are mostly used in parabolic trough plants. Those are toxic and highly flammable, thus increasing the risks of fire at the power plant. Energy storage possibility with this type of heat transfer fluid is quite low, as it has a low specific heat. Then, the maximum temperature they can stand is around 400°C, thus limiting the operation temperature of the plant.

Finally, those oils cannot be used as working fluid in the turbine, and a second loop needs thus to be created, with a heat exchanger between the oils and the working fluid running the turbine (water or organic fluids).

Other types of heat transfer fluids are also used, for example organic fluids, used in organic Rankine cycles, for low temperature plants. Then some other fluids are currently studied, as **air** (whose main advantage is that it is free and available everywhere, but its volumetric density is really low, which means that it would be needed to increase a lot the size of the pipes and plant) or **gases such as hydrogen and helium**, which can be used in dish Stirling collectors, and can reach temperatures up to 1200°C.

### b- Rankine cycle

The Rankine cycle is the most commonly used thermodynamic cycle with steam turbine thermal power plants. Its main components are the boiler (that heats water into steam), the turbine (that expands the steam and converts the energy of the steam into mechanical energy), the generator (that converts the mechanical energy from the turbine into electricity), the condenser (that condenses the steam into water) and pumps. Several others components can also be used, for example pre-heaters (using steam from the turbine to heat up the water after the condenser and thus increasing the efficiency of the plant), a deaerator ...

When used in a solar power plant, the solar field replaces the boiler, to heat up the water into steam, in the case of direct steam generation. Thus water/steam is used both as a heat transfer fluid and as a working fluid running the turbine. In other cases, the water can be heated up in a heat exchanger, using the heat from mineral or synthetic oils, or molten salts used as heat transfer fluids.

Figure II.25 represents the layout of a simplified solar power plant with direct steam generation.

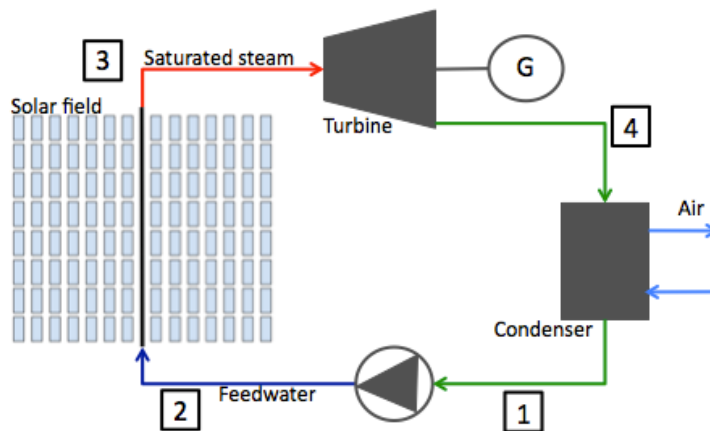
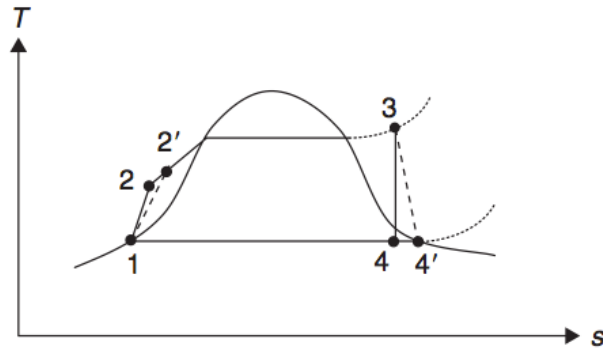


Figure II.25: Simplified layout of a solar power plant with direct steam generation and Rankine cycle

Figure II.26 represents the T-s diagram of a simple Rankine cycle (with no reheat) as described above.



*Figure II.26:* T-s diagram of a simplified Rankine cycle [Kalogirou 2009]

The ideal pumping process is represented by 1-2 and 3-4 represents the ideal isentropic expansion process in the turbine. The actual pumping process is however 1-2' and the real expansion process in the turbine is 3-4'.

The isentropic efficiency of the turbine is given by:

$$\eta_s = \frac{h_3 - h_{4'}}{h_3 - h_4} \quad (\text{II.9})$$

Figure II.27 represents the layout of a steam turbine cycle with two pre-heaters and one deaerator (or feed-water tank), which is used to remove non-desirable gases from the condensates. This layout is used further on to give the equations that describe the Rankine cycle.

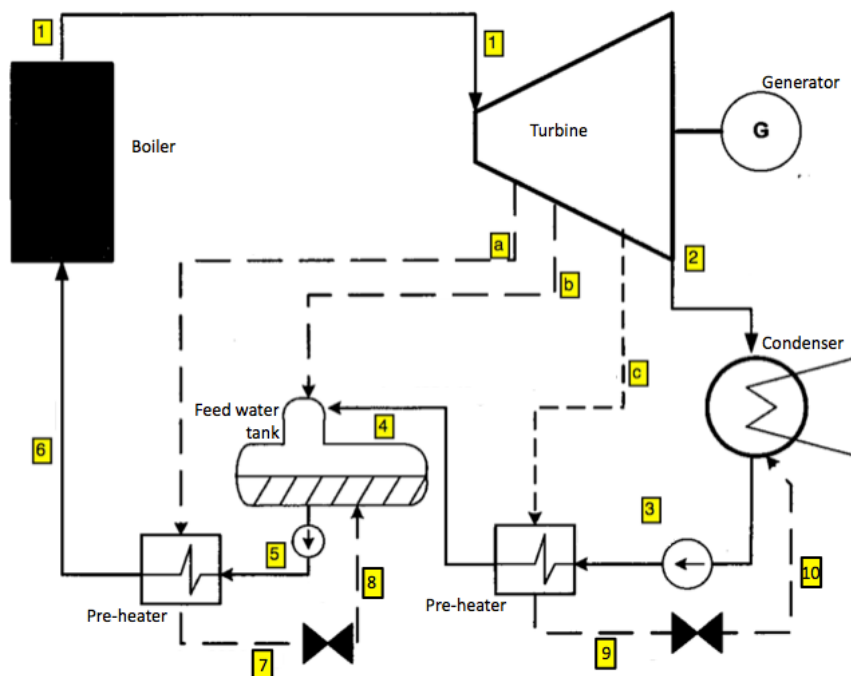


*Figure II.27:* Layout of a typical steam cycle with two pre-heaters and one feed-water tank [Petrov 2011]

The internal energy balance for an open system is given by the following equation:

$$\frac{dU}{dt} = \sum_{in-out} m h + W' + Q \quad (II.10)$$

Where  $U$  is the internal energy of the vessel,  $m$  is the mass flow (kg/s) and  $h$  is the enthalpy (kJ/kg) of the fluid entering the system (in) or leaving the system (out),  $W'$  is the work that is applied on the system and  $Q$  is the heat that is given to the system.

Thus it gives, for all the components of the cycle, the following equations.

The power given by the boiler is:

$$Q_{boiler} = m(h_1 - h_6) \quad (II.11)$$

The power produced by the turbine:

$$P_{turbine} = \left[ m(h_1 - h_a) + (m - m_a)(h_a - h_b) + (m - m_a - m_b)(h_b - h_c) + (m - m_a - m_b - m_c)(h_c - h_2) \right] \eta_{m+t} \quad (II.12)$$

where  $\eta_{m+t}$  is the mechanical and transmission efficiency of the generator.

The energy balance for the condenser is:

$$(m - m_a - m_b - m_c)h_2 + m_c h_{10} - (m - m_a - m_b)h_3 = m_{air} C_p (T_{out} - T_{in}) \quad (II.13)$$

Energy balance for the first (closed) pre-heater:

$$m_c(h_c - h_9) = (m - m_a - m_b)(h_4 - h_3) \quad (II.14)$$

Energy balance for the deaerator (open pre-heater):

$$m_b h_b + (m - m_a - m_b)h_4 = m h_5 \quad (II.15)$$

Energy balance for the second (closed) pre-heater:

$$m_a(h_a - h_7) = m(h_6 - h_5) \quad (II.16)$$

Many approximations can be made, to simplify the model: the pumps work can be neglected and the enthalpies after each of the heat exchanger (the two pre-heaters and the condenser) can be considered to be equal to saturated liquid water enthalpy.

In the end, the efficiency of the steam cycle is given by:

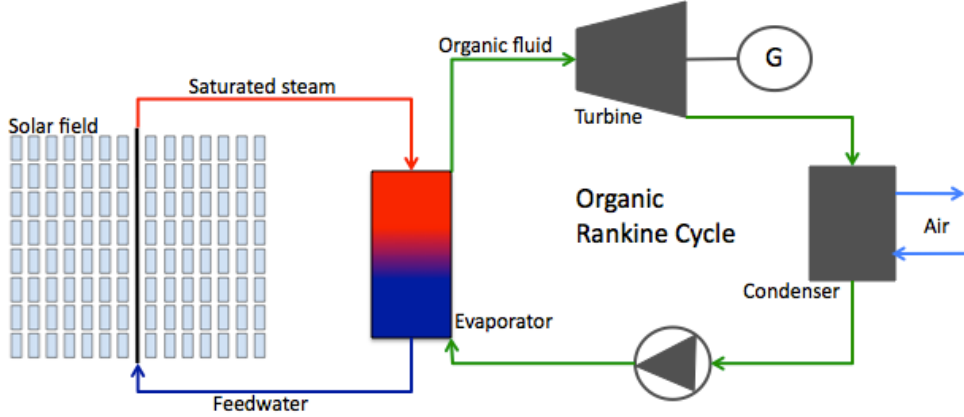
$$\eta = \frac{P_{turbine} - P_{pumps}}{Q_{useful}} \quad (II.17)$$

### c Organic Rankine cycle

Another type of Rankine cycle is sometimes used in solar power plants, most of all when the power that is produced is low (for example less than 5MWe). This is called the Organic Rankine Cycle, and it differs from the Rankine cycle that was described above by the fact that the working fluid is not water/steam, but an organic fluid with a boiling point lower than water.

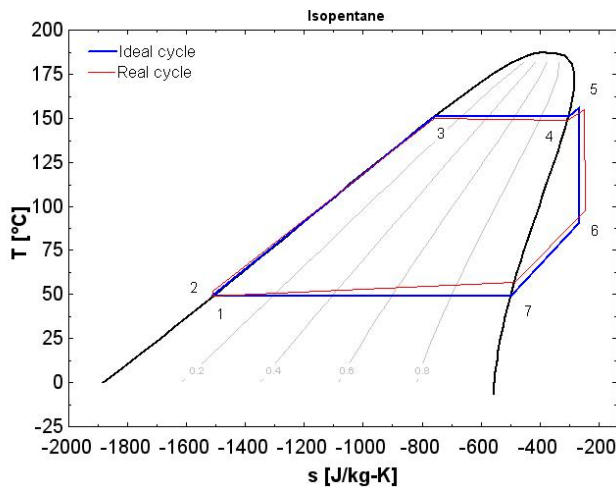
The organic fluid can be used as heat transfer fluid and working fluid, running the turbine. When water is the heat transfer fluid, an exchanger is used in order to transfer the heat from the water to the organic fluid.

Figure II.28 represents the simplified layout of such a plant with water as heat transfer fluid and an organic fluid as working fluid.



*Figure II.28: Simplified layout of a power plant with water as heat transfer fluid and an organic fluid as working fluid.*

Figure II.29 represents the T-s diagram of an organic Rankine cycle (the organic fluid being here isopentane).



*Figure II.29: T-s diagram of an Organic Rankine Cycle [Wikipedia]*

#### d- Solutions to increase the efficiency of a solar power plant

As the aim of this thesis is to optimise the operation of a solar power plant, different options to increase the efficiency are described in this section.

Some plants use a gas or fuel system as a **back up**. When the solar power plant is no longer producing, the back up system is started, thus increasing the operation time of the plant every day. For example in the SEGS plants in California, the natural gas back up produces up to 25% of the total production of the plant. It allows the plant to run during peak hours, when the electricity prices are the highest.

In other plants, some fuel is burnt in a boiler, in order to superheat or reheat the steam in the Rankine cycle. Some plants are also **hybridised** with a combined cycle. In those Integrated Solar Combined Cycle Systems (ISCCS), the energy from the solar field as well as the heat from the gas turbine are used in a heat exchanger to heat steam then running a turbine. Both the gas and steam turbines produce electricity.

Figure II.30 represents the layout of an ISCCS.

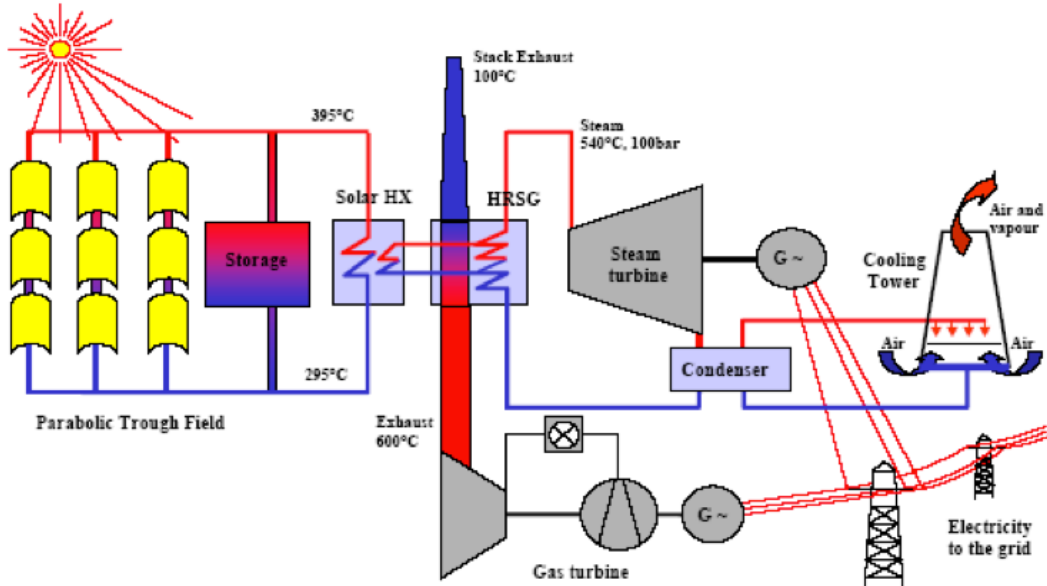


*Figure II.30: Layout of an Integrated Solar Combined Cycle System [Soler 2010]*

Other options can be used to increase the efficiency of the thermodynamic cycle. It is for example possible to reheat the steam, after a first, high-pressure turbine, and before a second, lower-pressure turbine. Superheating the steam is also a good mean to increase the efficiency of the plant, when the absorber tube materials allow it. Finally, one can use feed-water pre-heaters, after the condenser and before entering the solar field, to increase the efficiency of the cycle.

The last solution to increase the overall plant efficiency is to oversize the solar field compared to the turbine requirements and to store the excess energy. This energy can then be used during peak hours, when the electricity prices are higher. This last solution is further described in the next section of this thesis.

## 4 Energy storage in CSP

### a- Why an energy storage?

In some cases, it is possible to oversize the solar field, and thus produce more steam than what the turbine allows. The steam that is produced and cannot be used at once is stored, for example in a steam accumulator. When the heat transfer fluid is molten salt, those salts are stored before being used to produce steam in a heat exchanger.

The energy storage allows then compensating for insolation variations, due for example to the passage of clouds, during the day. It allows also using the stored energy at the end of the day, when the solar field cannot produce anything. Thus, energy storage is a mean to match the needs of a constant energy production. This can be illustrated with figure II.31 that represents the advantage of the energy storage in a solar power plant. The sum of the yellow and the white areas represents the available thermal energy at any time. Only the yellow area is used to produce power, while the white area is stored during the day, and then used at the end of the day to ensure a constant power production equal to the demand. The green area offers a comparison with a fuel burner production.

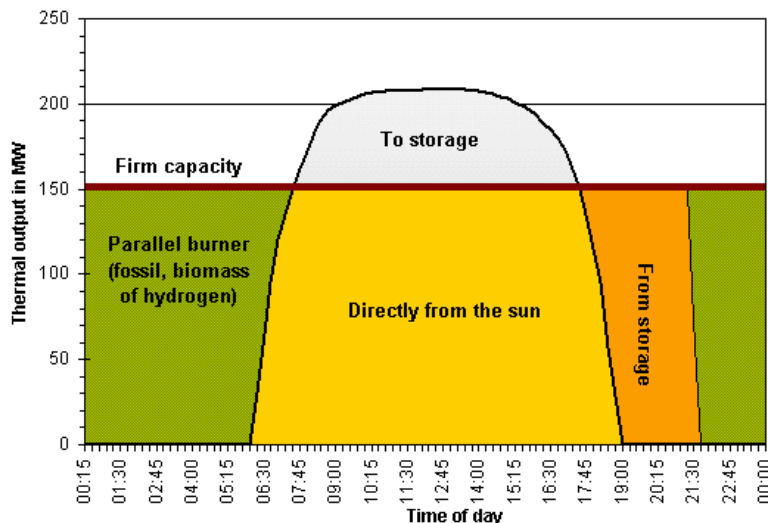


*Figure II.31: Advantages of thermal energy storage in solar power plant operation [Krothapalli 2011]*

When studying the prices of electricity and a solar power plant production during the day, one can see that the production peak is not at the same time as the electricity price peak. It can thus be interesting sometimes to store heat during the day and then use it when the electricity prices are high.

Different technologies of energy storage are described in next sections.

### b- Steam accumulator

A steam accumulator is a pressurized tank into which is stored a mix of saturated steam and saturated water.

The principle of steam accumulation is the following: when saturated steam from a boiler (and here from the solar field) enters the pressurized tank, the pressure increases in the tank, and thus the saturation temperature increases too. Then, the saturated steam condenses into saturated water. The heat is thus stored into pressurized water, which has a higher volumetric energy density than steam.

When the tank is discharged, the pressure decreases, as well as the saturation temperature. The saturated liquid vaporises and some steam is produced. The steam accumulator is operated with sliding pressure, which means that the pressure changes during the charging and discharging processes.

The following scheme represents a steam accumulator.

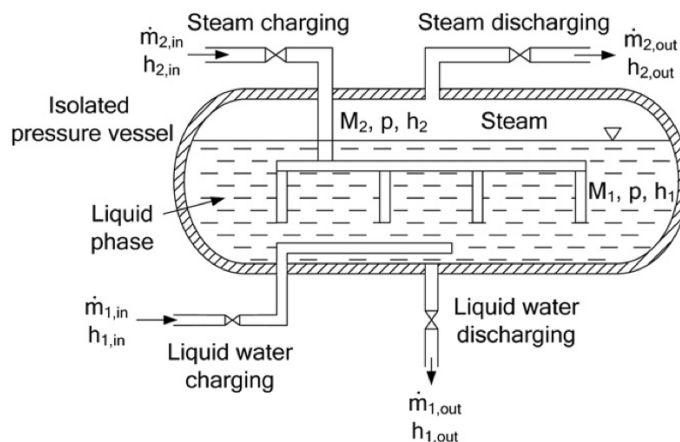


*Figure II.32: Steam accumulator layout [Stevanovic et al. 2012]*

### c- Molten-salts energy storage

Energy storage in solar energy field can be implemented with other, more expensive but also more efficient technologies, for example, direct or indirect storage of molten salts in two tanks (Andasol type plant, solar tower power plant).

The storage is said to be “direct” when the working fluid is stored directly, while it is said indirect when the working fluid is used to heat another fluid in a heat exchanger, the second fluid being then stored.

In solar power plants using molten salt as a storage medium, the solar energy is used to heat cold molten-salts pumped from a cold tank (around 290°C), which then are stored into a hot tank (around 565°C). When the stored energy is discharged, the hot molten-salts are used to heat water into steam, which is then used in a classical steam turbine. The cold salts are pumped back into the cold tank.

The molten salts are nitrate salts (a mix of NaNO<sub>3</sub> and KNO<sub>3</sub>).

An example of this type of power plant, using molten salts as storage mean, is the ANDASOL plant in Spain, represented in figure II.33.

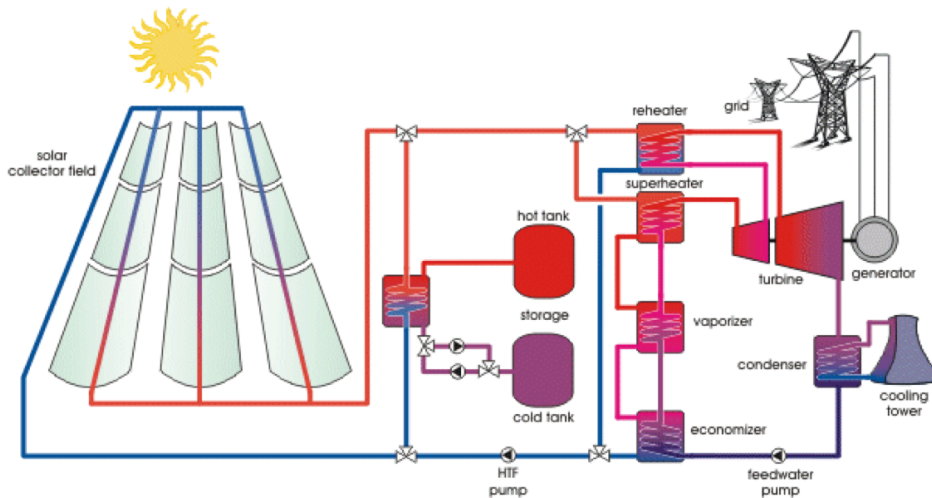


*Figure II.33: ANDASOL solar power plant's layout [Spelling 2011]*

In this case, the working fluid extracting the heat from the solar field is oil, which is used either to heat some water in a boiler, or to heat molten salts in a heat exchanger. This is an example of an indirect storage.

The GEMASOLAR power plant, shown in figure II.34 is an example of plant with direct molten-salt storage, as the molten salts are used both as working fluid and storage medium. As high temperatures are required to keep the salts in a liquid state, this technology requires solar tower plants that reach higher temperatures than for example parabolic trough plants.

The advantages of molten-salts storage are that it is a cheap and available product, with a high heat capacity and that is chemically inert. However, as those salts become solid at quite high temperatures (220°C), it adds complexity to the system.

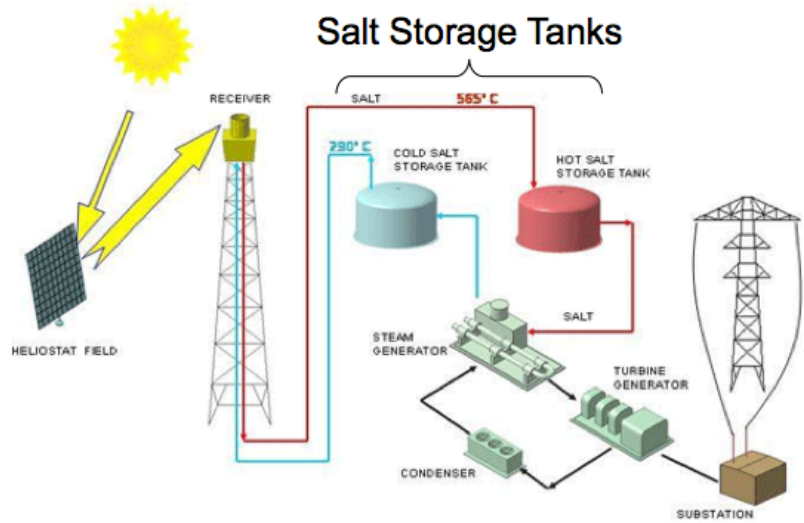


Figure II.34: GEMASOLAR power plant's layout  
[\[www.psa.es/webeng/areas/ussc/solartres.php\]](http://www.psa.es/webeng/areas/ussc/solartres.php)

#### d- Thermocline storage system

The thermocline technology is developed for economical reasons, as it needs only one tank for energy storage. The hot fluid coming from the solar field and the cold fluid coming from the power block are stored in the same tank. Hot fluids enter at the top of the tank, while cold fluids enter at the bottom of the tank. The system uses the natural convection, thanks to which the hot fluids remain on the top, and the cold fluids remain at the bottom. The zone of thermal gradient in the middle is called thermocline. The aim is to have a thermocline zone as thin as possible, thus having the best storage efficiency (as the heat is not transferred to the cold fluid). Figure II.35 describes a thermocline tank.

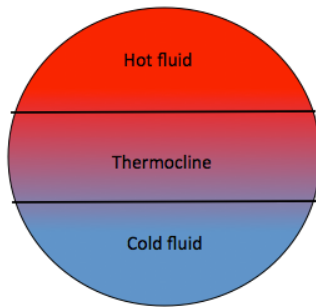
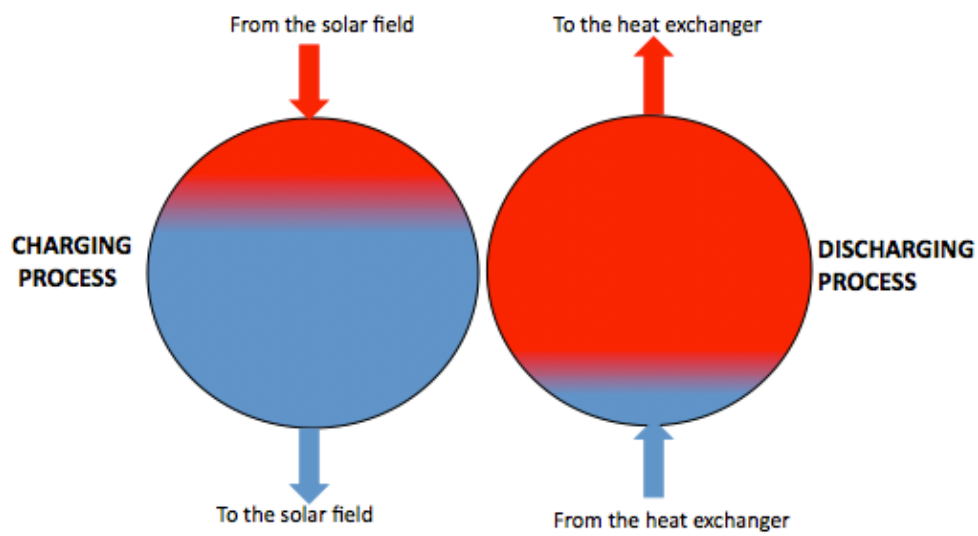


Figure II.35: Thermocline tank layout

During the charging process, hot fluid is added on top of the tank, thus enlarging the hot fluid zone, while cold fluid is extracted from the bottom, and then heated up in the solar field. This goes on until the tank is filled with hot fluid. During the discharging process, hot fluid is removed from the top of the tank, thus decreasing the volume of hot liquid, while the cold fluid from the heat exchanger is added in the bottom of the tank. This goes on until the tank is filled with cold fluid. Figure II.36 represents the thermocline storage system operation.



*Figure II.36: Operation of a thermocline energy storage system*

The tank can be filled with low cost materials such as rock and sand that are heated by the hot fluid during the charging process. [Feledziak 2012]

## III- Case study

### 1- Presentation of CNIM- Solar Division

The present thesis was led with the company CNIM Solar Division, which works on the development of thermal solar power plants. In this section, the company is described, as well as the technology that was developed by the Solar Division. Finally, the two projects that are treated by this thesis are described.

#### a- CNIM Solar Division

CNIM is a French group, located at La Seyne-sur-Mer, in Provence (south of France). It designs, builds and operates plants. The group works in three main domains: environment (waste processing and flue gas treatment), energy (boilers production for thermal or solar energy plants) and innovation and systems (military systems, for the nuclear industry...).

CNIM was created in 1856, and was at that time a company producing mainly tanks and boats. The Solar Division was created in 2009, even though CNIM invested in solar energy long before, taking part into the THEMIS project, a solar tower power plant built in Cerdagne (South of France) in the 1980's. The group designed and built the molten salts receiver (see section II.2.d, figure II.21).

The new solar division aims at designing and building thermal solar power plants. It built a prototype on the site of La Seyne-sur-Mer in 2010 and is now involved in two projects. The first one is the construction and operation of a 1MW pre industrial demonstrator (eCare) in Morocco. The second one is the construction and operation of a 9MW solar plant in Llo, in Cerdagne (south of France). Both projects are further detailed in the rest of this section.

#### b- CNIM technology

All those projects, as well as the prototype, use the same concentrating technology. The solar field is made of several lines of linear Fresnel collectors, using planar mirrors to concentrate the solar radiation onto a tube, where the radiation is absorbed and heats water into steam.

One line of Fresnel collectors is made of several modules. The prototype that was built in La Seyne-sur-Mer is the first module ever built by CNIM Solar Division. It is made of 14 lines of 8 mirrors (7 lines on each side of the receiver). It is about 50 metres long and 20 metres wide with an area of mirrors of about  $720 \text{ m}^2$ . The receiver is situated about 8 meters above the mirrors, and is about 0.40 metres wide.

Figure III.1 represents a module of linear Fresnel collector that is the constitutive element of all solar power plants.

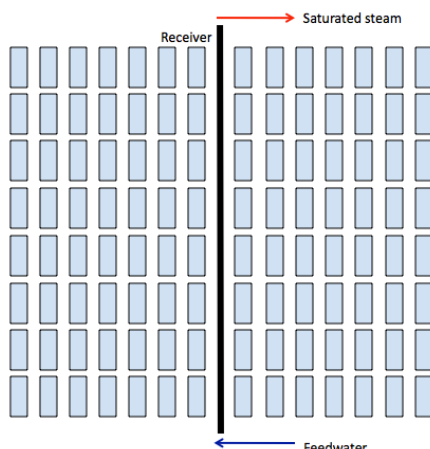
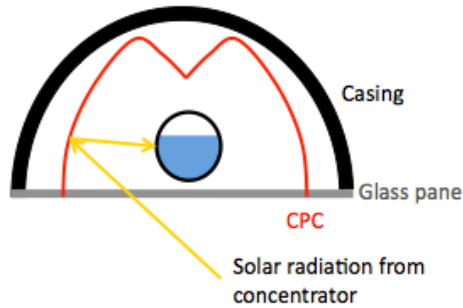


Figure III.1: Scheme of a module of CNIM linear Fresnel concentrator, viewed from above.

Figure III.2 represents a cut of the receiver. The absorber tube, inside which flows the working fluid, is protected by a high transmittance glass pane beneath it. This permits to reduce the convection losses along the absorber tube. Above the tube, a CPC (Compound Parabolic Collector) permits to reflect the radiations that miss the tube at first onto the tube. Indeed, the mirror field reflects the solar radiation onto the receiver with a wide spot, sometimes wider than the tube itself. The CPC thus increases the geometric efficiency of the power plant. A casing is situated above the CPC to protect it.



*Figure III.2: Cut of the receiver*

The absorber tube has a diameter of about 70 millimetres. The aim is to have a material with a high absorbance and a low emissivity. In this case, the tube is covered by a special coating with an absorbance of 0.95 on the visible spectrum, and an emissivity of 0.10 on the infrared.

The Compound Parabolic Collector (CPC) is made of aluminium covered with a special coating to increase the reflectivity (which is then equal to about 0.9 on the solar spectre). Its shape is a double parabola.

The glass pane is made of borosilicate (Pyrex), which has the advantage of being able to handle huge thermal shocks and high temperatures.

Finally, the casing is made of steel, as well as the structure that support the whole receiver.

The mirrors on the fields are all slightly bended. The mirrors of each line have a specific bend, in order to optimize the reflection and approximate a parabolic concentration.

Figure III.3 shows a picture of the prototype in operation on the site of la Seyne-sur-Mer.



*Figure III.3: Linear Fresnel direct steam generation prototype in La Seyne-sur-Mer (France) [CNIM]*

Two solutions are then considered to extract the heat from the solar field and produce power. The first one is direct steam generation. This solution is considered for plants over 5MWe. The second solution is to use pressurized water as the heat transfer fluid, and then to use an organic Rankine cycle to produce power. This solution being more efficient for lower temperature, is should be considered for plants below 5MWe.

### c - The projects

The Solar division of CNIM is currently working on the development of two projects.

The first one is called eCare. It is a 1MW pre-industrial demonstrator to be built in Morocco using the linear Fresnel collector technology developed by CNIM. The aim is to build a small-scale facility that could be then developed in all MENA countries (Middle East and North Africa). This project is led, since April 2012, with the funding of ADEME (the French agency for the environment and the energy) whose objective is to develop a French thermal solar industry able to become a major actor on the exportations market.

The eCare project was first designed with the organic Rankine cycle technology, as it is a power plant producing less than 5MWe, and with thermocline energy storage. However, considering that the theoretical global efficiency of such a plant was quite low (less than 20%) [Feledziak 2012], it was decided to lead an investigation for the same project but with direct steam generation (using saturated steam) and a steam accumulator for energy storage. This is the first part of this thesis.

The second project is a 9MW solar power plant to be built and then operated in Llo, (Cerdagne, France) using linear Fresnel collectors with direct (saturated) steam generation and a steam accumulator for energy storage.

This will be the first project to be led on an industrial scale for CNIM. It was a bid to the invitation to tender launched by the CRE (Commission for Energy Regulation) and the Minister for Environment and Energy. The aim is to develop new ways of producing energy in France.

## 2- Objectives

In this section is described the work that has to be done in this thesis.

The aim of the first part of the thesis is to estimate the global efficiency of a power plant with direct steam generation and energy storage using a steam accumulator, and then to compare it to the efficiency of the same plant that was calculated previously (during another thesis) with an organic Rankine cycle. In this purpose, it is necessary to estimate the plant annual performance, as well as the investment costs, to be able then to say if the project with direct steam generation is feasible.

The first part of the project is thus to choose a turbine, dealing with turbines manufacturers and developing specifications to ensure with the manufacturers that the global efficiency of the thermodynamic cycle is maximum. Once the specifications of the turbine are known, it is possible to design the layout of the plant (number of pre-heaters, re-heater...).

Then, a model of thermodynamic (Rankine) cycle is developed with Excel, calculating the electrical power produced for a known thermal power coming from the solar field. Data on the Ouarzazate (Morocco) site give the DNI, the wind speed, the ambient temperature, and the humidity for every hour of the year. This is the base of all the calculations, as it gives an idea of a typical year concerning solar radiation and weather conditions. This data is then used in the software developed by CNIM that calculates the thermal power provided to the heat transfer fluid by the solar field. This is the input data in the model that is developed. This model gives thus the annual production of the plant without storage.

In order to have a precise estimation of the power that can be extracted from the energy stored in the steam accumulator, a model of steam accumulator is developed with Excel, using the article of Stevanovic et al., that gives the evolution of the pressure, the volume and the steam and liquid water enthalpy inside the accumulator.

Once the annual production is known, it is necessary to estimate the investment costs, and thus to size every component of the plant and estimate its price, using data from previous projects led by CNIM.

In the end, all the parameters are optimized: the solar field and the steam accumulator are sized to have the best efficiency and the lowest investments costs, the way the stored energy is used (during peak hours, or to ensure a constant production during the day) is decided and the conclusion on the feasibility of the project are drawn.

**The specifications of the only steam turbine for less than 1MW gave that the maximum inlet pressure was equal to 12 bars. It gave a cycle efficiency of less than 16%, and thus the steam turbine was not efficient enough, compared to the organic Rankine cycle. The calculations were led no further and thus this part of work is not described in the present report that focuses more on the next part of the thesis.**

The second part of the project is to perform the same calculations of annual performances for the 9MW project in Llo.

## IV- Steam accumulator modeling

In order to be able to integrate an accurate model of thermal energy storage in the plant performance calculations, a steam accumulator was modeled, based on the papers “Dynamic of Steam Accumulation” by Stevanovic et al. [Stevanovic et al. 2012] and “Buffer Storage for Direct Steam Generation” by Steinmann et al. [Steinmann et al. 2005]. The equations given in [Stevanovic et al. 2012] were discretised in order to calculate the evolution of the different variables (enthalpies and pressure in the tank) every ten minutes. Some graphs were then drawn to know the evolution of the pressure in the tank throughout the time of the experiment. This evolution of the pressure, thus giving the evolution of the saturated steam enthalpy coming out of the tank was then integrated to the performance calculations.

### 1- Method

The steam accumulator model is based on the following equations. Figure IV.1 gives the different values that are used in this model.

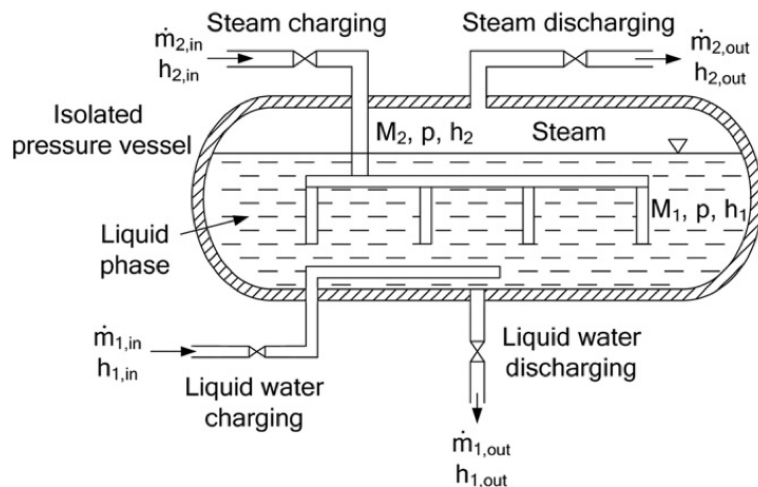


Figure IV.1: Steam accumulator layout [Stevanovic et al. 2012]

#### a- Mass balance

The liquid mass balance gives:

$$\frac{dM_1}{dt} = m_{1B} + m_{PT1} \quad (\text{IV.1})$$

$M_1$  being the liquid mass inside the tank,  $m_{1B}$  being the net mass balance of liquid water inlet and outlet flows and  $m_{PT1}$  being the liquid mass change due to evaporation and condensation inside the tank.

With  $m_{1B} = m_{1,in} - m_{1,out}$  where  $m_{1,in}$  is the liquid mass flow entering the tank and  $m_{1,out}$  is the liquid mass-flow leaving the tank; and  $m_{PT1} = m_c - m_e$  where  $m_e$  is the evaporation rate and  $m_c$  is the condensation rate.

Then the steam mass balance gives:

$$\frac{dM_2}{dt} = m_{2B} + m_{PT2} \quad (\text{IV.2})$$

$M_2$  being the steam mass inside the tank,  $m_{2B}$  being the net mass balance of steam inlet and outlet flows and  $m_{PT2}$  being the steam mass change due to evaporation and condensation inside the tank.

With  $m_{2B} = m_{2,in} - m_{2,out}$  where  $m_{2,in}$  is the liquid mass flow entering the tank and  $m_{2,out}$  is the liquid mass-flow leaving the tank; and  $m_{PT2} = m_e - m_c$  where  $m_e$  is the evaporation rate and  $m_c$  is the condensation rate.

### b- Energy balance

The internal energy balance for an open system (here the steam accumulator), when neglecting the potential and kinetics energies, is given by [Jamet 2011]:

$$\frac{dU}{dt} = \sum_{in-out} (m h) + W' + Q \quad (IV.3)$$

Where  $U$  is the internal energy of the tank,  $m$  is the mass flow (kg/s) and  $h$  is the enthalpy (kJ/kg) of the fluid entering the system (in) or leaving the system (out),  $W'$  is the work that is applied on the system and  $Q$  is the heat that is given to the system.

The internal energy is also given by  $U=H PV$  where  $H$  is the enthalpy of the system (kJ),  $P$  is the pressure of the system (bar) and  $V$  is the volume of the system ( $m^3$ ).

As the volume of the tank is constant, as there is no work applied on the steam accumulator, and as heat is lost by convection and conduction, the energy balance for the steam accumulator thus gives:

$$\frac{dH}{dt} = \sum_{in-out} (m h) + V \frac{dP}{dt} - Q_{losses} \quad (IV.4)$$

Here, the enthalpy of the system is equal to:  $H=H_1+H_2$  where  $H_1$  is the enthalpy of the liquid phase inside the tank and  $H_2$  is the enthalpy of the gaseous phase.

Equation (IV.3) can be used when considering the system of the liquid phase inside the tank. It gives:

$$\frac{dH_1}{dt} - V_1 \frac{dP}{dt} - P \frac{dV_1}{dt} = (m h)_{1B} + m_{PT1} h'' + W_1 + Q_{21} - Q_{losses,1}$$

where  $H_1$  is the enthalpy of the liquid phase ( $H_1=h_1 M_1$  with  $h_1$  being the enthalpy in kJ/kg) inside the tank (in kJ),  $(m h)_{1B}$  is the net energy balance of liquid inlet and outlet flows (in W),  $h''$  is the enthalpy of the saturated steam at the pressure of the tank (in kJ/kg),  $Q_{21}$  is the heat transfer rate from the superheated steam to the liquid (W),  $V_1$  is the volume of the liquid phase ( $m^3$ ) and  $P$  is the pressure inside the tank (bar).

The work applied on the system (W) being given by:  $W_1 = -P \frac{dV_1}{dt}$

Then, the liquid energy balance gives:

$$\frac{dH_1}{dt} = (m h)_{1B} + m_{PT1} h'' + V_1 \frac{dP}{dt} + Q_{21} - Q_{losses,1} \quad (IV.5)$$

with  $(\dot{m}h)_{1B} = \dot{m}_{1,in}h_{1,in} - \dot{m}_{1,out}h_{1,out}$  where  $h_{1,in}$  is the enthalpy of the liquid entering the tank and  $h_{1,out}$  is the enthalpy of the liquid leaving the tank.

Equation (IV.5) can be written for  $h_1$  (in kJ/kg) as:

$$\frac{dh_1}{dt} = \frac{1}{M_1} \left[ (\dot{m}h)_{1B} + \dot{m}_{PT1}h'' + V_1 \frac{dP}{dt} + \dot{Q}_{21} - \dot{Q}_{losses,1} - h_1 \frac{dM_1}{dt} \right] \quad (\text{IV.5})'$$

The same goes for the steam energy balance:

$$\frac{dH_2}{dt} = (\dot{m}h)_{2B} + \dot{m}_{PT2}h'' + V_2 \frac{dP}{dt} - \dot{Q}_{21} - \dot{Q}_{losses,2} \quad (\text{IV.6})$$

where  $H_2$  is the enthalpy of the steam phase ( $H_2=h_2.M_2$  where  $h_2$  is the enthalpy in kJ/kg) inside the tank (in kJ),  $(\dot{m}h)_{2B}$  is the net energy balance of steam inlet and outlet flows (in W), and  $V_2$  is the volume of the steam ( $\text{m}^3$ ).

With  $(\dot{m}h)_{2B} = \dot{m}_{2,in}h_{2,in} - \dot{m}_{2,out}h_{2,out}$  where  $h_{2,in}$  is the enthalpy of the steam entering the tank and  $h_{2,out}$  is the enthalpy of the steam leaving the tank.

Equation (IV.6) can also be written for  $h_2$ , as:

$$\frac{dh_2}{dt} = \frac{1}{M_2} \left[ (\dot{m}h)_{2B} + \dot{m}_{PT2}h'' + V_2 \frac{dP}{dt} - \dot{Q}_{21} - \dot{Q}_{losses,2} - h_2 \frac{dM_2}{dt} \right] \quad (\text{IV.6})'$$

The evaporation rate is given by  $\dot{m}_e = \frac{\rho_1 V_1 (h_1 - h')}{\tau_e r}$  for  $h_1 > h'$  and  $\dot{m}_e = 0$  for  $h_1 \leq h'$ . Where  $\rho_1$  is the liquid density ( $\text{kg/m}^3$ ),  $h_1$  is the liquid water enthalpy (kJ/kg),  $h'$  is the saturated liquid enthalpy (kJ/kg),  $r$  is the latent heat of vaporization (kJ/kg) and  $\tau_e$  is the evaporation relaxation time (s).

The condensation rate is given by  $\dot{m}_c = \frac{\rho_1 V_1 (h' - h_1)}{\tau_c r}$  for  $h_1 < h'$  and  $\dot{m}_c = 0$  for  $h_1 \geq h'$ . Where  $\tau_c$  is the evaporation relaxation time (s).

The condensation and evaporation relaxation times were taken equal to 85 seconds, as in [Stevanovic et al. 2012].

The heat transferred between the superheated steam and the liquid phase is given by  $\dot{Q}_{21} = (UA)_{21}(T_2 - T_1)$  where  $U$  is the overall heat transfer coefficient ( $\text{W/m}^2\text{K}$ ),  $A$  is the interface area,  $T_2$  is the superheated steam temperature and  $T_1$  is the liquid phase temperature.

However, [Stevanovic et al. 2011] states that the effect of this heat transferred between the two phases can be neglected, which was done in the model.

### c- Energy losses

The losses can be calculated considering that the tank is a cylinder with two half-spheres at each end, as shown in figure IV.2. The energy can be lost by conduction through several layers of different materials (metal, insulator) or by external convection (radiation is neglected). The calculations of the energy losses and the thermal resistances are described in paragraph V.12.

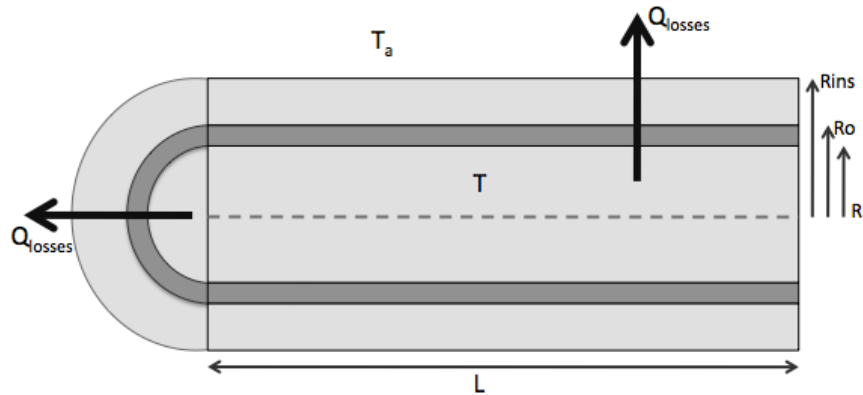


Figure IV.2: Layout of a tank with a layer of insulator

This calculation gives the losses for the whole accumulator. In order to have the losses for the liquid and the gaseous phases, equations (IV.5) and (IV.6) were used with the following relation between H, H<sub>1</sub> and H<sub>2</sub>: H=H<sub>1</sub>+H<sub>2</sub>.

This gives another relation:  $\dot{Q}_{losses} = \dot{Q}_{losses,1} + \dot{Q}_{losses,2}$ .

It was thus decided to estimate the losses from the liquid and gaseous phase as follow:

$$\dot{Q}_{losses,1} = \frac{V_1}{V_1 + V_2} \dot{Q}_{losses} \text{ and } \dot{Q}_{losses,2} = \frac{V_2}{V_1 + V_2} \dot{Q}_{losses}$$

#### d- Volume balance

Finally, the volume of the tank remains constant, thus giving:

$$V = V_1 + V_2 \quad (\text{IV.7})$$

It gives thus a set of five equations (IV.1), (IV.2), (IV.5)', (IV.6)' and (IV.7) for five unknown values that are the pressure P inside the tank, the liquid and steam enthalpy (h<sub>1</sub> and h<sub>2</sub>), and the steam and liquid mass inside the tank (M<sub>1</sub> and M<sub>2</sub>).

Those five equations were then discretised over a time step  $\Delta t$  and then implemented with Excel.

#### e- Discretisation

The exponent n indicates the current time, while the exponent n-1 refers to the time just before.

Equations (IV.1) and (IV.2) were discretised as follow:

$$M_1^n = M_1^{n-1} + (m_{1B} + m_{PT1})\Delta t$$

$$M_2^n = M_2^{n-1} + (m_{2B} + m_{PT2})\Delta t$$

Equations (IV.5)' and (IV.6)' were discretised as follow:

$$h_1^n = \frac{h_1^{n-1} + \frac{\Delta t}{M_1^n} \left[ (m h)_{1B}^n + m_{PT1}^n h_n^n + Q_{21}^n + V_1^n \frac{P_n - P_{n-1}}{\Delta t} - \frac{V_1^n}{V_1^n + V_2^n} Q_{losses}^n \right]}{1 + \frac{M_1^n - M_1^{n-1}}{M_1^n}}$$

$$h_2^n = \frac{h_2^{n-1} + \frac{\Delta t}{M_2^n} \left[ (m h)_{2B}^n + m_{PT2}^n h_n'' - Q_{21}^n + V_2^n \frac{P_n - P_{n-1}}{\Delta t} - \frac{V_2^n}{V_1^n + V_2^n} Q_{losses}^n \right]}{1 + \frac{M_2^n - M_2^{n-1}}{M_2^n}}$$

And finally, equation (IV.7) gives:

$$V = V_1^n + V_2^n$$

[Stevanovic et al. 2012] shows that equation (IV.7) leads to an equation for the variation of the pressure. This first equation was first implemented with Excel, along with equations (IV.1), (IV.2), (IV.5)' and (IV.6)'. However, the calculations were too complex to allow Excel to iterate alone, and it was thus necessary to make it iterate step by step with a VBA program. The results and calculation times not being what was expected, it was then decided to implement equations (IV.1), (IV.2), (IV.5)', (IV.6)' and make Excel iterate step by step once more in order to guarantee that equation (IV.7) is true, with a VBA program.

## 2- Results

Simulations were run for different cases, related to different initial values.

At first, the optimal initial water volume in the tank was estimated. For this purpose, four different simulations were run, with three sets of identical initial conditions, except for the initial volume of water inside the accumulator.

The initials conditions are given in Table IV.1:

*Table IV.1: Initial conditions for optimal initial water volume calculation*

		Simulation 1	Simulation 2	Simulation 3	Simulation 4
Accumulator volume	m <sup>3</sup>		360		
Maximal pressure	bar		70		
Minimal pressure	bar		15		
Time step	s		600		
Initial Pressure	bar		8		
Initial water volume	%	50%	60%	65%	70%

The optimal initial water volume is determined when comparing the amount of steam that can be stored in (and that can be discharged from) the accumulator.

The results that were obtained from the three simulations are described in table IV.2.

*Table IV.2: Results of simulations for initial water volume calculation*

		Simulation 1	Simulation 2	Simulation 3	Simulation 4
Initial water volume	m <sup>3</sup>	50%	60%	65%	70%
Mass of steam charged	ton	36	43,2	43,2	39,6

The optimal initial water volume was thus **60%**.

Knowing the optimal initial water volume, it was then necessary to have an estimation of the evolution of the pressure during the charging, discharging and storage processes. The simulation was run in the operation conditions for the Llo project.

It was decided to study a scenario with 3 accumulators of  $120 \text{ m}^3$  each. The minimum pressure (and initial pressure) was set at 12 bars and the maximum pressure was set at 70 bars. The initial liquid water volume was set at 60% of total accumulator volume. The inlet steam enthalpy was set to the enthalpy of saturated steam at 70 bars, as it is the nominal pressure for the turbine in Llo project, and as the steam accumulators are filled only when the nominal pressure is reached in the solar field. Initially, the liquid water and the steam in the accumulator are at equilibrium at the initial pressure (12 bars).

During the charging process, the inlet steam mass-flow was constant and equal to 2kg/s. The charging process was stopped when the pressure in the accumulator reached 70 bars. The charging process thus lasted 1h50.

During the discharging process, the outlet saturated steam mass-flow was constant and equal to 1kg/s. The discharging process was stopped when the accumulator pressure reached 12 bars. The discharging process lasted 3h30.

The results that are presented afterwards are drawn from a simulation launched for 1 accumulator described above.

Figure IV.3 shows the evolution of the pressure that was obtained after the simulation.

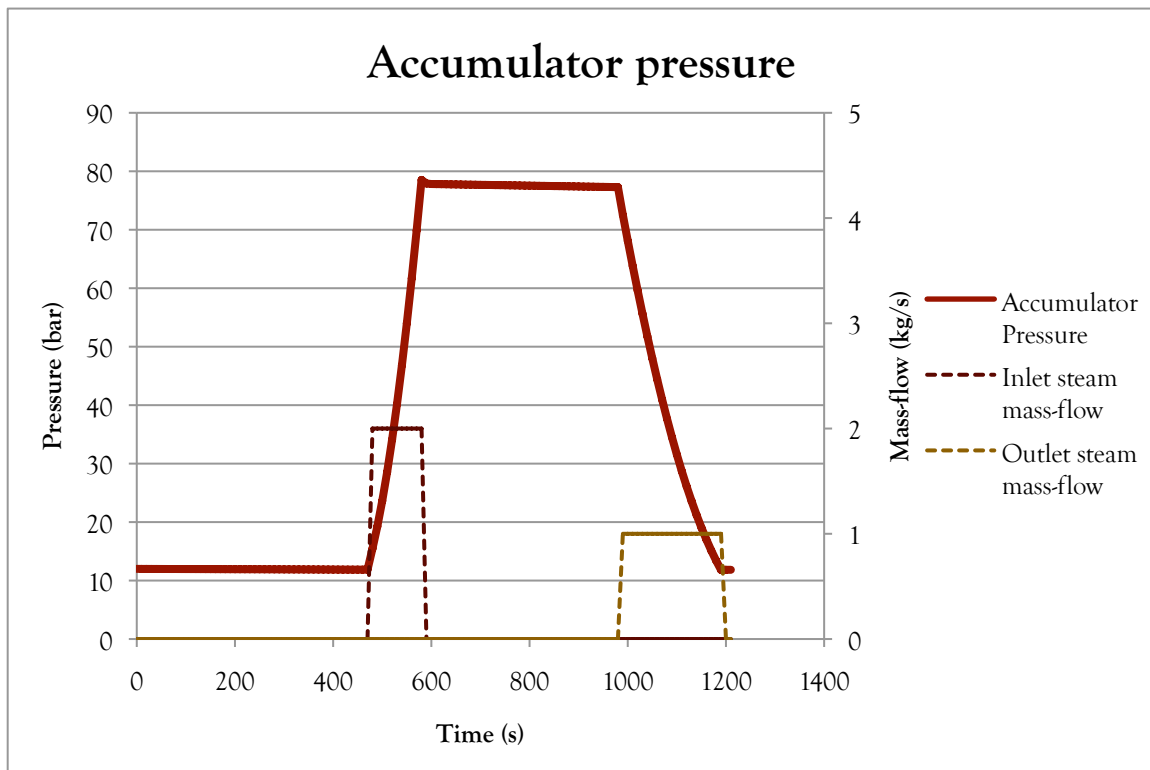


Figure IV.3: Evolution of the pressure, the inlet and outlet steam mass-flows during the simulation

During the storage processes at low and high pressure, the evolution of the pressure in the tank depends only on the time. Those two evolutions are shown in figures IV.4 and IV.5.

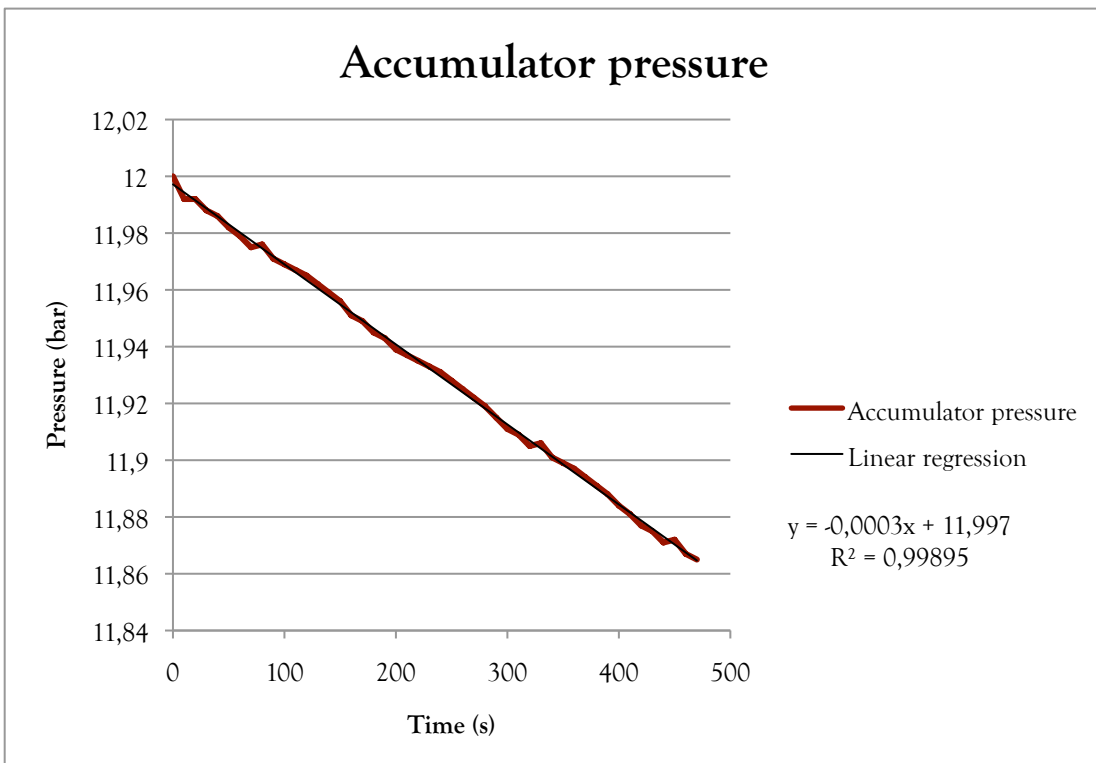


Figure IV.4: Evolution of the pressure with the time during the low-pressure storage process

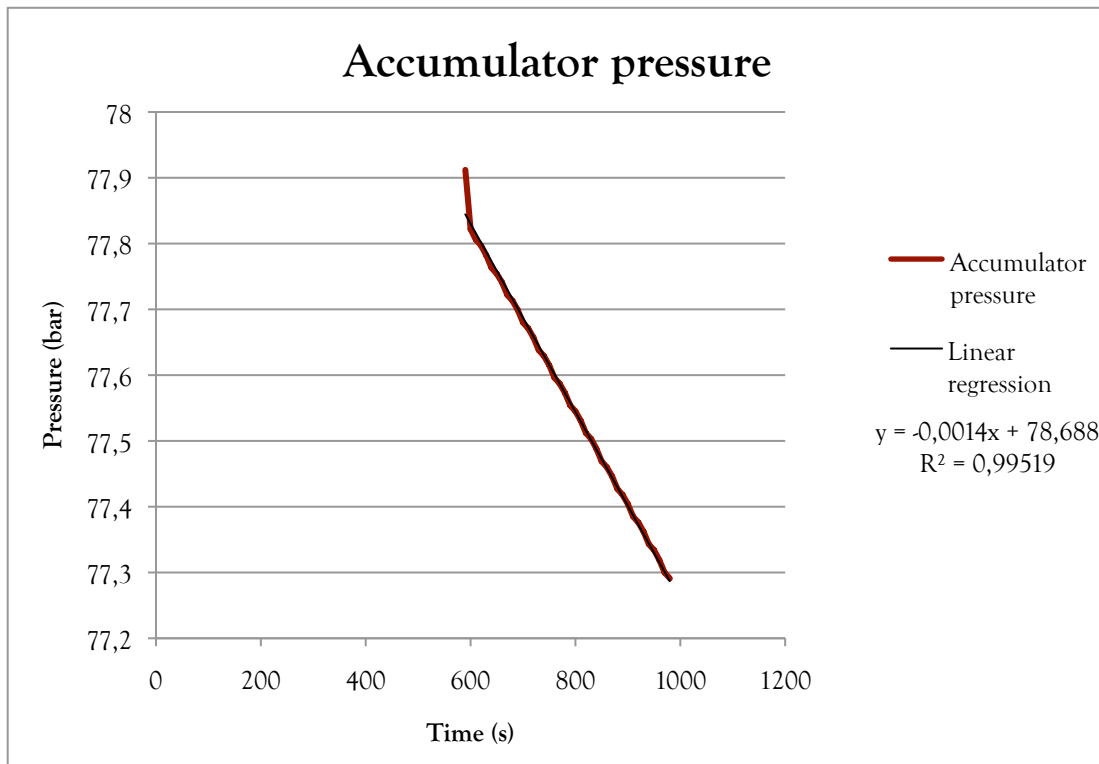
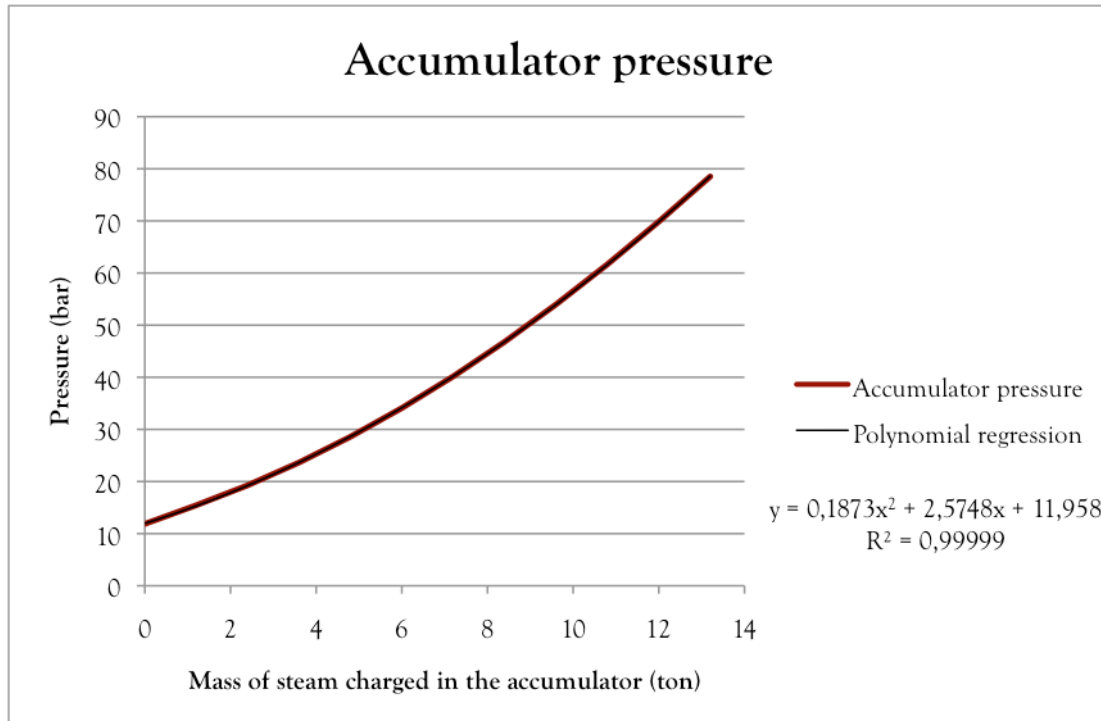


Figure IV.5: Evolution of the pressure with the time during the high-pressure storage process

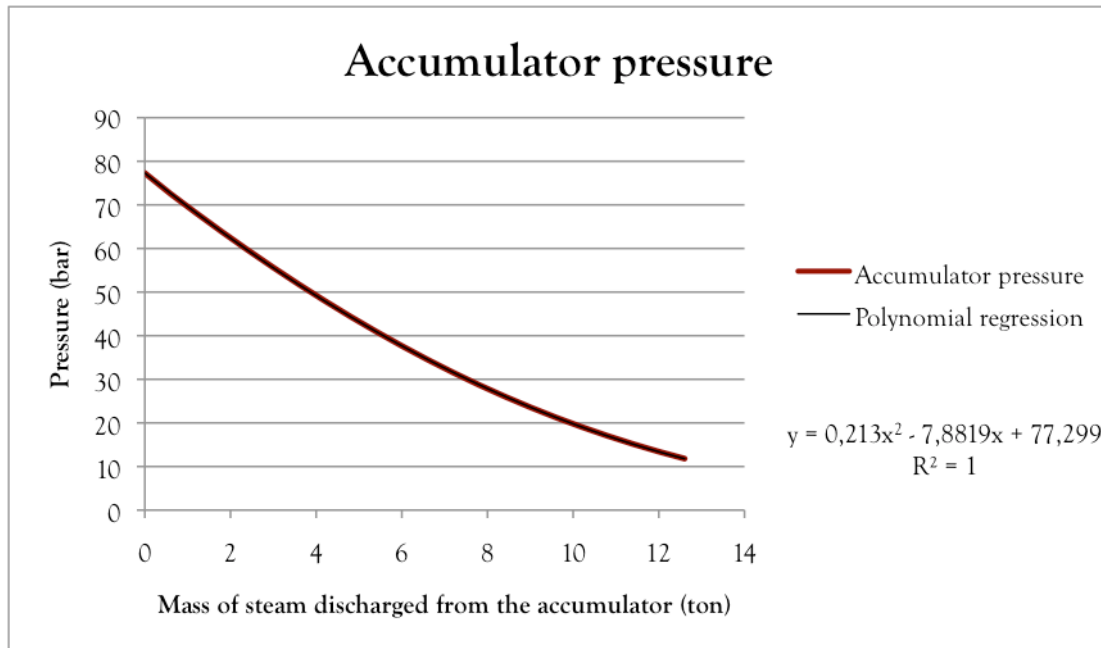
During the charging and discharging processes, the evolution of the pressure depends almost only on the mass of steam that was charged into or discharged from the accumulator (the losses are neglected).

Figure IV.6 represents the evolution of the steam accumulator pressure with the steam mass that is charged.



*Figure IV.6: Evolution of the pressure with the mass of steam charged inside the accumulator*

Figure IV.7 gives the evolution of the accumulator pressure with the mass of steam that is discharged.



*Figure IV.7: Evolution of the pressure with the mass of steam discharged from the accumulator*

The simulation was run for three different time steps (60, 600 and 1000 seconds) and the same curves were drawn. The same equations for the polynomial and linear regressions were obtained for charging, discharging, and storage processes. It shows that the results are independent of the time step. Moreover, the small variations that can be seen on the pressure curves are due to Excel iterations: those iterations

were made with a VBA program with low precision. When increasing the iterations precision, the variations disappear, but the simulation time increases drastically.

What can be easily calculated when simulating the plant operation every 10 minutes (or 600 seconds) is a sum of mass-flows, so the two previous graphs can also be obtained, depending on a sum of inlet or outlet mass-flow. The relation between the mass of steam (in tons) that is charged in the accumulator at a time  $t$  and the sum of mass flows (in kg/s) is as follow:

$$M_{steam} = \sum \frac{m_{steam} \cdot 600}{1000} = \frac{600}{1000} \cdot \sum m_{steam}$$

It gives then figure IV.8 and IV.9 representing the evolution of the pressure with the sum of inlet/outlet mass-flow.

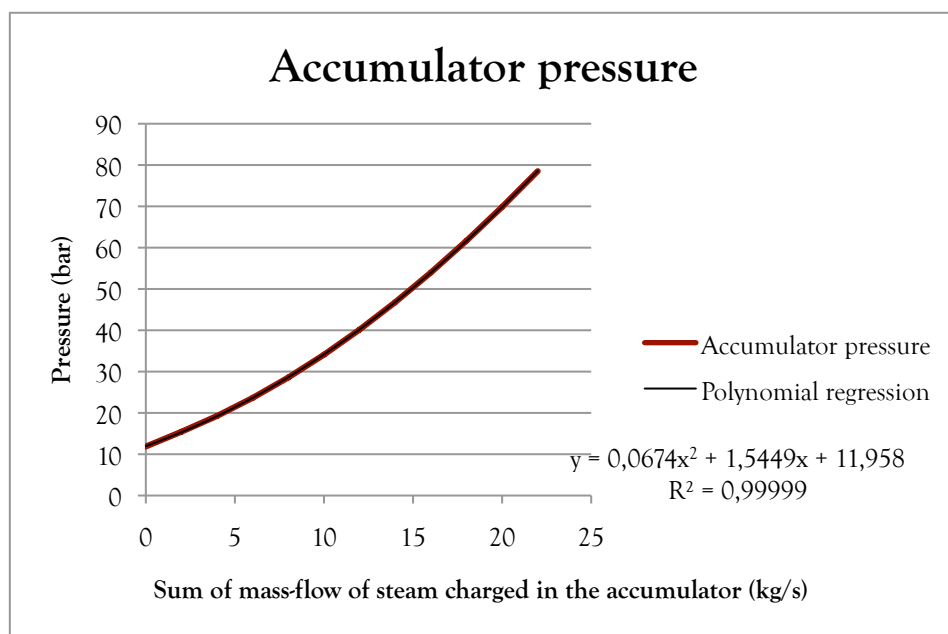


Figure IV.8: Evolution of the pressure with the sum of mass-flow of steam charged in the accumulator

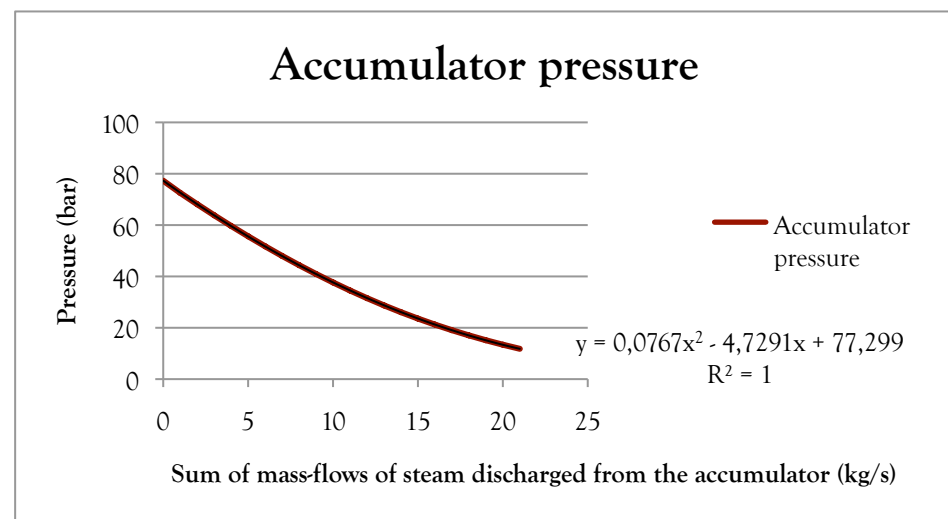


Figure IV.9: Evolution of the pressure with the sum of mass-flow of steam discharged from the accumulator

### 3- Discussion

When comparing the shape of the curve in figure IV.3, and the one described in [Stevanovic et al. 2012] and represented in figure IV.10, one can see that they are quite similar. One can notice the fact that the pressure reaches at first a higher value, before decreasing to the equilibrium value. This phenomenon is explained in [Stevanovic et al. 2012].

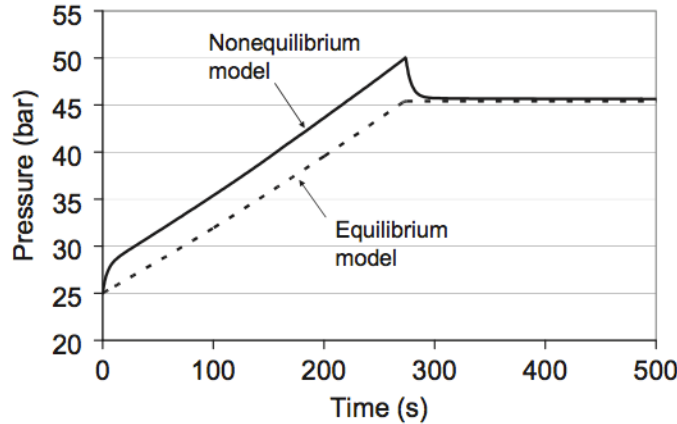


Figure IV.10: Results obtained for the charging process in [Stevanovic et al. 2012]

However, when comparing the amount of steam that can be charged with the theoretical value, one can observe that the simulation gives a result that is half what is expected in theory.

Indeed, the mass of steam that can be charged into the accumulator to pass from 12 bars to 70 bars is given when equating the equations obtained with the polynomial regression figure IV.6 to 70 bars. It gives:

$$M_{\text{charging}} = 12.02 \text{ tons or } 20.03 \text{ kg/s.}$$

The same reasoning goes to calculate the amount of steam that can be discharged from the tank to pass from 70 to 12 bars, this time using the equation on figure IV.7.

It gives:  $M_{\text{discharging}} = 10.13 \text{ tons or } 16.89 \text{ kg/s.}$

The theoretical steam mass that can be discharged from a tank between the pressures 70 and 12 bars is given by [Steinmann et al. 2005]:

$$M_{\text{discharging}} \Delta h_{\text{evaporate}} = M_{\text{liquid}} C_{\text{liquid}} (T_{\text{sat}}(P_{\text{start}}) - T_{\text{sat}}(P_{\text{end}}))$$

Where  $M_{\text{liquid}}$  is the mass of liquid in the tank, it is considered constant during the discharging,  $C_{\text{liquid}}$  is the liquid mean specific heat and  $\Delta h_{\text{evaporate}}$  is the mean heat of vaporization, given by:

$$\Delta h_{\text{evaporate}} = \Delta h_{\text{evaporate,ref}} \left( \frac{1 - (T + 273.15)/647}{1 - (T_{\text{ref}} + 273.15)/647} \right)^{0.38}$$

with  $\Delta h_{\text{evaporate,ref}} = 2257 \text{ kJ/kg}$  for  $T_{\text{ref}} = 100^\circ\text{C}$ .

In the end, it gives:  $M_{\text{discharging}} = 18.435 \text{ tons.}$

It represents a relative error of 45%. The same result was obtained when simulating exactly the same experience as in [Stevanovic et al. 2012]. As it was impossible to compare the simulation results with a real case, it was decided to rely on the theory of [Stevanovic et al. 2012] and [Steinmann et al. 2005].

It was thus decided to modify the equations obtained in figures IV.8 and IV.9 in order to obtain a mass of discharged steam of 18 tons.

The new amount of discharged steam being 1.8 times bigger than what was first calculated the equations were modified as follow.

For the charging process, M being the sum of inlet mass-flow:

$$P(M) = \frac{0.0674}{1.8^2} M^2 + \frac{1.5449}{1.8} M + 11.958$$

For the discharging process, M being the sum of the outlet mass-flow:

$$P(M) = \frac{0.0767}{1.8^2} M^2 - \frac{4.7291}{1.8} M + 77.295$$

The new amounts of steam that can be charged into and discharged from the accumulator are:

$$M_{\text{charging}} = 36.65 \text{ kg/s or } 21.99 \text{ tons}$$

$$M_{\text{discharging}} = 30.00 \text{ kg/s or } 18.00 \text{ tons}$$

#### 4- Conclusion

The main aim of the modelling of a steam accumulator was to be able to integrate the model into the performance calculation. For this purpose, the equations governing the evolution of the accumulator pressure during the charging, discharging, high-pressure and low-pressure storages processes were deduced from the theory as well as some simulations with the model. Those equations can be integrated to the performance calculations, as well as the total amount of steam that can be charged into and discharged from the accumulator.

Finally, it was decided to model 3 accumulators, in the performance calculations, and not all in 1 bigger accumulator. Otherwise, if only one bigger accumulator is modelled, the cases where some accumulators are only partially charged are not taken properly into account. Indeed, in such a case, the steam discharged from the big accumulator would have a lower pressure than 70 bars, while in the real case, the first accumulator would be totally charged and the pressure extracted from it would be at 70 bars initially.

## V- Performances calculations

Some performances calculations were made, in order to determine the annual electrical production, taking into account energy storage as well as the DNI variations throughout the year.

### 1- Method

#### a- Piping and Instrumentation Diagram

Figure V.1 represents the Piping and Instrumentation Diagram of the plant for the Llo project as it was modelled in the performances calculations program.

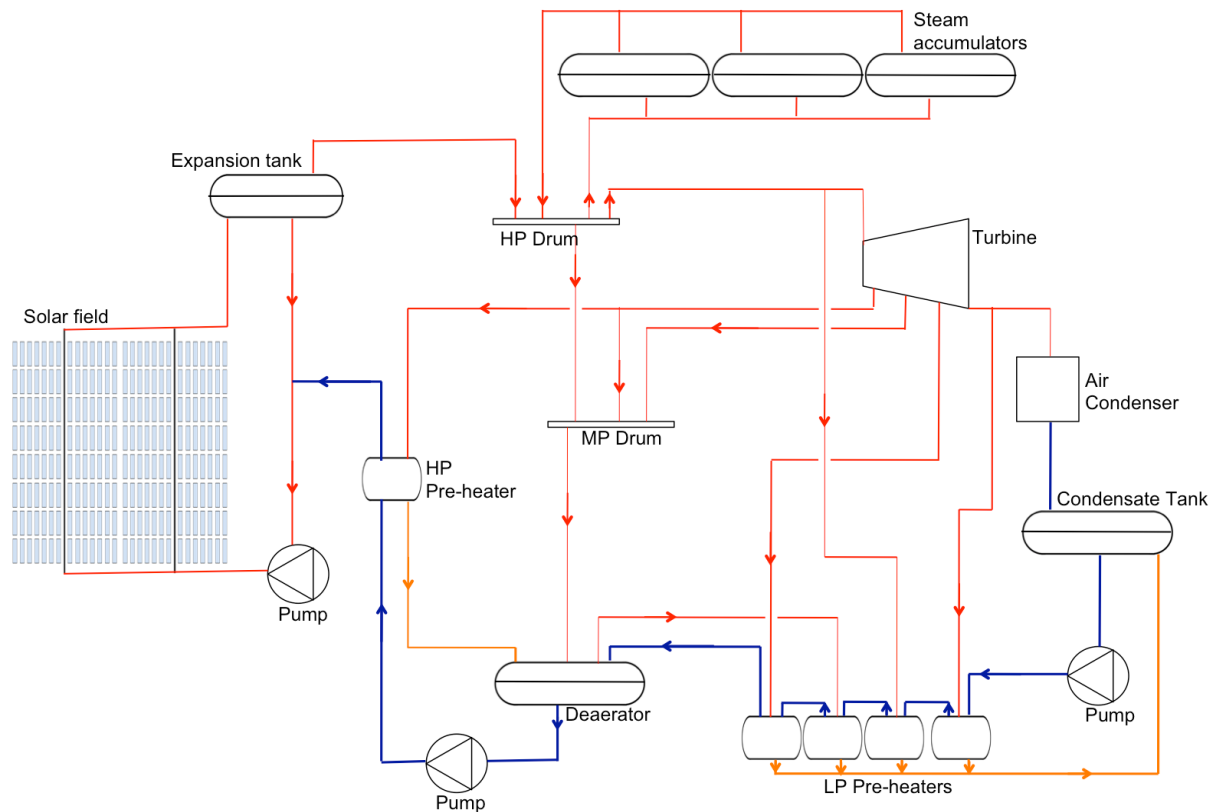


*Figure V.1: Piping and Instrumentation Diagram of the plant (Llo project)*

All the components, and the links between them, were modelled with Excel, thus creating a thermodynamic cycle. The program gives the production of electrical power, as well as the amount of steam that can be stored, for any thermal power.

This section describes the modelling of the thermodynamic cycle as well as the calculations that were made to obtain the annual performances.

### b- Solar field

The modelling of the solar field is not part of this program, and uses another program, called SimSol, developed by CNIM. SimSol uses the azimuth angle, the zenith angle, the Direct Normal Irradiation (DNI), the wind speed and the ambient temperature at the plant location (those data being given by MeteoNorm) to calculate the thermal power that can be used from the solar field. It takes into account the thermal losses as well as the geometrical losses.

A first calculation was made with SimSol in order to calculate the useful thermal power for every hour of the year. This data is given on a first Excel sheet of the program (“Données Llo”). It was calculated for the following input data:

- Number of lines: 26
- Number of modules per line: 5
- Number of rows of mirrors per module: 10
- Slope: 0%
- Mean DNI: 1931 kWh/m<sup>2</sup>/year
- Annual useful thermal energy: 75 558 MWh/year.

As the thermal power that is produced is proportional to the number of lines of mirrors as well as the number of modules per line, it is possible to calculate the thermal power that is produced for any configuration of the solar field quite easily.

In a “Discréétisation” sheet, the wind speed, ambient temperature and thermal power are discretised every 10 minutes. This is the input data for all the calculations made further on. Indeed, the calculation made is a static calculation made every ten minutes of the year. It was not possible to run a dynamic calculation. The time step 10 minutes was chosen as it seems to be the characteristic time in most problems linked to solar power, as can be deduced from [Bellard et al. 2012]. With a 10 minutes time step, simulations are running during several hours. It was thus technically not feasible to work with a shorter and more accurate time step.

### c- Expansion tank

At the end of the solar field is situated an expansion tank, where the two-phase flow leaving the receiver tube is stored. The liquid fluid is sent back to the solar field, while the steam is sent either to the turbine or to the storage tanks. The fluid is saturated in the expansion tank, which gives easily the enthalpy of the steam and liquid water, as well as the temperature in the tank, knowing the pressure. The steam quality is calculated with a program made by CNIM. The liquid mass flow that is sent back to the solar field is calculated as follow:

$$m_{water} = (1 - x) m_{SolarField}$$

Where x is the steam quality in the expansion tank,  $m_{water}$  is the mass-flow sent back in the solar field and  $m_{SolarField}$  is the mass-flow entering the solar field.

The steam mass-flow leaving the expansion tank is calculated in order to ensure saturation at nominal pressure in the expansion tank:

$$m_{steam} = \frac{P_{th} - m_{water}(h_{out,w} - h_{in})}{h_{out,st} - h_{in}}$$

Where  $m_{steam}$  is the steam mass-flow leaving the expansion tank,  $P_{th}$  is the thermal power,  $h_{out,w}$  is the enthalpy of the water leaving the tank,  $h_{out,st}$  is the enthalpy of the steam leaving the tank and  $h_{in}$  is the enthalpy of the water entering the solar field.

The volume of the tank was calculated in order to be able to store half an hour of water at full load. It gives about 50 m<sup>3</sup>.

#### d- Turbine

All the data that was used in the modelling of the turbine comes from the data sheet of two different turbines. The first one is a Thermodyn (GE) 70 bars and 9MW turbine. It should be the one used in the plant, but only the nominal case is known, and there is no data for partial loads. The second one is a GE 60 bars and 5 MW turbine for which the partial loads are known.

The Thermodyn data is given in table IV.1.

*Table V.1: Thermodyn 70 bars and 9MW turbine data sheet*

Inlet	Pressure	bar	70
	Temperature	°C	286
	Flow	kg/h	61 000
Bleed 1	Pressure	bar	14,27
	Enthalpy	kJ/kg	2 602,9
	Temperature	°C	196
	Flow	kg/h	7 239
	Isentropic efficiency		0,61
Bleed 2	Pressure	bar	3,06
	Enthalpy	kJ/kg	2 421,1
	Temperature	°C	134,2
	Flow	kg/h	3 977
	Isentropic efficiency		0,72
Bleed 3	Pressure	bar	1,12
	Enthalpy	kJ/kg	2 308,2
	Temperature	°C	102,9
	Flow	kg/h	4 658
	Isentropic efficiency		0,76
Exhaust	Pressure	bar	0,1451
	Enthalpy	kJ/kg	2 125,6
	Temperature	°C	54,8
	Flow	kg/h	45 070
	Moisture	%	19,9
	Isentropic efficiency		0,698
Global isentropic efficiency			0,727
Mechanical efficiency		%	95,05
Power at generator terminals		kW	9 010

The nominal thermal power was then determined in order to reach 70 bars and an inlet mass-flow in the turbine of 61 000 kg/h. It was estimated at 35 400 kW<sub>th</sub>, then producing 9 012 kW<sub>e</sub> (not taking into account the pumps and air condenser electrical consumption).

In order to calculate the partial loads, the data for the 60 bars and 5MWe turbine was used. The variations of the parameters (bleeds pressure, mass-flow and isentropic efficiency and mechanical efficiency) with the load were studied, and linear regressions were made. Those linear regressions were then applied to the 70 bars case (meaning that the slope of the curves remained the same but the equations were transformed so that it gave the nominal values for 100% load at 70 bars).

The nominal inlet pressure of the turbine for partial load was calculated in order to ensure a constant volume flow ( $\text{m}^3/\text{s}$ ) at the turbine inlet.

The results are summarized in table V.2.

Table V.2: Estimated partial loads for the turbine

		Load	100%	80%	60%	40%	20%
Inlet	Pressure	bar	70	57,3	44,4	31,2	18
	Flow	kg/h	61000	49031	37363	25970	14937
Bleed 1	Pressure	bar	14,27	10,67	7,07	3,47	2,854
	Flow	kg/h	7239	6412	5576	4741	3906
	Isentropic efficiency		0,61	0,617	0,624	0,631	0,638
Bleed 2	Pressure	bar	3,06	2,3	1,54	0,78	0,612
	Flow	kg/h	3977	3456	2908,8	2361,6	1814,4
	Isentropic efficiency		0,72	0,722	0,724	0,726	0,728
Bleed 3	Pressure	bar	1,12	0,79	0,46	0,13	0,224
	Flow	kg/h	4658	3912	3181	2449	1718
	Isentropic efficiency		0,76	0,767	0,773	0,780	0,786
Exhaust	Isentropic efficiency		0,698	0,681	0,664	0,646	0,629
	Global isentropic efficiency		0,727	0,725	0,723	0,73	0,716
	Mechanical efficiency	%	95,05	90,28	85,50	80,73	75,95

The relation between the enthalpies and the isentropic efficiency being:

$$\eta_{is} = \frac{h_{in} - h_{out}}{h_{in} - h_{out,is}}$$

Where  $\eta_{is}$  is the isentropic efficiency,  $h_{in}$  is the enthalpy of the steam entering a stage of the turbine,  $h_{out}$  is the enthalpy of the steam leaving the stage of the turbine, and  $h_{out,is}$  would be the enthalpy of the steam leaving the stage of the turbine, if the expansion was isentropic.

The following relation gives the electrical power that can be produced:

$$P_e = [m_{inlet}(h_{inlet} - h_{bleed1}) + (m_{inlet} - m_{bleed1})(h_{bleed1} - h_{bleed2}) + (m_{inlet} - m_{bleed1} - m_{bleed2})(h_{bleed2} - h_{bleed3}) + (m_{inlet} - m_{bleed1} - m_{bleed2} - m_{bleed3})(h_{bleed3} - h_{exhaust})]\eta_m$$

where  $P_e$  is the electrical power (in kW),  $h$  is the enthalpy at a specific point in the turbine (kJ/kg),  $m$  is the mass-flow (kg/s) and  $\eta_m$  is the mechanical efficiency.

The exhaust pressure is calculated knowing the air condenser specifications and the ambient temperature, as described in next paragraph.

The turbine was set to operate with variable pressure, between 70 bars (100% nominal load) and 12 bars (10% nominal load).

#### e- Air condenser

At first, the design ambient temperature was calculated. The design temperature is defined as the temperature such that the ambient temperature is equal or lower than the design temperature 2/3 of the time during the year. In Llo, the following curve was obtained for the ambient temperature.

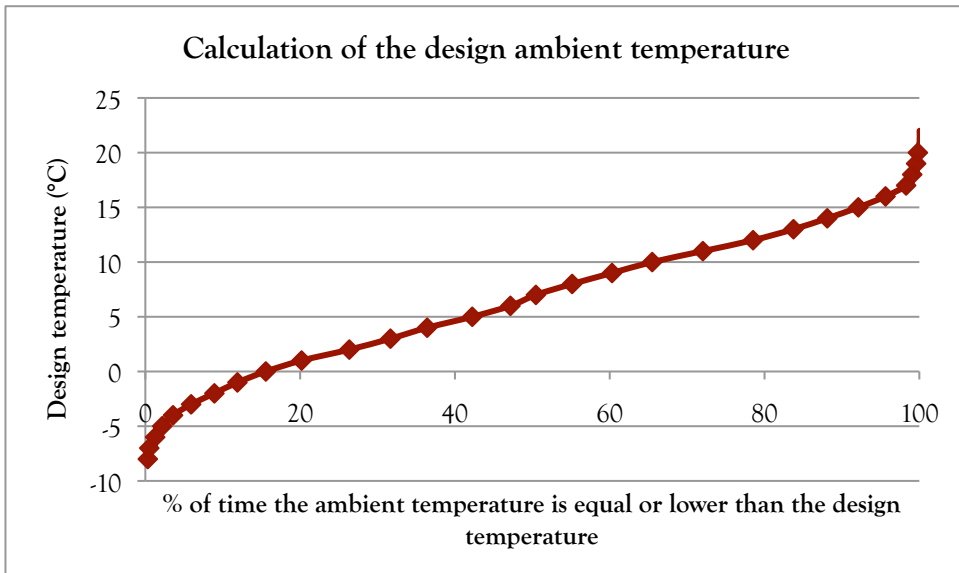


Figure V.2: Calculation of the design ambient temperature

The design ambient temperature is thus 10°C.

Then, the total heat exchanger area was calculated, using the formula from [Granryd et al. 2009].

$$Q_{cond} = U_{cond} A_{tot} \vartheta_m$$

where  $Q_{cond}$  is the heat exchanged in the air condenser (W),  $U_{cond}$  is the overall heat transfer coefficient ( $\text{W}/\text{m}^2\text{K}$ ),  $A_{tot}$  is the total heat exchanger area ( $\text{m}^2$ ) and  $\vartheta_m$  is the logarithmic mean temperature difference (K).

$$\vartheta_m = \frac{\vartheta_{in} - \vartheta_{out}}{\ln(\vartheta_{in}/\vartheta_{out})}$$

with  $\vartheta_{in} = T_{sat} - T_{cond,in}$  and  $\vartheta_{out} = T_{sat} - T_{cond,out}$ .

$T_{sat}$  being the saturation temperature at which the steam from the turbine is condensed,  $T_{cond,in}$  being the temperature of the air entering the condenser and  $T_{cond,out}$  being the temperature of the air leaving the condenser.

For air-cooled condensers, with finned coils and forced convection, the overall heat transfer coefficient is between 15 and 30  $\text{W}/\text{m}^2\text{K}$  [Granryd et al. 2009].

In this case, the overall heat exchanger coefficient was set at:  $U_{cond} = 26 \text{ W}/\text{m}^2\text{K}$  (from previous calculations made by CNIM).

The temperature of the air entering the air condenser was calculated as the design ambient temperature,  $T_{cond,in} = 10^\circ\text{C}$ .

The total heat exchanged in the air condenser is calculated in order to have 2°C sub-cooling at the outlet of the condenser.

The air temperature leaving the condenser is calculated with the following formula:

$$Q_{cond} = m_{steam} (h_{in} - h_{out}) = m_{air} C_{p,air} (T_{cond,in} - T_{cond,out})$$

Where  $Cp_{air}$  is the air heat capacity (1.004 kJ/kg.K) the air mass flow was set  $865.18 \text{Nm}^3/\text{s}$  (or  $1119 \text{kg/s}$ ), from previous air condenser specifications.

It gives, in the end, the following total heat exchanger area:  $A_{tot} = 33\ 111 \text{ m}^2$ .

For partial loads, the air mass-flows and (UA) coefficient for the different loads were approximated as follow:

$$m_{load} = m_{nominal} \left( \frac{P_{load}}{P_{nominal}} \right)^{0.7}$$

$$(UA)_{load} = (UA)_{nominal} \left( \frac{P_{load}}{P_{nominal}} \right)^{0.7}$$

where P is the load, (UA) is the overall heat transfer coefficient times the heat exchanger area. "Load" stands for partial load.

Then, the saturation temperature (for partial loads) was calculated using the equations [Granryd et al. 2009]:

$$\dot{Q}_{cond} = U_{cond} A_{tot} \vartheta_m$$

$$\vartheta_m = \frac{\vartheta_{in} - \vartheta_{out}}{\ln(\vartheta_{in}/\vartheta_{out})}$$

$$\vartheta_{in} = T_{sat} - T_{cond,in}$$

$$\vartheta_{out} = T_{sat} - T_{cond,out}.$$

All those equations put together give:

$$T_{sat} = \frac{T_{in} - T_{out} \exp\left(\frac{UA}{m_{air} Cp_{air}}\right)}{1 - \exp\left(\frac{UA}{m_{air} Cp_{air}}\right)}$$

Finally, knowing the saturation temperature, one can calculate the saturation pressure, that is also the turbine exhaust pressure.

## f Condensate tank

The volume of the condensate tank was calculated in order to be able to store the water from the storage. It was estimated (by calculation made previously by CNIM Solar Division) to be  $120 \text{ m}^3$ .

The condensate tank was modelled as an open pre-heater, and as such the condensate mass-flow leaving the tank was calculated as the sum of all the mass flows entering the tank. The enthalpy of the condensates leaving the tank was calculated as follow:

$$m_{out} h_{out} = \sum m_{in} h_{in} - \dot{Q}_{losses}$$

The thermal losses calculation is described in paragraph 12.

### **g- Deaerator**

The deaerator uses the steam from the second bleed to heat the condensate and remove the dissolved gases (such as the oxygen).

The volume of the deaerator was calculated previously by CNIM - Solar Division and was set at 40 m<sup>3</sup>. It was modelled as an open pre-heater with a temperature set at 150°C. The pressure is the saturation pressure. In reality, the pressure (and temperature) in the deaerator is set with a steam mass-flow coming from the high-pressure drum. The pressure must always be higher than 1 bar otherwise the deaerator does not work properly.

The pressure level of the second bleed in the turbine can also determine the pressure of the deaerator, as long as it remains above 1 bar.

The inlet steam mass-flow is set as the mass-flow from the second bleed.

The outlet mass-flow and enthalpy were calculated as in the condensate tank case, the calculation of the thermal losses is described in section V.12.

$$m_{cond,out} = \sum m_{in} - \sum m_{out}$$

$$m_{cond,out} h_{cond,out} = \sum m_{in} h_{in} - \sum m_{out} h_{out} - Q_{losses}$$

Where the index “cond,out” stands for the condensates leaving the deaerator.

### **h- Pre-heaters**

One high-pressure and four low-pressure closed pre-heaters were also modelled. The high-pressure one uses the steam from the first bleed to heat the condensates just before they enter the solar field. The inlet steam mass-flow and pressure are set as the mass-flow and pressure of the steam from the first bleed.

The low-pressure pre-heaters use the steam from the third bleed, or some steam from the turbine, or from the turbine outlet, or from the deaerator to pre-heat the condensates before they enter the deaerator. The mass-flow and pressure of the steam from the third bleed is set by the turbine data. The other inlet mass-flows are set to 1 kg/h for nominal load, and decrease proportionally with the load.

In all the cases, the cold condensates leaving the pre-heaters are set to be saturated liquid at inlet steam pressure. The enthalpies of the hot condensates  $h_{cond,out}$  leaving the pre-heaters are calculated as follow:

$$m_{cond}(h_{cond,out} - h_{cond,in}) = m_{steam}(h_{steam,in} - h_{liq,out})$$

### **i- Drums**

There are two drums in the system that are used as mixing tanks for steam coming from different parts of the system and entering the turbine or the deaerator.

Those drums were modelled as open pre-heaters, the mass-flow of the steam leaving the drum being the sum of all the mass flows entering the drum, and the enthalpy being calculated as follow.

$$m_{out} h_{out} = \sum m_{in} h_{in}$$

Thermal losses were not taken into account.

### j- Storage (charging / discharging)

The evolution of the pressure in the steam accumulators was modelled in another Excel sheet called "Stockage".

During the night, the pressure in the steam accumulators decreases because of thermal losses. The decrease is calculated with the results obtained from the steam accumulator model. It gives the following equation for the pressure decrease with the time:

$$P(t + \Delta t) = P(t) - 0.0003\Delta t$$

$\Delta t$  is the time step of the calculation, equal to 10 minutes (or 600s).

When the thermal load is higher than the nominal power, the exceeding steam mass-flow is calculated in the Excel sheet "Bilan de cycle" and integrated in the "Stockage" sheet. As long as the pressure in the steam accumulators is lower than the nominal pressure 70 bars, the accumulators are charged and the accumulator pressure increases with the mass of steam that is added according to the following equation:

$$P(M + \Delta M) = P(M) + \frac{0.0674}{1.8^2} (2M \cdot \Delta M + \Delta M^2) + \frac{1.5449}{1.8} \Delta M$$

Where  $M$  is the sum of all the mass-flows that were added previously (it is a sum of kg/s, even if it does not have much physical sense, it is easier for the simulation; an equivalent equation can also be given for tons of steam) and  $\Delta M$  is the mass-flow at the time  $t$ .

The total amount of steam that can be added in the accumulator in order to reach 70 bars is 36.65kg/s (or 21.99 tons, as the time step is 600s) per accumulator.

During the charging process, the different tanks are charged one after another, which means that the first accumulator is first filled in. When it is full, the second accumulator is filled in, and so on.

When all the steam accumulators are full, or when the thermal power is no longer higher than the nominal power, the steam is stored in the accumulators and nothing is released as long as the pressure in the accumulators is lower than or equal to the pressure in the system.

During this time, the pressure in the steam accumulators decreases because of thermal losses, according to the following equation:

$$P(t + \Delta t) = P(t) - 0.0014\Delta t$$

When the thermal power becomes lower than the nominal thermal power, and the pressure in the system becomes lower than the pressure in the accumulators, the accumulators are discharged, in order to maintain a constant mass-flow in the turbine inlet (61000 kg/h).

All the accumulators are discharged at the same time, if they have the same pressure. If one of the accumulators is partially charged (while at least one is fully charged) before the discharging process, it is discharged when its pressure is equal to the pressure in the other accumulators. If the first accumulator is partially charged before the discharging process, then it is discharged only when its pressure is equal to the pressure in the system.

The steam leaving the accumulators is saturated at the accumulator pressure. The accumulator pressure decreases with the amount of steam that leaves the tanks, according to the following equation:

$$P(M + \Delta M) = P(M) + \frac{0.0767}{1.8^2} (2M \cdot \Delta M + \Delta M^2) - \frac{4.7291}{1.8} \Delta M$$

The total amount of steam that can be taken from the accumulator in order to reach 12 bars is 30 kg/s (or 18 tons, as the time step is 600s) per accumulator.

The electrical power that is produced with the steam from the storage is calculated in another Excel sheet called “Déstockage”. In this sheet, only the turbine is modelled as in the sheet “Bilan de cycle”, but with no mass-flows in the bleeds.

An option in the “Stockage” sheet allows choosing the number of steam accumulator used in the system.

The steam-accumulators are discharged as soon as the circuit pressure becomes lower than the accumulators’ pressure, to maintain a constant electricity production. There is no need to wait for the electricity price peak in the evening, because the electricity production is sold at a constant price, 0.35 €/kWhe, and not at the market price.

### **k- Pumps**

Three pumps are used in the system: one condensate pump, one recirculation pump and one feedwater pump. The pumps electrical consumption was not calculated, as all the electricity that is produced is sold on the market at 35 c€/kWhe. The pumps and air condenser consumption is taken from the electrical network at the market price.

The work given to the condensate by the pumps was calculated with the following equations, from [Havtun et al. 2011].

$$\dot{W}_p = \eta_t \dot{E}_p = m_{cond} (h_{out} - h_{in})$$

$$\dot{E}_p = \frac{\dot{V}_{cond} \Delta P}{\eta_t} (1 + s)$$

Where  $\dot{E}_p$  is the pump power requirement (W),  $\dot{V}_{cond}$  is the condensates volumetric flow rate ( $m^3/s$ ),  $\Delta P$  is the pump pressure increase (Pa),  $\eta_t$  is the total pump efficiency and s is an additional factor to ensure that the motor is not overloaded.

The different parameters were set at the following values (depending on the pump):

$$\begin{aligned}\eta_t &= 0.65 - 0.71 \\ s &= 0.1 - 0.2\end{aligned}$$

The enthalpy of the condensates leaving the pump was thus calculated using the two previous formulas.

### **l- Thermal losses**

The thermal losses were calculated in another Excel sheet called “Pertes thermiques”. The estimation of the thermal losses is necessary to be able to calculate the energy needed to pre-heat the whole system after the night. Thermal losses were also integrated to the thermodynamic cycle on the “Bilan de cycle” sheet, in the deaerator and condensate tank modelling.

To calculate the energy loss during the night, the thermal losses were calculated at different spots of the circuit: in the expansion tank, in the condensate tank, in the deaerator, in the steam accumulators, in the solar field (receiver tube), in the high-pressure pipe from the solar field and in the low-pressure pipe going to the solar field.

#### **Thermal losses in pipes**

All the pipes were modelled as cylinders with conduction in several layers (metal and insulator) and convection inside (when there is a mass flow) and outside the pipe. The thermal resistances for each phenomenon were calculated.

The thermal resistance is defined as follow:

$$\Phi_{losses} = \frac{1}{R_{th}}(T_{in} - T_{out})$$

where  $R_{th}$  is the thermal resistance of a layer,  $\Phi_{losses}$  is the heat flux that is lost,  $T_{in}$  is the inner temperature and  $T_{out}$  is the outer temperature.

The conduction equation for a system of length  $dz$  with a cylindrical symmetry is given by [Taine et al. 2008]:

$$d\Phi = -\lambda \frac{dT}{dr} 2\pi r dz$$

where  $\lambda$  is the thermal conductivity (W/mK) and  $r$  is the radial distance from the centre of the cylinder.

When integrating this equation, it gives:

$$(T_{in} - T_{out}) = \frac{1}{\lambda 2\pi dz} \ln\left(\frac{r_{out}}{r_{in}}\right) d\Phi$$

where  $r_{in}$  is the layer inner radius, and  $r_{out}$  is the layer outer radius.

So the thermal resistance for the conduction in a cylindrical layer of length  $dz$  and comprised between  $r_{in}$  and  $r_{out}$  is:

$$R_{th} = \frac{1}{\lambda 2\pi dz} \ln\left(\frac{r_{out}}{r_{in}}\right)$$

The equation for convection is given by:

$$d\Phi = h^{conv}(T_{in} - T_{out})2\pi r dz$$

where  $h^{conv}$  is the convection coefficient (W/m<sup>2</sup>K).

The thermal resistance for the convection outside (or inside) a cylindrical pipe of length  $dz$  and radius  $r$  is given by:

$$R_{th} = \frac{1}{h^{conv} 2\pi r dz}$$

The pipe is modelled as shown in figure V.3.

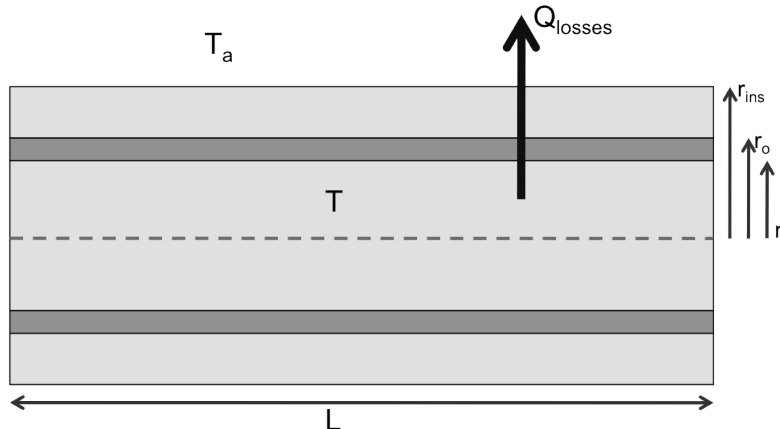


Figure V.3: Model of a pipe

The several thermal resistances are thus in series, in an electrical model of the system and can be added to calculate the overall thermal resistance.

It gives:

$$R_{th,tot}^{cyl} = \frac{1}{h_{in}^{conv} 2\pi L r_i} + \frac{1}{2\pi L \lambda_{metal}} \ln\left(\frac{r_o}{r_i}\right) + \frac{1}{2\pi L \lambda_{insulator}} \ln\left(\frac{r_{ins}}{r_o}\right) + \frac{1}{h_{out}^{conv} 2\pi L r_{ins}}$$

Finally, the thermal losses in the pipes are given by:

$$\Phi_{losses}^{\text{pipe}} = \frac{1}{R_{th,tot}^{cyl}} (T - T_a)$$

### Thermal losses in tanks

All the tanks are modeled as cylinders with one half-sphere at each end, as shown in figure V.4.

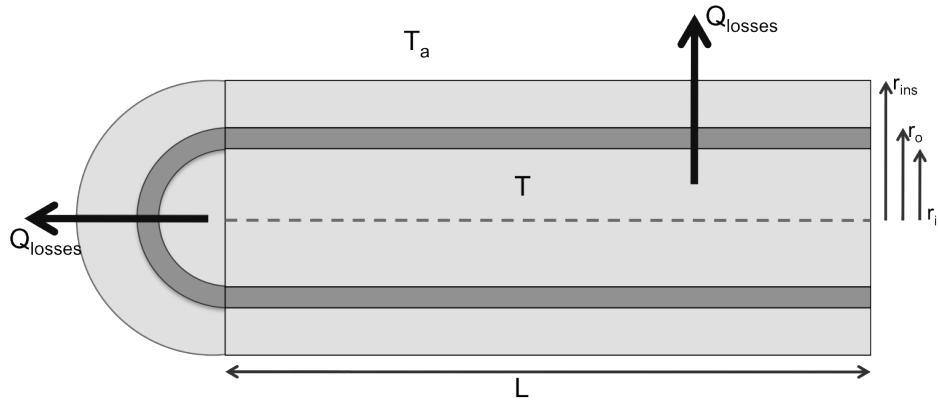


Figure V.4: Representation of a tank

The calculation for the overall thermal resistance in the cylindrical part is the same as what was done in previous section.

The calculation for the spherical parts is led in the same way.

The conduction equation in a sphere is given by [Taine et al. 2008]:

$$d\Phi = -\lambda \frac{dT}{dr} 4\pi r^2$$

When integrating this equation between two radiuses, it gives:

$$(T_{in} - T_{out}) = \frac{1}{\lambda 4\pi} \left[ \frac{1}{r_{in}} - \frac{1}{r_{out}} \right] d\Phi$$

The expression of the thermal resistance for the conduction in a sphere is thus:

$$R_{th} = \frac{1}{\lambda 4\pi} \left[ \frac{1}{r_{in}} - \frac{1}{r_{out}} \right]$$

The equation for the convection outside a sphere is:  $d\Phi = h^{conv}(T_{in} - T_{out})4\pi r^2$

And the expression of the thermal resistance for the convection outside a sphere is:  $R_{th} = \frac{1}{h^{conv} 4\pi r^2}$

With the same reasoning as for the cylindrical case, the overall thermal resistance for the spherical part is calculated as follow:

$$R_{th,tot}^{sph} = \frac{1}{4\pi\lambda_{metal}} \left[ \frac{1}{r_i} - \frac{1}{r_o} \right] + \frac{1}{4\pi\lambda_{insulator}} \left[ \frac{1}{r_o} - \frac{1}{r_{ins}} \right] + \frac{1}{h_{out}^{conv} 4\pi r_{ins}^2}$$

In the tanks, the energy losses can go through either the cylindrical part, or the spherical part. Those two parts are thus in parallel in an electrical model of the tank, and the overall thermal resistance for the tank is given by:

$$R_{th,tot}^{\text{tank}} = R_{th,tot}^{sph} // R_{th,tot}^{cyl} = \frac{R_{th,tot}^{sph} R_{th,tot}^{cyl}}{R_{th,tot}^{sph} + R_{th,tot}^{cyl}}$$

Finally, the thermal losses in the tanks are given by:

$$\Phi_{losses}^{\text{tank}} = \frac{1}{R_{th,tot}^{\text{tank}}} (T - T_a)$$

### Thermal losses in the solar field

The shape of the receiver tube casing (represented Figure V.5) made it more difficult to calculate the thermal losses.

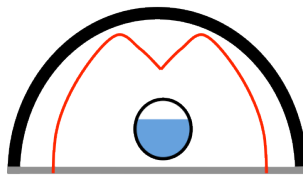
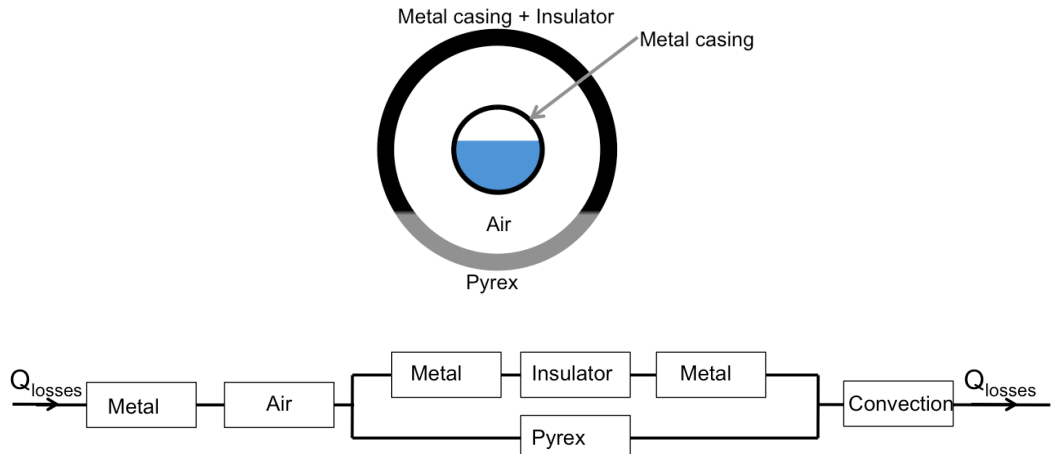


Figure V.5: Casing of the receiver tube

It was decided to model the receiver casing as a cylinder with two different areas (made of different materials), separated from the receiver tube by an air layer. The model of the receiver is given in figure V.6, as well as the electrical and simple equivalent. It was decided to neglect the solid angles and to consider a very simple model, as the influence of this thermal resistance is quite low in the performances calculations.



*Figure V.6: Modelling of the receiver tube and casing, and its electrical equivalent*

All the thermal resistances are calculated as was described in section V.11.a.

#### Calculation of convective heat transfer coefficients

For external convection, it was decided to use equations for a flow along a circular cylinder. [Taine et al. 2008] gives the following relation, /Knudsen & Katz, 1958/:

$$Nu_D = \frac{\bar{h}D}{\lambda} = C Re_D^n$$

Where  $Nu_D$  is the Nusselt number based on the cylinder diameter,  $\bar{h}$  is the convective heat transfer coefficient, D is the cylinder diameter,  $\lambda$  is the thermal conductivity (W/mK) and  $Re_D$  is the Reynolds number based on the cylinder diameter.

The coefficients C and n can be determined knowing the Reynolds number and the composition of the external flow, according to table V.3.

*Table V.3: Coefficients for Knudsen & Katz equation*

$Re_D$	n	C	
		Gas	Liquid
1 to 4	0,33	0,891	$0,989Pr^{1/3}$
4 to 40	0,385	0,821	$0,911Pr^{1/3}$
40 to 4 000	0,466	0,615	$0,683Pr^{1/3}$
4 000 to 40 000	0,618	0,174	$0,193Pr^{1/3}$
40 000 to 250 000	0,805	0,0239	$0,0266Pr^{1/3}$

The expression for the Reynolds number is given by:  $Re_D = \frac{\rho v D}{\mu}$

Where  $\rho$  is the fluid density ( $\text{kg}/\text{m}^3$ ), v is the flow speed ( $\text{m}/\text{s}$ ), D is the cylinder diameter (m) and  $\mu$  is the dynamic viscosity ( $\text{N}/\text{sm}^2$ ).

The Prandtl number Pr expression is:  $Pr = \frac{\mu C_p}{\lambda}$  where  $C_p$  is the specific heat of the fluid ( $\text{kJ}/\text{kgK}$ ).

For internal convection, it was decided to use the equation for turbulent flows given by [Taine et al. 2008] /Dittus & Boelter 1930/:

$$Nu_{Dh} = 0.023 Re_{Dh}^{0.8} Pr^{0.4}$$

This equation is valid for  $0.7 \leq Pr \leq 120$  and  $10^4 \leq Re_{Dh} \leq 1.2 \cdot 10^5$ .

Where Dh is the hydraulic diameter, given by the cylinder diameter in this case.

The flow speed is calculated using the following relation:  $m_{fluid} = \rho A v_{fluid}$  where  $v_{fluid}$  is the flow speed (m/s) and  $m_{fluid}$  is the fluid mass-flow (kg/s).

### **m- Pressure losses**

Pressure losses were calculated in the solar field by a program made by CNIM and integrated to the thermodynamic cycle balance in the sheet “Bilan de cycle”.

### **n- Pre-heating**

To obtain a performance calculation as accurate as possible, it is necessary to estimate the energy needed to pre-heat the system. It is the amount of energy needed to obtain 12 bars in the system, after the system cooling during the night.

It is thus first necessary to calculate the energy lost during the night, in all the parts of the system (deaerator, condensate tank, expansion tank, pipes and solar field).

In this purpose, the evolution of the temperature with the time during the night was studied. [Havtun et al. 2011] gives the following equation for the evolution of the temperature in a building during a transient situation.

$$mCp \frac{dT}{dt} = \dot{Q}_{sun} - \dot{Q}_{losses} = \dot{Q}_{sun} - \frac{1}{R_{th}}(T - T_0) \quad (V.1)$$

During the night, the energy received from the sun is equal to 0 and thus the equation becomes:

$$mCp \frac{dT}{dt} = \frac{1}{R_{th}}(T - T_0)$$

After integration, it gives:  $T(t) = T_a + (T_0 - T_a) \exp\left(-\frac{t}{mCpR_{th}}\right)$

Then, the evolution of temperature during the day was studied, this time with some energy received from the Sun.

After integration of equation (V.1), it gives:

$$T(t) = T_a + R_{th} \dot{Q}_{sun} + (T_0 - T_a + R_{th} \dot{Q}_{sun}) \exp\left(-\frac{t}{mCpR_{th}}\right)$$

With those two equations, the evolution of the temperature in the circuit was studied, during the night and then during the early day, when the system is pre-heated.

The pressure in the expansion tank being the saturation pressure, the pre-heating energy is calculated as the amount of energy from the sun that is needed to reach a pressure of 12 bars in the expansion tank.

A simulation is run during one day, calculating the evolution of pressure and temperature in all the tanks and in the pipes and solar field with a time step of 600 seconds.

When a thermal power is available, a mass flow is set to 10 kg/s to pre-heat the system.

The pre-heating energy needed was calculated for several days and references values were set for winter, summer and spring/autumn days, to be integrated to the performance calculations.

## 2- Results

A simulation was run, to calculate the electrical power that is produced every 10 minutes, with the method described above. The slope at the plant location was first not taken into account. The starting point, and stoping point for the turbine was set at 20 bars, which represents approximately 18% of nominal load. The simulation was run with 26 lines of 5 modules and 3 steam accumulators.

The thermodynamic cycle efficiency for nominal load is **25.46%** and the nominal electrical production is **9 012 kWe**.

The company asked that those results were not made public. All the following results will thus be given as dimensionless numbers, divided by the thermal power that was given in the business plan made for the Llo project  $P_{BP}$ , and that is the value of the annual electricity production that needs to be reached or exceeded in order to be able to launch the project.

The following results, described in Table V.4, were obtained.

*Table V.4: Monthly electrical energy production with and without storage (dimensionless results, compared to  $P_{BP}$ )*

Month	Total electricity production ( $\times 10^3$ )	Electricity production without storage ( $\times 10^3$ )	Electricity production from storage ( $\times 10^3$ )
1	38,67	38,49	0
2	46,25	46,42	0
3	100,30	95,88	4,42
4	83,94	78,21	5,73
5	121,27	111,16	10,11
6	126,61	116,12	10,49
7	144,55	131,69	12,86
8	117,62	108,89	8,73
9	84,44	79,56	4,88
10	42,01	41,59	0,42
11	31,07	30,66	0,41
12	22,76	22,79	0
<b>Total (x1)</b>	<b>0,959</b>	<b>0,901</b>	<b>0,058</b>

It gives the following graph, represented on figure V.7.

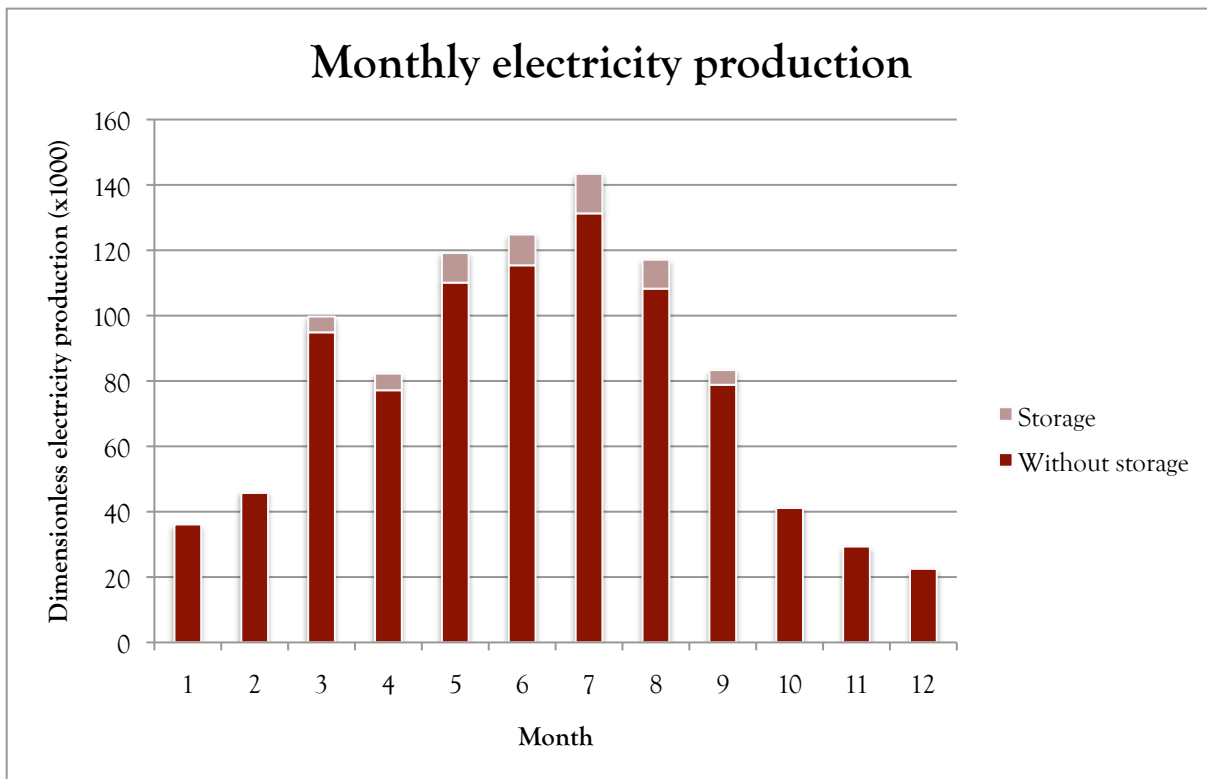


*Figure V.7: Monthly electrical production with and without storage.*

In this case, the storage was used **121 days** a year with at least one accumulator fully charged (86 days during which the three accumulators were fully charged). The turbine operated during **2333 hours a year**. And the total amount of energy stored into the accumulators was  **$0.332P_{BP}$  GWh**. The efficiency of the steam accumulators was thus of **17.5%**.

### 3- Discussion

The results that were obtained were not satisfying, even though the reasoning was checked and validated by the team. The problem was that the business plan was based on the value for the annual energy production  $P_{BP}$ , while the value that was obtained with the simulation was  **$0.959P_{BP}$** .

It was thus decided to study different solutions to improve the annual production, without increasing the costs.

First, the influence of the slope at the plant location was studied. Then it was decided to modify the turbine operation conditions.

The influence of every parameter was studied, as well as their combined influence on the annual production. The results are given in next section.

## VI- Results improvement

### 1- Influence of the location slope

A rule of thumb says that the best inclination for solar panels located at latitude  $\lambda$  is precisely the angle of the latitude  $\lambda$ . Indeed the geometric efficiency increases with the inclination of the panel, as the cosine effect is reduced. As there is a slight slope at the plant location, calculations were made to take it into account, to see its influence on the annual energy production.

The average slope at Llo is calculated on a topographic map and is set as  $\varepsilon_{LLO}$  and is equal to  $4.21^\circ$ .

In order to obtain the useful heat from the solar field, taking into account the slope, it is necessary to modify the program made by CNIM calculating the thermal power.

The program calculates the thermal power knowing the following parameters:

- Azimuth angle,  $\varphi$
- Elevation angle,  $\theta$
- DNI ( $\text{W/m}^2$ )
- Ambient temperature
- Wind speed

Knowing the two first parameters, it calculates two other angles: the angle between the projection of the sun and the vertical in the North-South plane  $\alpha$  and in the East-West plane  $\beta$ . All those angles are represented in figure VI.1.

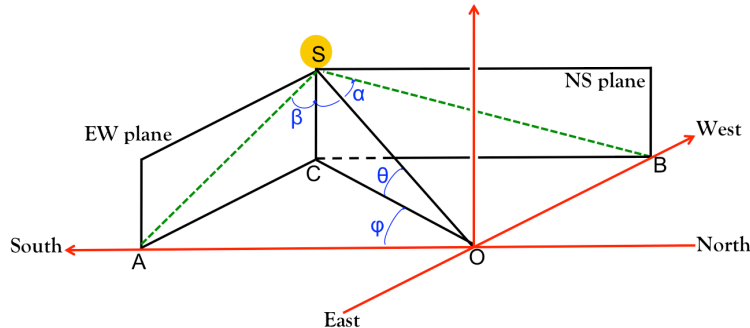


*Figure VI.1: Definition of the angles used in the thermal power calculation program*

Taking into account the slope at the location site is equivalent to change the coordinate system, rotating it by the angle  $\varepsilon_{LLO}$ , as shown in figure VI.2.

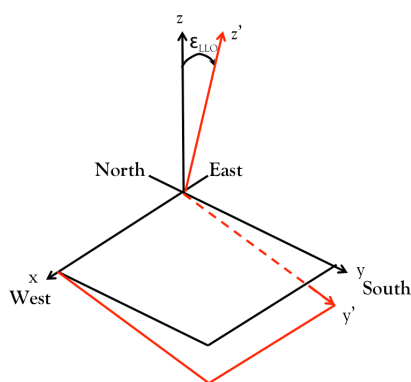


*Figure VI.2: Change of spherical coordinates system*

The equations to change the spherical coordinates, given by [Paturel 2007], use angles that are measured from the axis x. The azimuth angle thus evolves between 0 and  $\pi$ . In real conditions, the azimuth angle that is measured every day is calculated from the axis y (from the South). The azimuth angle thus evolves between  $-\pi/2$  and  $\pi/2$ .

The calculations were first made using the notation of [Paturel 2007], here using a \* to precise that it is not the notation used in real conditions. The change of variable is then done in the equations.

In a Cartesian coordinate system, and if one considers that the Sun is on a sphere of radius 1, the position of the Sun is given by:

$$\begin{aligned} X &= \cos\theta \cos\varphi \\ Y &= \cos\theta \sin\varphi \\ Z &= \sin\theta \end{aligned}$$

X,Y,Z being the coordinates on the axis x,y,z, as defined in figure VI.2.

[Paturel 2007] gives the following relations to change spherical coordinates.

$$\begin{bmatrix} X' \\ Y' \\ Z' \end{bmatrix} = \begin{bmatrix} 1 & 0 & 0 \\ 0 & \cos\epsilon_{LL0} & -\sin\epsilon_{LL0} \\ 0 & \sin\epsilon_{LL0} & \cos\epsilon_{LL0} \end{bmatrix} \begin{bmatrix} X \\ Y \\ Z \end{bmatrix}$$

Where the notations with the sign ' represent the notations in the new coordinate system.

This gives, using the equations of the coordinates in a Cartesian coordinate system and the equations of change of coordinate system:

$$\begin{aligned} X' &= \cos\theta' \cos\varphi' = \cos\theta \cos\varphi \\ Y' &= \cos\theta' \sin\varphi' = \cos\theta \sin\varphi \cos\epsilon_{LL0} - \sin\theta \sin\epsilon_{LL0} \\ Z' &= \sin\theta' = \cos\theta \sin\varphi \sin\epsilon_{LL0} + \sin\theta \cos\epsilon_{LL0} \end{aligned}$$

From these equations, it is possible to obtain relations for the azimuth and elevations angles in the new coordinates system:

$$\begin{aligned} \cos\theta' &= \sqrt{\cos^2\theta \cos^2\varphi^* + (\cos\theta \sin\varphi^* \cos\epsilon_{LL0} - \sin\theta \sin\epsilon_{LL0})^2} \\ \sin\theta' &= \cos\theta \sin\varphi^* \sin\epsilon_{LL0} + \sin\theta \cos\epsilon_{LL0} \\ \cos\varphi'^* &= \frac{\cos\theta \cos\varphi^*}{\sqrt{\cos^2\theta \cos^2\varphi^* + (\cos\theta \sin\varphi^* \cos\epsilon_{LL0} - \sin\theta \sin\epsilon_{LL0})^2}} \\ \sin\varphi'^* &= \frac{\cos\theta \sin\varphi^* \cos\epsilon_{LL0} - \sin\theta \sin\epsilon_{LL0}}{\sqrt{\cos^2\theta \cos^2\varphi^* + (\cos\theta \sin\varphi^* \cos\epsilon_{LL0} - \sin\theta \sin\epsilon_{LL0})^2}} \end{aligned}$$

The relation between the azimuth angle in [Paturel 2007], noted with a \*, and the azimuth angle that can be measured is:

$$\varphi^* = \frac{\pi}{2} - \varphi$$

The same goes with the new coordinate system:  $\varphi^* = \frac{\pi}{2} - \varphi'$

Using basic trigonometric relations, it is possible to obtain the following equations, for the azimuth and elevation angles in the new coordinates system.

$$\begin{aligned}\cos\theta' &= \sqrt{\cos^2\theta\sin^2\varphi + (\cos\theta\cos\varphi\cos\epsilon_{LLO} - \sin\theta\sin\epsilon_{LLO})^2} \\ \sin\theta' &= \cos\theta\cos\varphi\sin\epsilon_{LLO} + \sin\theta\cos\epsilon_{LLO} \\ \sin\varphi' &= \frac{\cos\theta\sin\varphi}{\sqrt{\cos^2\theta\sin^2\varphi + (\cos\theta\cos\varphi\cos\epsilon_{LLO} - \sin\theta\sin\epsilon_{LLO})^2}} \\ \cos\varphi' &= \frac{\cos\theta\cos\varphi\cos\epsilon_{LLO} - \sin\theta\sin\epsilon_{LLO}}{\sqrt{\cos^2\theta\sin^2\varphi + (\cos\theta\cos\varphi\cos\epsilon_{LLO} - \sin\theta\sin\epsilon_{LLO})^2}}\end{aligned}$$

With those four equations, it is possible to obtain the new azimuth and elevation angles. It is now necessary to calculate the angles  $\alpha$  and  $\beta$  in the new coordinates system.

With figure VI.1, one obtains the following relations:

$$\begin{aligned}\tan\alpha^{(i)} &= \frac{CB}{CS} = \frac{\cos\varphi^{(i)}}{\tan\theta^{(i)}} \\ \tan\beta^{(i)} &= \frac{CA}{CS} = \frac{\sin\varphi^{(i)}}{\tan\theta^{(i)}}\end{aligned}$$

The relations are the same in the new coordinates system. From the six last equations, it is possible to calculate the angles  $\alpha'$  and  $\beta'$ .

## Results

One can check that at solar noon, when  $\varphi=0$ , the equations for the azimuth and elevation angle in the new coordinates system give that:

$$\begin{aligned}\varphi' &= 0 \\ \theta' &= \theta + \epsilon_{LLO}\end{aligned}$$

The new elevation angle is the sum of the elevation angle without the slope and the slope, which is true in reality.

Another way of checking the values obtained was to model the change of coordinate system with Google Sketchup. The values that were measured with the 3D model were the same as the values that were calculated. Finally, a last checking was made comparing the total amount of thermal power available at Llo and at Murcia. The latitude difference between those two locations is equal to the slope at the plant location,  $4.21^\circ$ . Murcia is thus the equivalent location of Llo when taking into account the slope.

For a same time of sunshine, the available thermal power in Murcia is 86254 MWh a year, while it is 86449 MWh a year at Llo. The model to take into account the slope at the plant location is thus validated.

For the same conditions as in section V.1, but taking into account the location slope, the annual useful thermal energy obtained is: **86449 MWh**.

The improvement is thus quite significant (+14.4%), as is the increase of annual energy production, which is shown in section VI.3.

The results show that the thermal power increase is much more significant in the winter than in the summer, as can be seen in figure IV.3. For the same conditions at solar noon, one can calculate up to 60% more thermal power when taking into account the slope, compared to the original case, during the winter. During the summer, the increase is about 5%.

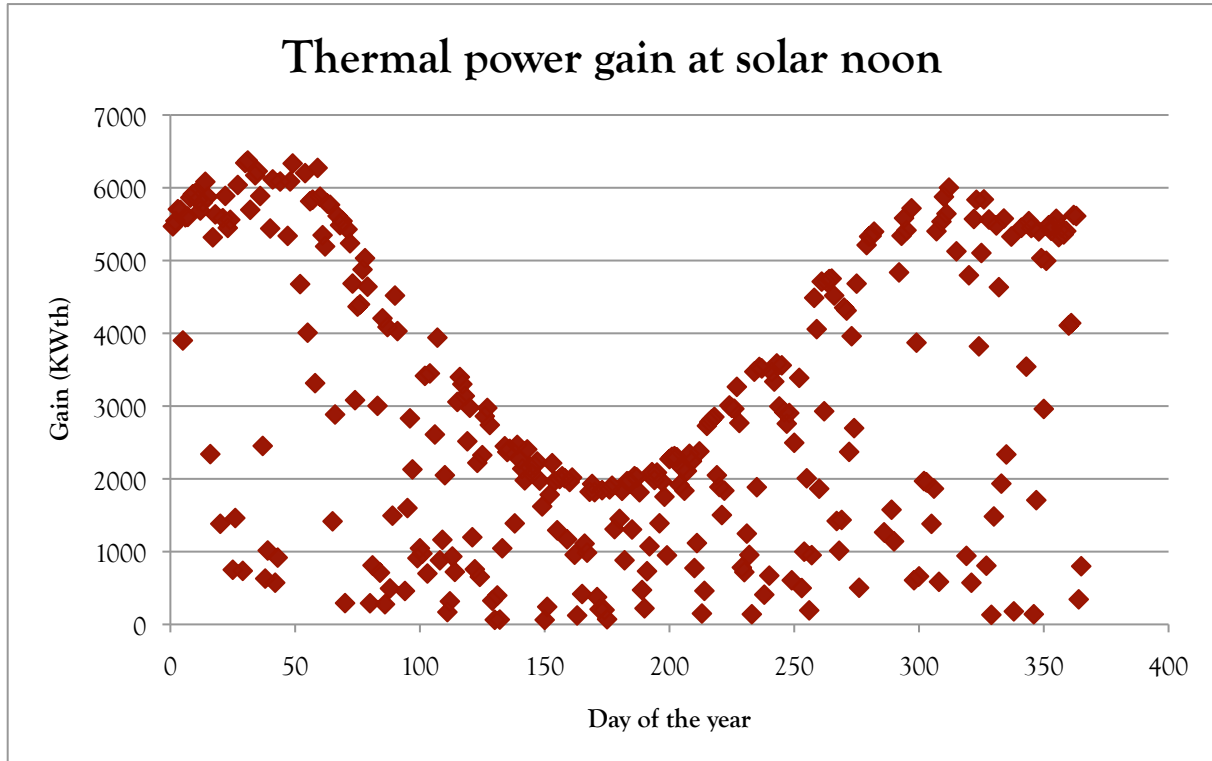


*Figure VI.3: Thermal-power gain with location slope at solar noon*

## 2- Modification of turbine operation conditions

The next solution that was considered to improve the annual energy production was to let the turbine operate up to 105% and/or down to 10% (12 bars) of its nominal load. The second option would mean to let the turbine operate down to the end of the day, which means that during a short time (about 1 hour), the turbine operates below its minimal partial load.

It required only small modifications of the program that are not described here, and led to the results described in section VI.3.

## 3- Influence of the weather conditions

It was then decided to estimate the influence of the weather conditions on the energy production. The cloudy or rainy days are already taken into account in the simulation, with the data from MeteoNorm. However, the effect of high winds, or of the frost on the mirrors during winter days might have a real influence on the electricity production.

The highest wind speed at which the plant can operate is 50 km/h. When studying the MeteoNorm data, one can see that this wind speed is never reached; the highest wind speed measured being 30 km/h. However, this data is made with hourly average measures, which means that the gusts are not really taken into account. The dominant wind in the region, called the Tramontane, is a North West wind with gusts that can reach easily 100 km/h.

It is not possible to take into account the effect of the wind with the information that is known.

In order to take into account the influence of the frost, it is necessary to know the number of days during which there is condensation or frost on the mirrors.

To have condensation on the mirrors, it is necessary to have a mirror surface temperature lower than the dew point.

The mirror surface temperature is calculated with the following balance equation (between convection and radiation):

$$h_{conv}(T - T_a) + \sigma(T^4 - T_{sky}^4) = 0$$

where  $h_{conv}$  is the convective heat transfer coefficient,  $T$  is the mirror surface temperature,  $T_a$  is the ambient temperature,  $T_{sky}$  is the sky temperature and  $\sigma$  is the Planck constant (equal to  $5.669 \times 10^{-8} \text{ W/m}^2\text{K}^4$ ).

For convenience, it is possible to write the same equation with  $h_r$  the radiation heat transfer coefficient.

$$h_{conv}(T - T_a) + h_r(T - T_{sky}) = 0$$

One can then define an average temperature  $T_m$  as:  $T_m = \frac{T + T_{sky}}{2}$ .

The radiation heat transfer coefficient can then be approximated by:  $h_r = 4\sigma T_m^3$

Which gives the following equation for the mirrors surface temperature:

$$T = \frac{h_{conv}T_a + h_rT_{sky}}{h_{conv} + h_r}$$

The sky temperature can be calculated with the following formula [RET Screen 2004] /Swinbank, 1963/:

$$L_{clear} = 5.31 \times 10^{-13} (T_a + 273,15)^6$$

where  $L_{clear}$  is the radiation coming from clear sky ( $\text{W/m}^2$ ).

The radiation from the sky can also be given by the Stephan-Boltzmann equation for a black body:

$$L_{sky} = \sigma(T_{sky} + 273,15)^4$$

From those two equations can be deduced the sky temperature.

The convective heat transfer coefficient is calculated with external forced convection equations.

It is then necessary to estimate the dew point, with the following equations /Magnus - Tetens/ [Wikipedia]:

$$T_r = \frac{b\alpha(T_a, RH)}{a - \alpha(T_a, RH)}$$

$$\alpha(T, RH) = \frac{aT_a}{b + T_a} + \ln RH$$

$$a = 17.27$$

$$b = 237.7 [\text{°C}]$$

Where RH is the relative humidity.

Finally, there is frost formation when the mirror surface temperature is lower than the dew point and below 0°C.

To estimate the energy losses in the electrical production because of the frost, the number of days during which there is frost on the mirrors was estimated. Then, the energy that is necessary to heat up the mirrors and melt the frost was calculated, depending on the frost thickness and the ambient temperature, with the following equation:

$$E_{melt} = M_{ice} C_{ice} (T_{melt} - T_a) + M_{ice} r$$

Where  $M_{ice}$  is the ice mass on the mirror (kg),  $C_{ice}$  is the ice specific heat (kJ/kgK),  $T_{melt}$  is the temperature at which the ice melts (0°C) and  $r$  is the latent heat of fusion (kJ/kg).

An average energy needed to melt the ice was determined for two frost thicknesses (2 and 5 mm). Then the electrical production was estimated, once the amount of global energy received by the mirrors is higher than the energy needed to melt the ice, and once the thermal energy received from the solar field is higher than the energy needed to preheat the circuit.

## Results

For an average frost thickness of 2mm, the annual electrical energy loss is equal to **1.28%** of annual electricity production.

For an average frost thickness of 5mm, the annual electrical energy loss is equal to **2.86%** of annual electricity production.

## 4 Load management

The electrical network manager, called RTE in France, can sometimes ask a renewable energy plant owner to shut down the plant, in order to ensure the balance between production and consumption as well as the security of the line.

This is called load management, and has to be taken into account in the electrical production calculation.

At the plant location, in Llo, it is theoretically not possible to connect new plants anymore to the electrical network. This is due to the fact that, during the spring months, the snowmelt increase the electrical production of all the dams situated in the Pyrenees, all around Llo. During those months, the line capacity is thus saturated, and it is not possible to connect another plant to it. Some projects are currently led to improve the electrical network, but it might take several years before the network can receive more plants.

However, as the line capacity is not saturated during the whole year, it was decided to grant a dispensation to CNIM and to allow the company connecting the new solar energy plant. The only condition was that during the snowmelt months, the solar plant might have to shut down during several days.

RTE calculations gave an average of 230 hours a year of shut down. Those hours are distributed over the snowmelt months (May, June, July), as well as September, as described in table VI.1.

*Table VI.1: Repartition of shutdown hours.*

	May	June		July	September
Number of hours during which the production is stopped during one day, ranked from longest to shortest	11	11	6	8	2
	11	11	6	3	2
	10	11	5	2	2
	9	11	5	1	1
	8	11	4		1
	6	10	4		
	6	9	3		
	4	9	3		
	4	8	3		
	1	7	1		
Sum	70	138		14	8

This table can be read as follow: there are two days in May during which the production must stop during 11 hours.

Knowing this, the production losses were estimated, with three different scenarios. In an optimistic scenario, the shutdown days are the days during which the production is the lowest. In a pessimistic scenario, the shutdown days are the days during which the production is the highest. And a median scenario studied the case in between.

In the optimistic and median scenarios, the shutdown hours are in the evening. In the pessimistic scenario, the shutdown hours are in the afternoon, during the production peak.

## Results

The results that were obtained with this calculation are given in table VI.2.

*Table VI.2: Electricity production losses with the load management*

Scenario	Optimistic	Median	Pessimistic
Losses (%)	8,02%	10,08%	11,57%

The losses are not negligible, as the snowmelt months correspond to the peak production months for the solar plant.

## 5- Results

Many simulations were then run, taking into account the different improvements that were described previously. The results are given in Table VI.1.

Then, it was decided to further detail the case where the slope is taken into account and the turbine operates down to 10% load, as it is the case that is the closest to what should be turbine operation in real life.

*Table VI.3: Dimensionless results of the simulations for different cases (compared to  $P_{BP}$ )*

	Thermal power from solar field	Electrical energy production without storage	Production from storage	Total electrical energy production	Number of hours of turbine operation (h)	Stored energy	Storage efficiency	Number of days of storage utilization (day)
Base Case	75558	0,901	0,058	0,959	2334	0,332	17,5%	121 (86)
Up to 105% load	75558	0,932	0,057	0,988	2334	0,269	21,2%	122 (88)
Down to 10% load	75558	0,903	0,058	0,962	2566	0,332	17,5%	121 (86)
105% load and 10% load	75558	0,934	0,057	0,991	2566	0,269	21,2%	122 (88)
Slope and 10% load	86449	1,020	0,063	1,083	2722	0,396	15,8%	152 (104)
105% and 10% and slope	86449	1,055	0,064	1,119	2722	0,323	19,7%	153 (104)

The number of days of storage utilisation represents the number of days in the year during which at least one accumulator is fully charged. The number in parenthesis represents the number of days during which the three accumulators are fully charged.

The following tables and figures present the result in the case where the slope is taken into account and the turbine operates down to 10%.

First, table VI.2 presents the monthly electrical production with and without storage.

*Table VI.4: Dimensionless monthly electrical energy production with and without storage*

Month	Total electrical energy production ( $\times 10^3$ )	Electrical energy production without storage ( $\times 10^3$ )	Electrical energy production from storage ( $\times 10^3$ )
1	52,08	52,08	0
2	59,24	58,26	0,97
3	115,31	107,61	7,69
4	91,04	85,16	5,88
5	128,69	118,84	9,85
6	133,87	123,83	10,04
7	151,65	139,61	12,04
8	126,92	118,02	8,90
9	94,33	88,45	5,88
10	51,90	50,42	1,48
11	42,59	42,59	0
12	34,98	34,98	0
Total	1,083	1,020	0,063

Figure VI.4 presents the monthly electrical energy production with and without storage.

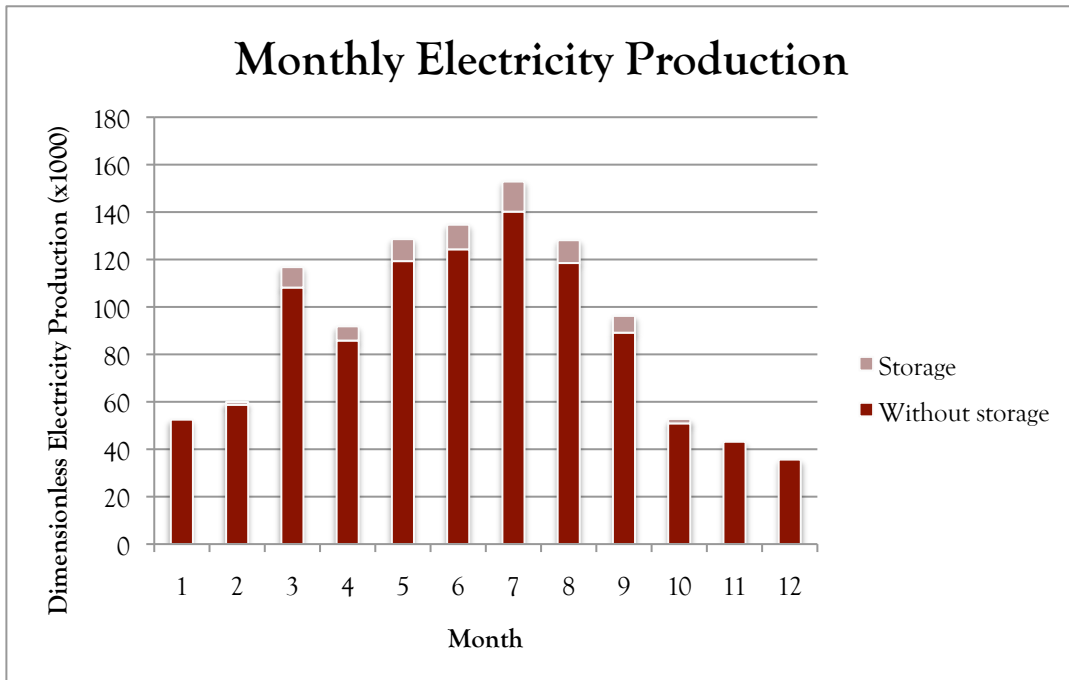


Figure VI.4: Monthly electrical energy production with and without storage.

Figure VI.5 gives the utilisation of the thermal power during the summer. The red area represents the total amount of energy that is directly sent to the turbine, the green area is the amount of energy that is stored during the day and the blue area is the energy that is lost.

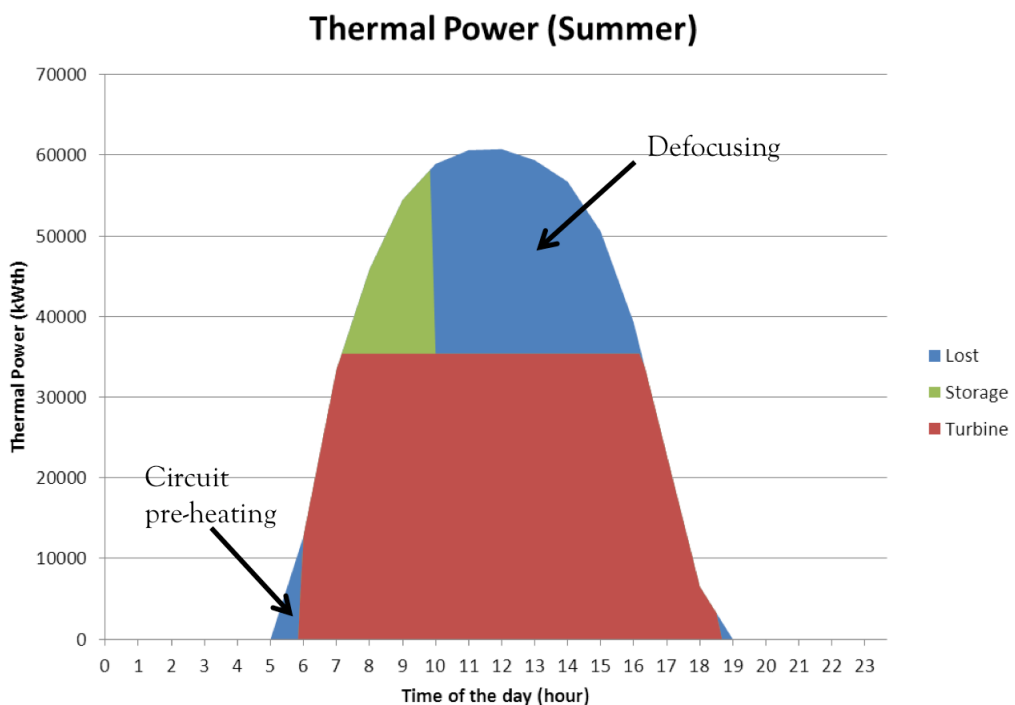
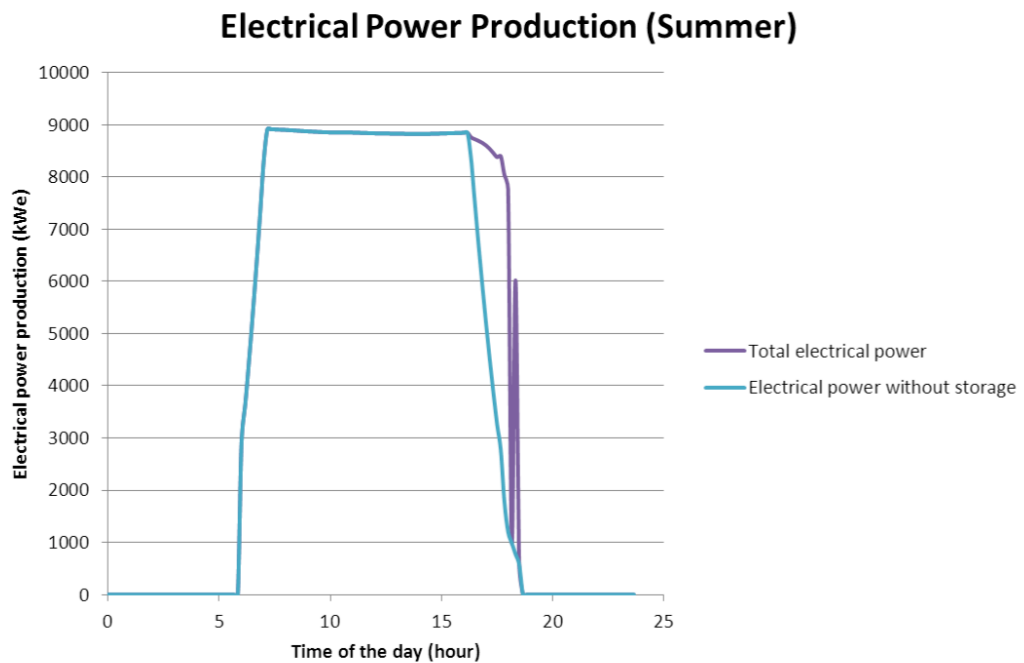


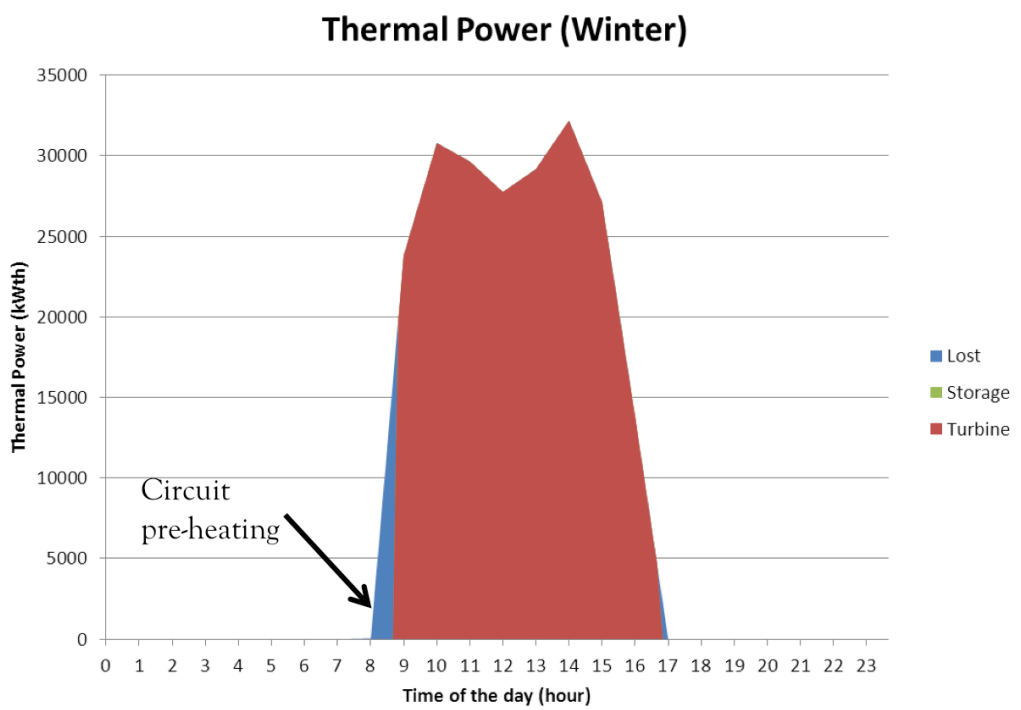
Figure VI.5: Utilisation of thermal power on a summer day.

Figure VI.6 gives the electrical production with and without storage on a summer day.



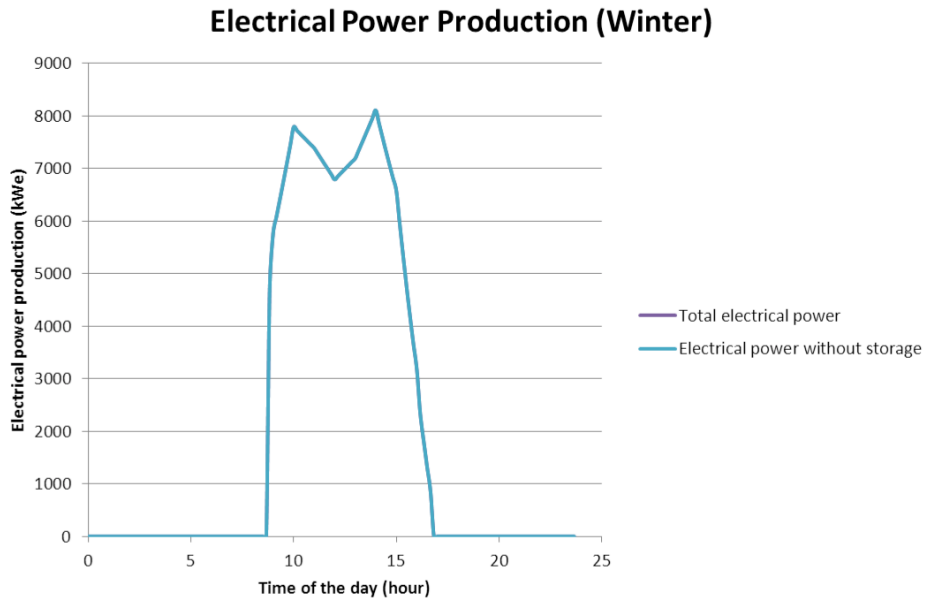
*Figure VI.6: Electrical power production with and without storage on a summer day*

Figure VI.7 shows the utilisation of the thermal power during a winter day.



*Figure VI.7: Utilisation of thermal power on a winter day*

Figure VI.8 gives the electrical production with and without storage on a winter day.



*Figure VI.8: Electrical power production with and without storage on a winter day*

Finally, table VI.5 presents the results when taking into account all the parameters (location slope, weather condition, load management).

*Table VI.5: Results summary (dimensionless annual production)*

Scenario	Electrical production (GWhe)
Base case	0,960
Ideal case (slope + 10%)	1,083
Ideal case + frost	1,069
Ideal case + load management	0,973
Ideal case + frost + load management	0,960

## 6- Discussion

Table VI.1 describes the influence of each way to improve the annual performance on the electrical production.

One can see that each way increased the annual electricity production, but for different reasons.

When allowing the turbine to operate down to 10% of nominal load, it increases the turbine annual operation time. As the turbine runs longer every day, it produces more energy. This can be checked in the results: the annual electricity production increases of 0.211% when the turbine runs down to 10% load.

The amount of energy stored in the accumulators is the same, as well as the amount of energy that is discharged from the storage.

When allowing the turbine to operate up to 105% of nominal load, the maximal power that can be reached is higher. For periods when the thermal power is higher than the nominal thermal power, the turbine produces more energy than in the base case, while less steam is stored in the accumulators (or later, only when the thermal power reaches 105% load). However, in this case, the turbine operation

time remains constant. The results in table VI.1 show that the annual electricity production increases by **2.96%**.

The slope has the greatest influence on the annual electricity production, as can be seen in Table VI.1. Indeed, the annual electricity production increases by **12.59%** when taking into account the slope at the plant location.

The slope decreases the optical losses on the solar field (most of all, the cosine effect), which thus increases the useful thermal power leaving the solar field. As the thermal power is higher, more power is produced at any time in the turbine, and in the meantime, more energy is stored in the accumulator. Those two phenomena explain the drastic increase in total energy production, as well as the increase in the turbine operation time (the 10% load is reached later every day), and the number of days during which the storage is used.

It was then decided to study the case where the slope is taken into account and the turbine runs down to 10% load. This case is the one that should be implemented in reality. Indeed, even though the slope that was calculated is an average, the slope always has an influence on the electricity production. When discussing with the turbines manufacturers, it appears that running the turbine down to 10% every day is not a problem if it does not last too long. However, running the turbine at 105% of nominal load is possible but difficult, not because of the turbine itself (one can specify this characteristic to the turbine manufacturer, in order to be able to run at 105% load), but because of the electrical network. Indeed, it would mean that the nominal production would no longer be 9MW, which creates problem when balancing the electricity production and consumption on the global network.

The results for this scenario are described in table VI.4 and figure VI.4 that present the same monthly production but in two different ways.

It shows that the electricity production follows the variation of the thermal energy from the solar field, which is maximal during the summer, and minimal during the winter.

Something else worth noting is the fact that the storage is useless during 5 autumn/winter months: January, February, October, November and December. Knowing that the price of an accumulator is about 1 million Euros, it shows that the number of accumulator must be optimized, taking into account the investment costs as well as the thermal energy available.

Finally, some graphs for some typical days were drawn, in order to show the utilisation of the thermal energy, as well as the production of electrical energy during a day.

Figure VI.5 shows how the thermal energy from the solar field is used during a sunny summer day. One can see that the system pre-heating lasts about 50 minutes, and that the nominal load is then reached in about 1 hour and 10 minutes. During the whole day, the turbine then operates at nominal power, while the available thermal energy keeps on increasing. This allows some energy storage. However, one can see that only a little share of the thermal energy that is not used in the turbine can be stored. When all of the accumulators are fully charged, the remaining thermal energy cannot be used in the turbine, nor stored. It is thus necessary to de-focus the mirrors on the solar field, to increase the optical losses and thus decrease the amount of thermal energy available, otherwise it would heat up the receiver and endanger the solar field. It means however that the resource cannot be fully exploited during sunny days in the summer, and this energy is lost. It could thus be interesting to optimize the size of the field, of the turbine and the number of accumulators to be able to take advantage of the whole energy resource.

Figure VI.6 shows the variation of electricity production during the same summer day.

It shows that as long as the turbine runs at nominal load, no storage is used, and the electricity production is maximal (9 MW). However, one can observe two phenomena here.

First, the maximal electricity production is less than 9 MW, while it should be equal to 9.012 MW, which is the nominal power. Then, one can see that the amount of electricity that is produced

throughout the day slightly decreases between the time when the nominal power is reached and noon. Then it slightly increases during the afternoon.

Those two phenomena are due to the fact that the air condenser was designed for a temperature of 10°C. As during the summer the temperature is higher than 10°C, the air condenser is less efficient, and thus the turbine exhaust pressure is higher. This leads to the fact that less electricity is produced.

As during the day, the temperature increases during the morning and early afternoon, and then decreases, it explains the variations of the electricity production during the day.

Then, when the thermal power becomes lower than the nominal load, the electricity production decreases quite quickly (about 2 hours), as the cycle efficiency decreases at partial load (between 25.46% at nominal load, and 21.21% at 20% load).

The energy from the storage permits to maintain the nominal mass flow in the turbine during about 1 hour and a half. It does not mean however that the nominal turbine power is maintained, as the turbine operates at the solar field pressure, which is then lower than the nominal pressure.

Then, the steam accumulators are emptied and the electricity production decreases quickly.

The rapid oscillation of the electricity production with the storage (violet) that can be seen on figure VI.6 should not be taken into account. It is due to the fact that in the simulation with Excel, the steam accumulators can be discharged only when the accumulators' pressure is higher than the expansion tank pressure. Because the data was discretised every 10 minutes, the pressure in the steam accumulators sometimes decreases faster than the pressure in the expansion tank, while in real life it should decrease at the same speed. In the simulation, it led to moments when the storage was not discharged anymore, before the pressure in the accumulator was once more higher than the pressure in the expansion tank, and this explains the variations that can be observed.

Figure VI.7 shows the thermal energy utilisation during a sunny winter day. One can see that the nominal load is never reached in this case, which explains the results described previously, about the fact that the storage is useless in autumn and winter. There is thus no energy stored, and all of the thermal energy available is used to produce electricity in the turbine.

The pre-heating lasts about 50 minutes, and some energy is lost at the end of the day, when the thermal power is lower than 10% of nominal load.

Figure VI.8 shows the variations of electricity production during the same winter day. One can see once more that the storage is not used, and that the variations of the electricity production follow the variations of the thermal energy available throughout the day.

It was decided to check the model with a known linear Fresnel plant operating in Spain: Puerto Errado 2 Thermosolar power plant, operated by Novatec. Their estimated annual electrical power production is 50 GWhe/year, with two 15 MW turbines and 302 000 m<sup>2</sup> mirrors surface. For a plant with the same characteristics, the simulation results gave 51.04 GWhe/year. This is 2% above the value from Novatec, knowing that the thermal power available was not perfectly known, nor the turbine data. It was thus decided that the model gave accurate enough results for the company.

To increase the reliability of the results, the influence of the frost on the mirrors was studied and it showed that the losses might reach up to 2.8% of the annual electricity production. Which is thus not negligible. However, these calculations were made with a very simple frost model, assuming that the frost layer is always the same, as well as the energy needed to heat up and defrost the mirrors. Other weather conditions should also be taken into account, such as the snow on the mirrors (what would be the optimum angle of the mirrors to ensure that the snow does not stay on the mirrors?) and the high

wind speeds. As the gusts were not taken into account in the weather data, it was not possible to estimate the production losses because of the too high wind speeds.

The influence of mandatory shutdowns forced by the electrical network manager was also estimated. The plant being situated in the Pyrenees where many dams are installed, the shutdown periods are during the snowmelt months, that is to say May, June and July. Those months are also the months of highest production for the solar plant.

This triggers annual electrical losses between **8 and 12%** of total production, depending on the scenario that is taken into account.

These losses might however be only temporary, before the electrical network is improved in the region, which might mean that the electrical production could be reduced during 5 to 10 years, and then could be improved during the following years. It might also be possible for the solar plant manager to negotiate with the dams owner in order to be able to produce solar energy during the days, during which the dams might store energy; the dams then being able to produce when the solar plant shuts down in the evenings. This solution would allow the network manager to take full profit from the solar resource in the region, as well as the hydropower resources.

Moreover, the periods after heavy rains were not taken into account by the data from RTE, it would then be possible to have longer shutdown periods during the year, if some sunny periods happen just after some very rainy ones.

As one might note, many other solutions to improve the efficiency of the solar plant were not studied. Among those solutions could be counted: the steam superheating, or reheating, the improvement of the storage method (with another technology, such as molten salts). The reason for not studying those solutions was first that the steam superheating was made impossible by the materials of the receiver tube (which cannot stand temperatures higher than 300°C). Another reason was finally that the aim of the company was designing a low costs plant built to meet the day load. The storage was only aimed at maintaining a constant production during the day, and ensuring a production slower decrease in the evening.

Finally, one should state that to increase the accuracy of the results, one should take into account the real dimensions for all the pipes and tanks in the thermal losses calculations and try to take into account the real slope (not an average slope). It would be also interesting to model the air condenser more accurately, as it seems that the calculations made under-estimated the condenser efficiency.

Being able to run dynamic simulations for some typical days would also increase the reliability of the results, as it would give more accurate estimation of the energy necessary to pre-heat the system, and energy that could be produced from the storage.

I would be also interesting to take into account the availability of the plant. This data is not known now, as no industrial power plant has ever been built by CNIM before.

## VII – Economic optimisation

### 1- Method

The costs for all the components of the power plant were estimated by CNIM before this thesis was performed. All those prices being confidential, it was not possible to report them in this thesis.

When studying the different prices given by all the suppliers, it is possible to draw a repartition of the investments costs, as shown in figure VII.1.

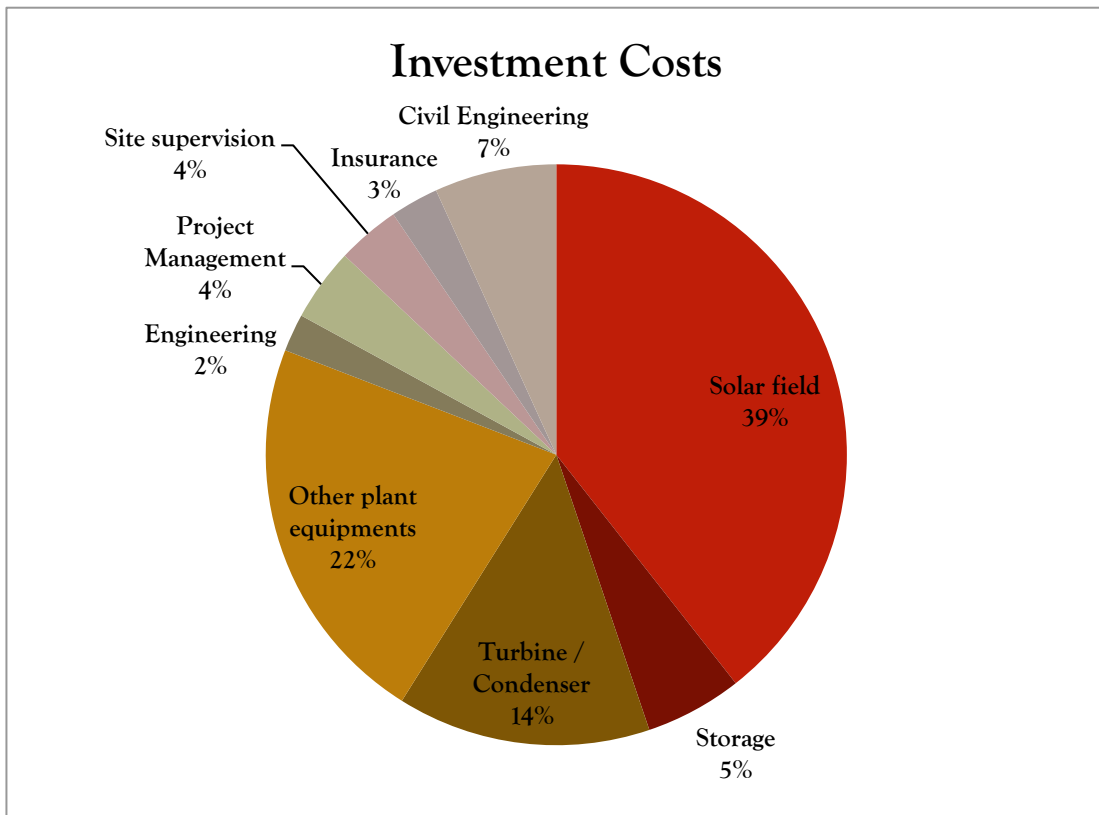


*Figure VII.1: Repartition of investments costs*

One can thus see that plant components fabrication, transport and commissioning represents 80% of the total investment price. Other human resources (engineers, project managers but no operators) represent 10%. The civil engineering is considered alone, as it is not done by CNIM but by a collaborator.

The same was done for the annual operation and maintenance costs, as shown in figure VII.2. One can see that the major part of the operation costs is due to human resources. Operation costs includes electricity (the pumps, motors electrical consumption being bought from the network at the market price, while the electrical production is sold at 35c€/kWh), and water consumption.

The components renewal costs are estimated over a time period of 15 years.

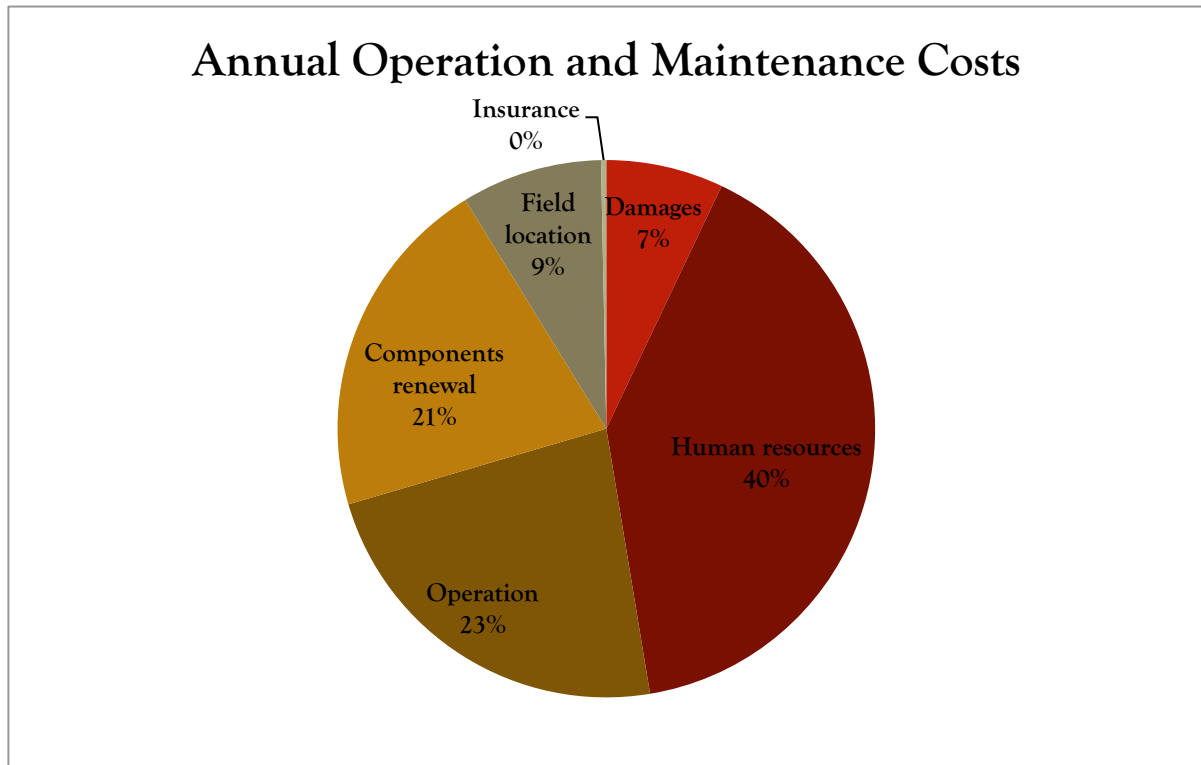


*Figure VII.2: Annual operation and maintenance costs repartition*

For both the investment costs and the operation and maintenance costs, the costs were divided between constant costs and variable costs, depending on the number of lines of mirrors, or on the number of steam accumulators.

Concerning the investment costs, it was estimated that the cost of the solar field (fabrication, transport and commissioning) and the storage accumulators was proportional to the number of lines or of accumulators respectively. The cost of the turbine and air condenser, when changing the rated power  $P$  of the turbine, was calculated as follow:

$$Cost(P) = Cost(P_{ref}) \left( \frac{P}{P_{ref}} \right)^{0.7}$$

Where  $P_{ref}$  is the reference rated power.

All the other costs were considered constant.

Concerning the operation and maintenance costs, the water, electricity and reactants (used to purify the water inside the circuit) consumption was considered proportional to the number of lines of mirrors. All the other costs were considered constant, even though it might be more accurate to modify the costs for the components renewal.

The investment costs, the operation and maintenance costs as well as the annual electricity production were then calculated for different plant design, with 26 to 31 mirrors lines, with 1 to 6 steam accumulators and with a 9MW and a 10MW turbine.

The best design was estimated comparing the payback times. The payback time is the period of time that is required for the return on an investment to repay the sum of the original investment [Wikipedia].

The payback time is calculated as:

$$PaybackTime[\text{year}] = \frac{\text{Investment}[\text{€}]}{\text{Production}[GWhe/\text{year}] \times \text{Electricity Price}[\text{€}/GWhe] - \text{Operation Costs}[\text{€}/\text{year}]}$$

## 2- Results

Table VII.1 and table VII.2 below describe the results obtained for a 9MW and a 10MW turbine.

*Table VII.1: Economic optimisation in the 9MW turbine case*

Dimensionless annual electricity production (GWhe/year)	Number of lines					
	26	27	28	29	30	31
Number of accumulators	1	1,03	1,06	1,08	1,10	1,12
	2	1,06	1,08	1,10	1,13	1,15
	3	1,08	1,10	1,13	1,15	1,17
	4	1,09	1,11	1,14	1,16	1,19
	5	1,11	1,13	1,15	1,18	1,21
	6	1,12	1,14	1,17	1,20	1,22

Payback time (year)	Number of lines					
	26	27	28	29	30	31
Number of accumulators	1	10,566	10,470	10,379	10,292	10,209
	2	10,517	10,413	10,315	10,221	10,131
	3	10,407	10,318	10,234	10,153	10,075
	4	10,544	10,420	10,303	10,191	10,085
	5	10,519	10,454	10,326	10,204	10,088
	6	10,607	10,471	10,342	10,220	10,104

The red cells show the optimal storage configuration for a specific solar field design. The text marked in green shows the case that was studied in all previous calculations.

In the 10 MW case, the simulations were run with the same data as in the 9 MW case, thus assuming that the same turbine runs at a higher nominal load (39 500 kWth instead of 35 400 kWth). This is not the real case, but it was necessary to make assumptions as no data was known concerning a 10 MW turbine.

*Table VII.2: Economic optimisation in the 10 MW turbine case*

Annual electricity production (GWhe/year)	Number of lines					
	26	27	28	29	30	31
Number of accumulators	1	1,08	1,11	1,13	1,15	1,18
	2	1,10	1,12	1,15	1,17	1,20
	3	1,09	1,12	1,14	1,16	1,18
	4	1,12	1,15	1,18	1,20	1,23
	5	1,14	1,16	1,19	1,22	1,25
						1,28

Payback time (year)	Number of lines					
	26	27	28	29	30	31
Number of accumulators	1	10,143	10,042	9,946	9,854	9,767
	2	10,163	10,049	9,941	9,838	9,740
	3	10,392	10,305	10,221	10,141	10,065
	4	10,274	10,135	10,003	9,878	9,759
	5	10,280	10,204	10,060	9,923	9,793
						9,600

### 3- Discussion

When comparing the results obtained during the economic optimisation simulations, one can observe that the best payback time for the project is **9.887 years** with a 9 MW turbine, and **9.600 years** with a 10 MW turbine, with a 31 lines solar field and 5 steam accumulators.

In the worst scenario, that is to say with the longest payback time, the payback time is 10.566 years. The difference between the shortest and longest payback times is about 1 year. For the solar field design and storage configuration that was considered in previous calculations (that is to say, 26 lines of 5 modules, 3 steam accumulators and a 9MW turbine), the payback time is **10.407 years**. It would thus be possible to decrease the payback time of half (0.52) a year with the same turbine, a solar field designed to occupy the whole location area (with 31 lines) and 5 steam accumulators. It would be possible to decrease the payback time of 0.8 year (about 9 months) with a solar field with 31 lines, 5 steam accumulators and a 10 MW turbine.

The payback time decrease is not really significant when changing the plant design, but it can be interesting to take it into account anyway.

As the data concerning the prices was only based on assumptions, it was decided to test the sensibility of the results with the prices evolution.

In the 9 MW turbine case, it was seen that an increase of 77% in the solar field price would change the best scenario from the [31 lines, 5 accumulators] scenario to the [26 lines, 3 accumulators scenario]. And in the 10 MW turbine case, it was seen that an increase of 82% in the solar field price would change the best scenario from the [31 lines, 5 accumulators] scenario to the [31 lines, 3 accumulators] scenario.

However, such increases in the solar field price remain quite unlikely.

It was then seen that a 30% increase in the storage price would change the best scenario from the [31 lines, 5 accumulators] scenario to the [31 lines, 2 accumulators scenario] in the 9MW turbine case, and from the [31 lines, 5 accumulators] scenario to the [31 lines, 1 accumulator] scenario in the 10 MW case. This price increase remains quite unlikely. However, in the 10 MW case, an increase of 9% of the storage price would change the best scenario from the [31 lines, 5 accumulators] scenario to the [31 lines, 2 accumulators] scenario. This increase could have a higher probability and must thus be taken into account.

## Conclusion

This master thesis was led with the company CNIM, to estimate the annual electricity production of a 9MW linear Fresnel CSP plant that will be installed in Llo, in the French Pyrenees.

At first, a steam accumulator model was created, in order to obtain data on the charging and discharging processes and thus deduce the curves of the pressure variations during those periods. Those results were then integrated to the annual production calculation programmed with Excel. The plant performances calculation was made modelling each components of the thermodynamic cycle with Excel, and then running simulations for data estimated every ten minutes of one year. The simulation was not dynamic but quasi-static. The modelling with Excel, and with a time step of 600 seconds led to some approximation problems that were considered as negligible as the results accuracy matched with what was expected by the company.

The results accuracy was then improved, taking into account different parameters such as the plant location slope, the frost on the mirrors, and the plant shutdowns due to load management.

The influence of the slope at the plant location showed a real improvement of the annual electricity production. Indeed, as it increased the thermal energy available at the end of the solar field by **14.4%**, it increased the annual electricity production by **12.59 %**.

The study of the influence of the weather conditions showed that the frost on the mirrors during cold and humid nights could lead to annual electricity losses of up to **2.84%** of the total production.

Then, the plant shutdowns due to load management by the electrical network operator RTE, during the snowmelt months (May, June and July) trigger losses between **8.02** and **11.57 %** of annual electricity production, as the snowmelts months are the same as the high production months for the solar power plant.

Finally, an economical optimisation, based on prices calculated by CNIM, showed that the best design for the solar field was the one using all the space on the plant location (with 31 lines) and with 5 accumulators. It would then mean a payback time of **9.887 years**. Changing the turbine for a 10 MW one would also decrease the payback time.

However, the plant operation optimisation was limited by the company objectives of building a low-cost solar plant designed to meet the day load. This meant that solutions such as steam superheating, steam reheating or molten salts thermal storage were not studied, as it would have meant higher investments.

The company is satisfied with the model that was created, and with the results that were obtained. The results were validated by the estimation of the annual production of a known solar plant built in Spain by Novatec. It will be a base for future negotiations with investors and RTE (the electrical network manager). However, it would be interesting to run dynamic simulations to have more accurate estimations of the energy needed to preheat the circuit, the reaction of the plant to load variation (because of clouds during the day), and the storage behaviour during charging and discharging processes.

This master thesis was the opportunity to discover the issues linked to the design and construction of a solar thermal power plant, both on a theoretical and industrial point of view. It was also an opportunity to learn VBA programming, learn how to create simple and accurate models of complex problems, and develop methods to tests results.

## References

- [Bellard et al. 2012] *Experimental characterization of a High-Temperature Pressurized Air Solar Absorber for the PEGASE Project*, SolarPACES Conference Marrakech
- [Feledziak 2012] *Etude du Couplement d'une Installation Solaire Thermodynamique avec un groupe turbo-alternateur ORC*, Master Thesis at CNIM
- [Granryd et al. 2009] *Refrigerating Engineering*, Sustainable Energy Utilization course material, KTH, p 9.5
- [Havtun et al. 2011] *Sustainable Energy Utilization*, course material, KTH, pp 76 and 143
- [Jemet 2011] *Thermodynamique appliquée*, Thermodynamic course material, ECP
- [Kalogirou S. 2009] *Solar Energy Engineering, Processes and Systems*, Elsevier, chapters 2, 3 and 10
- [Krothapalli A. 2011a] *Solar Energy: an Introduction*, Renewable Energy Technology course material, KTH
- [Krothapalli A. 2011b] *Flat plate and Concentrating Collectors*, Renewable Energy Technology course material, KTH
- [Paturel 2007] *Trigonométrie sphérique*, Observatoire de Lyon, 2007
- [Petrov M. 2011] Sustainable Power Generation, Course material, KTH
- [RET Screen 2004] *Analyse de projet de chauffage solaire de l'eau*, RET Screen International, Natural Resources Canada
- [Soler R. 2010] *Etat de l'Art des Technologies CSP*, Renewable Energy course material, ECP
- [Spelling J. 2011] *Solar Thermal Power Fundamentals*, Renewable Energy Technology, Advanced course material, KTH
- [Steinmann et al. 2005] *Buffer Storage for Direct Steam Generation*, Solar Energy 80 (2006), pp 1277-1282
- [Stevanovic et al. 2012] *Dynamic of Steam Accumulation*, Applied Thermal Engineering 37 (2012) pp 73-79
- [Taine et al. 2008] *Transferts Thermiques*, Heat Transfer course material, ECP, pp 28, 179, 197, and 241
- [Trieb F. 2009] *Global Potential of Concentrating Solar Power*, SolarPACES Conference Berlin